



MAGISTERARBEIT

Titel der Magisterarbeit

“Astero seismic modelling of the roAp star gamma Equulei
based on observations obtained by the MOST satellite”

angestrebter akademischer Grad

Magister der Naturwissenschaften (Mag. rer. nat.)

Verfasser:	Michael Gruberbauer, Bakk. rer. nat.
Matrikel-Nummer:	0301587
Studienrichtung lt. Studienblatt:	Astronomie
Betreuer:	Univ.-Prof. Dipl.-Ing. Dr. Werner W. Weiss

Wien, im November 2008

Zusammenfassung

roAp (rapidly oscillating Ap) Sterne sind pulsierende Sterne mit starken organisierten Magnetfeldern, die zur Gruppe der (im Allgemeinen nicht pulsierenden) Ap Sterne gehören. Erst wenige Objekte dieser Art wurden bisher entdeckt. Mit ihren chemisch-pekuliaren Sternatmosphären, ihren heterogenen Eigenschaften, was Rotation, Magnetfeldstärke und Pulsationscharakteristik betrifft, sowie ihrer geringen Anzahl, stellen roAp Sterne ein interessantes aber sehr komplexes Thema in der stellaren Astronomie dar. Eine äußerst vielversprechende Möglichkeit, die Vielzahl an physikalischen Effekten aufzulösen, die in diesen Objekten eine Rolle spielen, ist die Asteroseismologie. Sie untersucht, was Pulsationen über den Sternaufbau verraten.

Diese Magisterarbeit berichtet vom Versuch, bei einem roAp Stern erstmalig lediglich mittels der Pulsation auf die Fundamentalparameter und den Aufbau des Sterns rückzuschließen. Mit Hilfe des MOST-Asteroseismologiesatelliten wurden Helligkeitsschwankungen des roAp Sterns γ Equulei (γ Equ) über 19 Tage lang gemessen, wobei insgesamt beinahe ca. 50000 Datenpunkte gewonnen werden konnten. Diese Daten wurden dann mit den aktuellsten Pulsationsmodellen dieses Sterntyps verglichen. Der MOST-Datensatz ermöglicht durch seine außergewöhnliche Qualität zum ersten Mal eine eindeutige Auflösung von γ Equ's Frequenzen, und liefert somit die Grundbedingung für eine derartige Untersuchung.

Nach einer ausführlichen Einführung in das Thema der Ap und roAp Sterne, wird der Satellit MOST detailliert vorgestellt. Da die Kalibration von Satellitendaten äußerst schwierig ist, und MOST in nicht unerheblichem Maße der Kontamination von Störsignalen ausgesetzt ist, muss auch explizit auf die MOST-Dateneigenschaften eingegangen werden. Anschließend wird Punkt für Punkt erläutert, welche Datenreduktionsschritte für die Bearbeitung der γ Equ-Daten notwendig waren, um eine Liste an Pulsationsfrequenzen zu extrahieren, die mit höchster Wahrscheinlichkeit nur intrinsisches Signal enthält. Hier wird besonderes Augenmerk auf die Frequenzanalyse gelegt.

Anschließend folgt in dieser Arbeit eine Beschreibung der theoretischen Modelgitter, die für den Vergleich zu den beobachteten Daten verwendet wurden. Diese Gitter wurden mit Hilfe von Interpolation noch zusätzlich erweitert, weshalb auch eine Analyse der Verlässlichkeit dieses Eingriffes vorgelegt wird. Im Folgenden wird der Algorithmus, mit dem Theorie und MOST-Daten verglichen wurden, ausführlich beschrieben, und die Ergebnisse des Vergleichs besprochen. Zuletzt werden die Implikationen der Ergebnisse für zukünftige Untersuchungen dieser Art aus Sicht des Autors präsentiert.

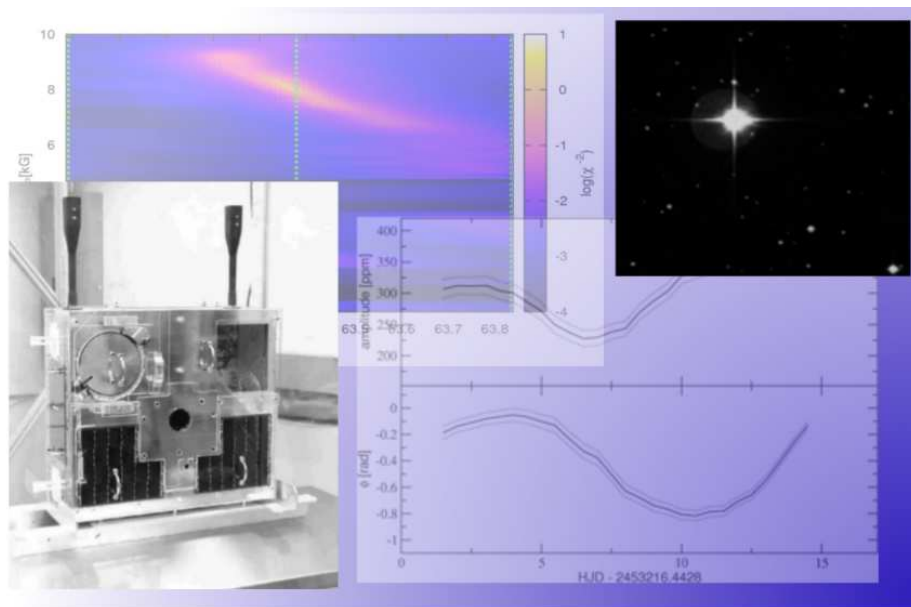
Abstract

roAp (rapidly oscillating Ap) stars are pulsating stars with strong, organized magnetic fields. They belong to the larger group of (in general non-pulsating) Ap stars. Only a few objects of this class are known up to now. Due to the many convoluted effects, like their peculiar atmospheres, their heterogeneity concerning rotation, magnetic field strength, and pulsation characteristics, they are interesting but difficult stars to study. One of the most promising tools to improve our understanding of this class of stars is asteroseismology, which tries to infer details of stellar structure simply from a star's pulsation.

This thesis reports on the first attempt to use asteroseismology for a roAp star as a way to derive the fundamental stellar parameters from pulsation modes alone. With the help of the MOST-satellite, which was explicitly designed for asteroseismological purposes, the varying brightness of the roAp star γ Equulei (γ Equ) has been monitored for over 19 days. All in all, about 50000 measurements were obtained. These were then compared to the latest generation of roAp pulsation models. Due to its impressive quality, the MOST-data set fulfils the requirements for such a study by being the first to unambiguously resolve γ Equ's frequencies.

After an extensive introduction to the topic of Ap and roAp stars, the MOST satellite is introduced in detail in the introductory chapters. Also, the characteristics of the data it delivers are explicitly discussed, since it is most important to not misidentify instrumental signal, which most astronomical satellites suffer from, as being intrinsic to the star. What follows is a step-by-step report on the data reduction techniques employed, as well as a detailed discussion of the frequency analysis that was performed to yield a set of intrinsic pulsation frequencies.

Subsequently, a description of the grids of theoretic pulsation models used to fit to the observations is given. These grids were further refined and extended by interpolation. Therefore, the validity of this process had to be evaluated, which is also discussed. Then, the fitting algorithm, which is employed to compare observations and theoretic models, is explained in great detail. Eventually, a profound report on the results, as well as their implications for future studies of this kind, concludes this work.



Asteroseismic modelling of the roAp star γ Equulei
based on observations obtained by the MOST satellite

M.Sc. THESIS

BY

MICHAEL GRUBERBAUER

IfA
University of Vienna



UNIVERSITY OF VIENNA

DEPARTMENT OF ASTRONOMY

Images used to create the cover illustration have been taken from:

- Walker et al. (2003)
- Image from the second Palomar Observatory Sky Survey (POSS, Reid et al. 1991) centred on γ Equ obtained via the ALADIN interactive sky atlas (Bonnarel et al. 2000)
- Gruberbauer et al. (2008)

Contents

Preface	1
Part I: Introduction	3
1 roAp stars and γ Equ	5
1.1 Ap stars	5
1.2 roAp stars	10
1.3 The observational history of γ Equ	17
1.4 Motivation for this work	19
2 The MOST satellite	21
2.1 The benefits of observing from space	21
2.2 MOST - design and relevant properties	25
Part II: Data reduction and analysis	31
3 The MOST data of γ Equ	33
3.1 The γ Equ data set in the time domain	33
3.2 Frequency analysis	38
3.3 The frequencies and amplitudes of γ Equ	41
Part III: Modelling	45
4 Modelling γ Equ's pulsation	47
4.1 Pulsation models	47
4.2 Model fitting	52
Conclusion and outlook	61
5 Conclusion and outlook	63
5.1 A list of discoveries	63
5.2 Implications for future studies - space photometry as a keyplayer	64
5.3 Conclusion	65
Acknowledgements	67
A χ^2-plots	69
Bibliography	79

Preface

The astronomer's laboratory is quite unlike the experimental environment of most natural sciences. While physicists or chemists are able to perform controlled experiments, employing elaborately designed apparatuses to test their theories, an astronomer has to remain a passive observer¹. We cannot create interstellar clouds to act as nurseries for stars, in order to study stellar birth, life, and death. We are not able to let galaxies collide at will, and we cannot build planetary systems. We can point our telescopes at the skies, however, and try to deduce the principles that govern the inner workings of these objects, simply by employing what is called the principle of universality: the idea that the laws of nature, as we observe them on Earth, are the same everywhere and at every time in the universe.

By simply measuring electromagnetic radiation from countless and diverse celestial objects, using photometry, spectroscopy, and interferometry, astronomers have been able to shed light on the mysteries of stellar evolution, galaxy formation, cosmology, and more. Still, many key questions remain unanswered to this day. As these questions, e.g., concerning the details of stellar structure, continue to become more detailed and intricate, scientists are more and more dealing with a convolution of multiple physical effects. The chemically peculiar Ap stars are a good show case for this problem, exhibiting effects like diffusion, stratification, global magnetic fields, intrinsic variability, non-local thermodynamic equilibrium effects (non-LTE), convection, etc., which results in a very complicated picture.

Often a single factor cannot be isolated, and the fundamental parameters of a star², which ultimately govern all of these physical processes, are not very well known. Clearly, in such cases developing a satisfying theory that describe these details is a difficult thing to do. For astronomers, the focus must therefore shift to figuring out new ways of how to isolate a specific phenomenon, and how to be able to obtain a good estimate of the fundamental parameters.

Stellar astronomers have found such a way a century ago. By discovering the famous period-luminosity relation in 1908 (Leavitt, 1908), astronomers realized for the first time, that stars undergo changes on the dynamical time-scale that are dependent on their structure and fundamental parameters. Previously, it was thought that only by observing many similar stars, spanning the whole range in age from birth to death, something could be learned about a class of stellar objects and eventually inferred about specific members of this class. Also, due to the nature of photometric and spectroscopic measurements, astronomers were observationally constrained to the atmospheres of stars. What would later be called asteroseismology, however, showed that by only knowing the periods of a pulsating star and the reason why it pulsates, a multitude of physical

¹Even though the Heisenberg uncertainty principle might suggest otherwise, at such vast scales as astronomers are interested in, the term “passive observer” probably is no contradiction.

²For stars in general, these are mass, luminosity, temperature, radius, and metallicity. In the case of Ap stars, however, one might also add the global magnetic field strength.

process in the stellar interior, as well as the stellar atmosphere, could be studied.

Asteroseismology has since been refined to not only study the “simple” Cepheids or RR Lyrae stars. Our highly detailed knowledge about the interior Sun mostly comes from asteroseismic investigations of its stochastically excited “solar-type oscillations”. In addition, many different classes of pulsating stars all over the HR-diagram (HRD) have been identified and studied, ranging from the well-known δ Scuti (δ Sct) stars, to more exotic objects like pulsating white dwarfs. Finally, asteroseismology has also become important in the domain of the Ap stars, in specific the rapidly oscillating Ap stars (roAp stars). This sparsely populated group of stars exhibits some of the most puzzling problems for stellar astrophysicists. As I will try to show in this work, based on data of the roAp star γ Equulei (γ Equ) obtained by the MOST (Microvariability and Oscillation of STars) satellite, new developments in theory of the pulsation of roAp stars, as well as the ever-increasing precision in measuring their oscillations, paints a very optimistic picture for solving these puzzles in the near future.

DISCLAIMER: This work is largely based on the publication “*MOST photometry and modeling of the rapidly oscillating Ap (roAp) star γ Equ*”, which was published in *Astronomy and Astrophysics* (Gruberbauer et al. 2008). It is therefore necessary to mention which part I played in this investigation, and also which sections of this thesis rely on my original work. Concerning the cited article, I was responsible for all literature research, the comparison of reduced light curves, frequency analysis, model interpolation, model fitting, and most of the writing. It was also my task to interpret the results and investigate their implications. Daniel Huber, who is a co-author of the paper, produced the decorrelated light curve. Thomas Kallinger devised the “doughnut”-fitting routine and was in charge of applying it to the raw data of γ Equ. Hideyuki Saio computed all theoretic models, which I subsequently expanded using interpolation, and which I fitted to the observed data. Finally, all remaining co-authors assisted in editing the journal article. In conclusion, I am certain that this thesis gives credit where credit is due and is a valid representation of my original work.

Part I: Introduction

Chapter 1

roAp stars and γ Equ

In this chapter, I give a basic introduction to the topic of chemically peculiar A stars. I will focus on the more specific topic of roAp stars. Their serendipitous discovery and a chronicle of the major advances in understanding these stars, in particular their oscillations, will be discussed. Eventually, the attention shifts to γ Equ. I present a detailed review of what was already known about this star prior to the MOST observations, especially concerning its pulsational characteristics. This will provide the necessary context, in which my investigations have to be understood. The chapter concludes with a section on the motivation for the work presented in this thesis, which necessarily has to build on the preceding introductory sections.

1.1 Ap stars

The discovery of chemically peculiar (CP) stars dates back to the first half of the 20th century, when the first serious efforts were made to characterize stars according to their spectra. The term “peculiar” initially was used to describe any spectrum that was difficult to classify according to the Harvard sequence. Soon, many of these objects were identified as non-stellar objects, spectroscopic binaries or other types of variable stars (Fleming & Pickering 1912). However, with improving spectral resolution and atomic line data, true chemical peculiarities in some stars became apparent. Morgan (1933) found that this phenomenon seemed to extend from early F type stars¹ towards higher temperatures, up to the very hot B stars. Spanning such a vast range of effective temperatures, studying and determining the cause for these apparent anomalies became a necessary and promising task to better understand stellar atmospheres and evolution.

Various classification systems were proposed, but one of the simpler ones prevailed until today (Preston 1974). Preston divided CP stars into 4 categories. Since only the cooler stars of type A-F are considered to be possible candidates for roAp pulsation, what he called CP2 stars and what are commonly referred to as (magnetic) Ap stars, are the focus of this section. They are distinct in showing large-scale organised magnetic fields, which had been detected as early as in the middle of the 20th century (Babcock 1947, 1958), as well as abundance anomalies, in particular an overabundance in rare earth elements (REE, e.g., Er, Eu, Nd, Pd, ...).

¹It was actually γ Equ which was identified as a chemically peculiar F0 star in Morgan’s work. This classification was not far off, as the star is today considered to be of type A9p.

1.1.1 Magnetic field geometry and the oblique rotator model

Monitoring the magnetic fields of these CP2 stars soon revealed an effect that would later be explained by the oblique rotator model (Stibbs 1950). Variations of the strength and polarity of the magnetic fields were going hand in hand with variations of mean light, as well as observed element abundances. This suggested that in many Ap stars the magnetic field, which is correlated with these quantities, is essentially dipolar and its axis inclined to the rotation axis. As a consequence, the obliquity of the magnetic axis would produce a modulation of the measured magnetic field strength over the course of one rotation cycle. Mathematically, this can be expressed by

$$\cos \alpha = \cos i \cos \beta + \sin i \sin \beta \cos 2\pi\phi, \quad (1.1)$$

where α is the angle between the axis of the magnetic field and the observer, i is the inclination of the rotation axis towards the line of sight, β is the inclination of the magnetic axis to the rotation axis, and ϕ is the phase of rotation with respect to the maximum of the magnetic field measurements. Fig. 1.1 shows the main characteristics of this geometry. The initial assumption of a simple

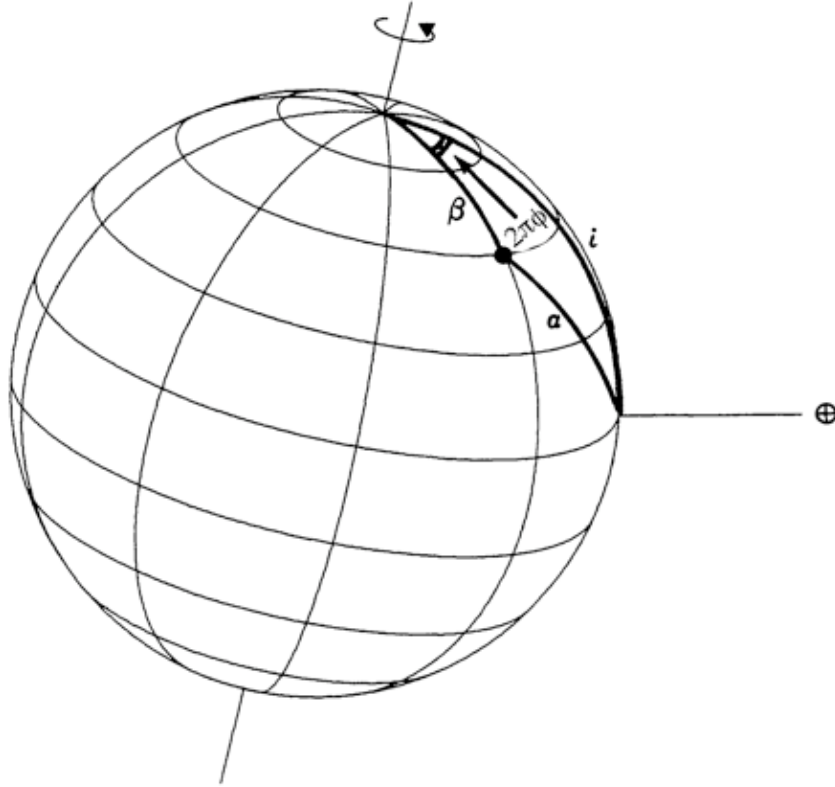


Figure 1.1: Schematic visualisation of the the oblique rotator model. (Modified from Kurtz (1990))

magnetic dipole, however, is too inaccurate for many Ap stars. As an example, Landstreet (1988), when observing the Ap star 53 Cam, found that combining a dipolar, a quadrupolar, and an octupolar component was necessary in order to fit the magnetic field measurements. Through the recent advent of Magnetic Doppler Imaging (MDI) an even more intriguing test for the magnetic

field configuration of Ap stars has been established. For 53 Cam, the same object Landstreet observed in 1988, the results of such a MDI analysis by Kochukhov et al. (2004a) is presented in Fig. 1.2. Nonetheless, some axial symmetry is still prevalent in even the most complex magnetic field geometries of Ap stars.

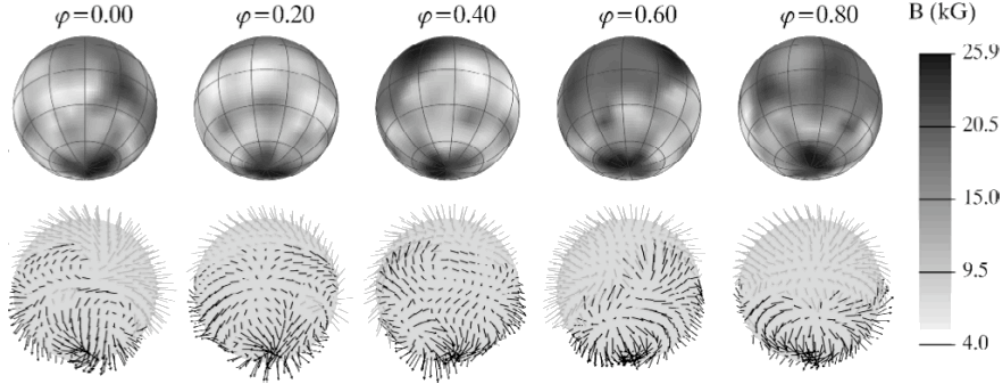


Figure 1.2: Results of MDI for the Ap star 53 Cam. The figure shows the surface magnetic field distribution, as well as the surface field orientation, as a function of rotation phase measured from the Fe II line at λ 5169.03 Å. (Modified from Kochukhov et al. (2004a))

Overall, the oblique rotator model still applies for crude estimates of the magnetic field geometry, determination of rotation periods, maximum field strength, and abundance inhomogeneities, while demanding not nearly as powerful instruments and computation as the (M)DI techniques. Also, not only did it solve the problem of the observed time-dependent properties of Ap stars, but it also inspired the explanation of roAp pulsation observations via the oblique pulsator model (see Sec. 1.2.2).

1.1.2 Origin of the magnetic fields

Stellar magnetism has only been observed in relatively few non-degenerate stars². Aside from the Sun, and the considerably hotter Bp stars, Ap stars account for the majority of definite detections. Many cooler non-peculiar stars are expected to exhibit stellar spots correlated with surface magnetic field extrema not unlike the Sun. However, only recently has instrumentation improved by such an amount as to actually measure these effects reliably (Berdyugina et al. 2008). The reason for this observational dominance of Ap stars is of course the impressive magnitude of their observed magnetic field strengths, owing to the global scale of these fields and their organised structure.

These impressive magnetic field configurations, and their seeming exclusivity to Ap and Bp stars, however, are still puzzling to astronomers. Various hypotheses attempting to ascertain their origin have been proposed. Possible explanations range from fossil magnetic fields, i.e., stellar magnetic fields that originate from the magnetic properties of the interstellar medium from which the stars formed, to various propositions of dynamo activity and magneto-hydrodynamic instabilities. The

²This is of course referring to excluding pulsars or white dwarfs, which possess excessive magnetic fields due to conservation of their progenitor's total surface magnetic flux. Interestingly, for those white dwarfs with the largest measured magnetic fields the progenitors certainly could not have been anything but Ap stars.

evidence to prefer any of these hypotheses is still missing or, at best, inconclusive. Elaborate discussions on this subject can be found in Mathys (2004) and Arlt (2008), and references therein.

1.1.3 Explaining the abundance anomalies

In order to explain the abundance anomalies in Ap stars, several hypotheses have been proposed over the years. It was obviously a very difficult thing for theorists to come up with a viable theory of “how to make Ap stars”. Many researchers focussed on the seemingly necessary, excessive formation of rare-earth elements. It was proposed that either in the material from which Ap stars had formed, or in their atmospheres themselves, nuclear reactions had to take or have taken place to generate the observed abundances. However, since some Ap stars are members of clusters that do not show general abundance peculiarities, the first hypothesis was soon disregarded. To think of particular nuclear reactions, so effective and ubiquitous that they would lead to the observed peculiarities, led scientists on curious paths.

A brilliant example for this is the paper by Fowler et al. (1965). In a very profound discussion the authors first give a summary of the abundance characteristics of different kinds of peculiar A stars. Then they proceed by proposing a rather complicated scenario that could explain, from their point of view, the existence of Ap stars. They suggest that these stars have already gone through the red giant phase but returned to near the main sequence. Multiple flashes of carbon during the red giant phase should have led to a disruption of the degenerate core, lifting the degeneracy, increasing the number of heavy elements like REEs by neutron capturing processes, and bringing an interior magnetic field and heavy elements to the surface. Atmospheric abundances of He and other elements heavier than hydrogen would, according to Fowler et al., have been diminished through spallation. By lifting the degeneracy, and without losing a lot of mass, the stars then would return to a quasi-main sequence state and settle down. The prerequisites for this to happen (e.g., multiple C-flashes, acceleration of elements in the atmosphere by very strong magnetic fields in order for spallation to occur, post-RGB stars), some of which contradicting theory of stellar evolution at the time, as well as the chain of events proposed, nowadays renders this hypothesis useful only in a historical sense. The principle of Occam’s Razor would suggest that simpler explanations should be available.

A different solution for the Ap enigma, nominating a stellar companion that has undergone all the evolutionary changes up to the white dwarf stage as the reason for the observed abundances and magnetic fields, is also discussed in Fowler et al. (1965). The mass ejected from this star would have been accreted onto the A star’s atmosphere, producing the chemical peculiarities. The remnant white dwarf then would evolve a strong magnetic field through conservation of total surface magnetic flux. In conclusion, the system, if not spectroscopically resolved, could produce the observational impression of a magnetic, chemically peculiar A star. This scenario, however, was highly questionable even at the time of publication, since many Ap stars were considered to be single stars with relative certainty. Therefore, all of the available explanations were considered to be somehow inadequate. As so often throughout the history of science, a much simpler hypothesis soon was developed that is still considered the most probable today: the diffusion hypothesis.

It was introduced to the field of Ap stars through the landmark paper by Michaud (1970) and builds on the simple idea that radiative accelerations from bound-bound and bound-free transitions can counteract or even surpass the gravitational forces on some elements (Mn, Sr, Y, Zr and REEs). As explained in Michaud (1970) these elements then would be pushed towards the top of the atmosphere, while other elements like He would settle down. In order for this to happen, the stellar atmosphere needs to be relatively stable. Since Ap stars possess large magnetic fields which

suppress convection and are found to be relatively slow rotators compared to typical A stars, this basic prerequisite is fulfilled. Diffusion is nowadays widely accepted to be indeed the key player in the formation of the abundance anomalies in Ap stars. The theoretical framework for diffusion in stellar atmospheres has been revisited and improved many times, and recent investigations even indicate that these processes also play an important role in non-peculiar stars. Observations require for instance that the "Standard Solar Model" must account for gravitational settling of He, in order to produce a lower temperature gradient. Without this effect, theory would mismatch the neutrino production rate by 7 % (Bahcall et al. 1995). More details on the application of diffusion in non-CP stars can be found in Vauclair (2003).

In the exceptionally detailed review on the topic of roAp stars by Kurtz & Martinez (2000), the authors summarise the effects of diffusion on the atmospheres of CP stars. In particular, they list observational properties of Ap stars that can be reproduced qualitatively with the help of the diffusion hypothesis. The following checklist contains paraphrases of the most important arguments given in their paper.

- **Abundances of Fe-peak, rare earth and lanthanide elements:** Due to numerous absorption lines with energies near the flux maximum at the temperature of the radiative zone, these elements are levitated to the surface layer and therefore appear to be overabundant.
- **Ages of Ap stars:** Diffusion is able to produce observable anomalies on time scales on the order of 10^6 years. This is compatible with the observed ages of Ap stars.
- **Non-detection of chemical anomalies in red giants with Ap precursors:** Were the mentioned observed overabundances actually real, i.e., due to significantly higher abundances in the stars' mean chemical composition, these properties would remain observable throughout their lifetimes. Since diffusion only produces apparent overabundances, the build-up of a growing surface convection layer as required by stellar evolution, is sufficient for the anomalies to vanish due to convective mixing.
- **Slow rotation:** Ap stars show considerably lower $v \sin i$ values ($< 100 \text{ km s}^{-1}$) than normal A-type stars ($\approx 250 - 300 \text{ km s}^{-1}$). The low rotational velocities are needed for diffusion to be effective, because faster rotation would produce meridional circulations that would inhibit diffusion.
- **Magnetic fields and diffusion:** The global magnetic fields in Ap stars are probably the reason for their lower rotation velocities by means of magnetic braking. Additionally, they help to stabilise the envelope against convection. Both consequences make diffusion feasible.
- **Ap- δ Sct dichotomy:** Numerous Ap stars are situated in the δ Sct instability strip but show no pulsation of this type. The reason for this again is diffusion, since under the influence of diffusion He settles gravitationally. Without sufficient amounts of Helium in the He II ionisation zone for the κ -mechanism to act on, δ Sct-like pulsation cannot be excited.

With the introduction of the oblique rotator model and the diffusion hypothesis, the basic characteristics of Ap stars seemed to be understood³. With the discovery of the roAp stars and the first publication reporting on this new class of variables in the early 1980s, a whole new phenomenon was unveiled.

³There is still one largely unanswered question however. Why do some A stars become Ap stars while most do not ?

1.2 roAp stars

1.2.1 Discovery and observational properties

The discovery of roAp stars is a story of serendipity. Although most Ap stars lie within the classical instability strip, their particular properties were thought to inhibit pulsation. Kurtz (1982) elaborates that the strong (and global) magnetic fields would probably have a stabilising effect on any oscillations. In addition, as alluded to in Section 1.1.3, diffusion leads to He deficiencies in the He II-ionisation zone, where stellar oscillations are usually excited due to the κ mechanism in δ Sct stars. Very high-overtone pulsations in particular, such as those eventually discovered in roAp stars, were not at all expected. As described in Kurtz (1990) the discovery of the roAp phenomenon was a consequence of the claimed detection of δ Sct-like pulsation in stars that nonetheless showed a spectroscopic signature similar to that of an Ap star⁴. In the particular case of HD 188136 (Wegner 1981) a strong spectroscopic similarity to HD 101065 was established. As a test of the boundaries of possible δ Sct-pulsations among Ap stars, D.W. Kurtz observed HD 101065 in 1978. To cite the discoverer himself:

“I tested HD 101065 for light variability in April 1978 using differential photometry with two comparison stars giving a time resolution of about 8 min. The appearance of its light curve seemed to suggest that variations were occurring on a time scale too short to see with the differential photometry, so the next month I observed the star through a Johnson B filter with continuous 20-s integrations. The 12.14-min variations were immediately (and unbelievably) obvious.” (Kurtz 1990)

Soon after this initial discovery reported in Kurtz (1982), many more roAp stars were found. At the time of this writing about 40 stars of this class are known. They exhibit pulsation periods between 5 and 21 minutes and very few modes with amplitudes above a few mmag seem to be excited. Their spectral types range from A-F and most stars seem to lie on the main sequence. From spectroscopical observations roAp stars appear strikingly similar to non-pulsating Ap (noAp) stars, as reported by Ryabchikova et al. (2004). These two related groups exhibit a similar chemical composition, comparable rotation periods and magnetic fields. However, noAp stars generally appear to have higher effective temperatures. On the other hand, Ryabchikova et al. find that the so-called “REE anomaly”, a dependence of the results of abundance determination on the ion used for the analysis⁵, strikingly is more pronounced in roAp stars.

The very high frequencies, which are actually close to the frequency region inhabited by the more elusive solar-type oscillations, point to high radial overtones on the order of 20. Although the variations were “obvious” in the case of HD 101065, in general, the amplitudes of roAp stars are only a few mmag, which explains why, in terms of the history of variable stars, they were only identified quite recently. A very interesting characteristic that is shared by many of these pulsators is the property of showing equidistant multiplets of frequencies in the Discrete Fourier Transform (DFT) of their light curves and radial velocity time series (e.g., Kurtz 1982). This means, of course, that in the time domain the signal is varying in amplitude with a frequency given by the difference of the adjacent multiplet components (= beating). Although γ Equ does not exhibit these multiplets, it is important to discuss their implications. It was these equally spaced frequencies in the DFT that led to the highly successful model of the oblique pulsator.

⁴Although, as mentioned in Section 1.1.3, there should be a dichotomy between Ap stars and δ Sct variables, these observations have remained valid and other similar stars have been found. A discussion on this problem can be found in Kurtz & Martinez (2000).

⁵In the case of the roAp star 33 Lib, Ryabchikova et al. (2003) derive differences in abundance of Pr and Nd of more than 2 dex, depending on whether they use lines of the first or second ions of these elements.

1.2.2 The oblique pulsator model

Not only did D.W. Kurtz report the finding of this new class of pulsating stars in his paper from 1982, he also introduced a model that could explain their seemingly strange variations. As stated in the previous section, for most roAp stars each prominent frequency is surrounded by multiple equally spaced frequencies. These frequencies are much too close to correspond to p-modes of increasing radial order, according to the asymptotic theory as described by Tassoul (1990). Consequently, one might identify those additional frequencies with non-axisymmetric ($m \neq 0$) modes, i.e., rotational splitting. However, such m -modes would have to follow the well-known relation by Ledoux (1951)

$$f_{\ell,m} = f_{\ell,0} \pm m(1 - C_{k,\ell})f_{\text{rot}}, \quad (1.2)$$

where $f_{\ell,m}$ is the observed m -mode frequency of spherical degree ℓ and azimuthal order m , $f_{\ell,0}$ is the frequency of the axisymmetric mode with same spherical degree as the m -mode, $C_{k,\ell}$ is the Ledoux constant which depends on the stellar structure and the type of pulsation, and f_{rot} is the rotation frequency of the star. Kurtz observed, however, that the multiplet frequencies were spaced with **exactly** the rotation frequency to within the observational uncertainties, thus yielding $C_{k,\ell} \sim 0$. Although this value rather close to zero is not outside the realm of physical possibility, another factor makes it very improbable that non-axisymmetric modes are the correct solution. In Kurtz (1982), the author also reports that the pulsation amplitude maximum occurs simultaneously with the magnetic maximum⁶ and that this coincidence remains valid over the whole duration of the observations, i.e., several rotation cycles. This is only probable if indeed $C_{k,\ell} = 0$, since any $C_{k,\ell} \neq 0$ would, over time, lead to a drift between the two different maxima, because the oblique rotator model implies that the magnetic field varies with exactly the rotation frequency.

Consequently, Kurtz proposed a different explanation inspired by the oblique rotator - the oblique pulsator model (OPM). Just as in the oblique rotator model describing the magnetic field variations, the modulation of the signal from a dipole pulsation would vary over the course of a rotation cycle. This variation results in an amplitude modulation that produces a frequency triplet in the frequency domain, centred at the actual frequency of the dipole pulsation and spaced with exactly the rotation frequency. This can be expressed as described in Kurtz (1982) like a signal

$$\Delta m = A \cos(\omega t + \phi), \quad (1.3)$$

where $\omega = 2\pi f$ and ϕ is some phase of the pulsation, but with an amplitude varying as a sinusoidal function of time according to

$$A(t) = A_0 + 2A_1 \cos(\Omega t) \quad (1.4)$$

with $\Omega = 2\pi f_{\text{rot}}$. Substituting A in equ. 1.3 with equ. 1.4 then yields

$$\Delta m = A_0 \cos(\omega t + \phi) + A_1 \cos[(\omega + \Omega)t + \phi] + A_1 \cos[(\omega - \Omega)t + \phi] \quad (1.5)$$

A DFT of such a signal will consequently show the required three frequencies: a central frequency $\omega/2\pi$ with amplitude A_0 , and two frequencies $(\omega + \Omega)/2\pi$ and $(\omega - \Omega)/2\pi$ with amplitudes A_1 . In order to produce this amplitude variability, the pulsation axis must be inclined to the rotation axis. Since Kurtz observed the pulsation maxima at exactly the same time as the magnetic maxima, he concluded that the roAp stars pulsate about their magnetic axis.

Following the derivation from Kurtz (1982), by adapting this assumption one can write the relative change in luminosity as

$$\frac{\Delta L}{L} \propto P_l(\cos \alpha) \cos(\omega t + \phi) \quad (1.6)$$

⁶The temporal behaviour of the apparent magnetic field strength can of course be described according to the oblique rotator model (see Section 1.1.1).

by introducing α , the angle between the pulsation pole (= magnetic pole) and the line-of-sight, and a Legendre polynomial $P_\ell(\cos \alpha)$ which depends on the shape of pulsation. In the case of dipole pulsation ($\ell = 1$) the Legendre polynomial is simply $\cos \alpha$ and equation 1.5 immediately follows from equation 1.6. Just as in the model of the oblique rotator, $\cos \alpha$ can be expressed as in equation 1.1. Using the same symbols as in equations 1.3 to 1.5 this amounts to

$$\cos \alpha = \cos i \cos \beta + \sin i \sin \beta \cos(\Omega t), \quad (1.7)$$

with

$$A_0 = \cos i \cos \beta \quad (1.8)$$

and

$$A_1 = \frac{1}{2} \sin i \sin \beta. \quad (1.9)$$

Thus, the ratio of the amplitudes

$$\frac{A_1}{A_0} = \frac{1}{2} \tan i \tan \beta. \quad (1.10)$$

Evidently, the oblique pulsator can be used to infer the inclination of the rotation axis (i) and the obliquity of the magnetic axis to the rotation axis (β), because the ratio of the amplitudes A_1/A_0 depends on these geometric factors. In the case of quadrupole pulsation ($\ell = 2$) the associated Legendre polynomial produces

$$\begin{aligned} \frac{\Delta L}{L} &\propto A_0(\cos \alpha) \cos(\omega t + \phi) + A_1 \cos[(\omega + \Omega)t + \phi] + A_1 \cos[(\omega - \Omega)t + \phi] \\ &+ A_2 \cos[(\omega + 2\Omega)t + \phi] + A_2 \cos[(\omega - 2\Omega)t + \phi] \end{aligned} \quad (1.11)$$

with

$$A_0 = 12 \cos^2 i \cos^2 \beta + 6 \sin^2 i \sin^2 \beta - 4, \quad (1.12)$$

$$A_1 = 12 \cos i \cos \beta \sin i \sin \beta, \quad (1.13)$$

and

$$A_2 = 3 \sin^2 i \sin^2 \beta. \quad (1.14)$$

In general, according to the simple OPM, an axisymmetric mode of spherical degree ℓ will produce a multiplet with $2\ell + 1$ components. Special emphasis has to be given again, however, to the fact that this model predicts equal amplitudes for the positively and negatively shifted components, i.e., $A_\ell = A_{\ell+1} = A_{\ell-1}$. In many roAp stars that show frequency multiplets due to rotation, the amplitudes do not exhibit this equality. Refined versions of the OPM have partially solved this problem by incorporating rotational effects like the coriolis force (Bigot & Dziembowski 2002). Nonetheless, by looking at time-resolved amplitudes and phases, some stars still do not exactly obey even the refined OPM (e.g., Handler et al. 2006). In these cases a combination of $\ell = 1, 2$, or even higher is necessary to reproduce the temporal behaviour of amplitudes and phases. This is due to the fact that the assumption of modes characterised by a single spherical harmonic is not applicable in the presence of a global magnetic field (Kurtz 1992, also see Section 1.2.4).

The OPM is a very powerful and important tool to infer the pulsation geometry of roAp stars, but it cannot be applied to each object of this class. γ Equ, the subject of this study, is one of these few example. It does not show any significant rotation on an observationally relevant time scale of months to a few years. Hence, I will now leave this topic since a basic understanding of the OPM and its relevance for the study of roAp stars has already been established.

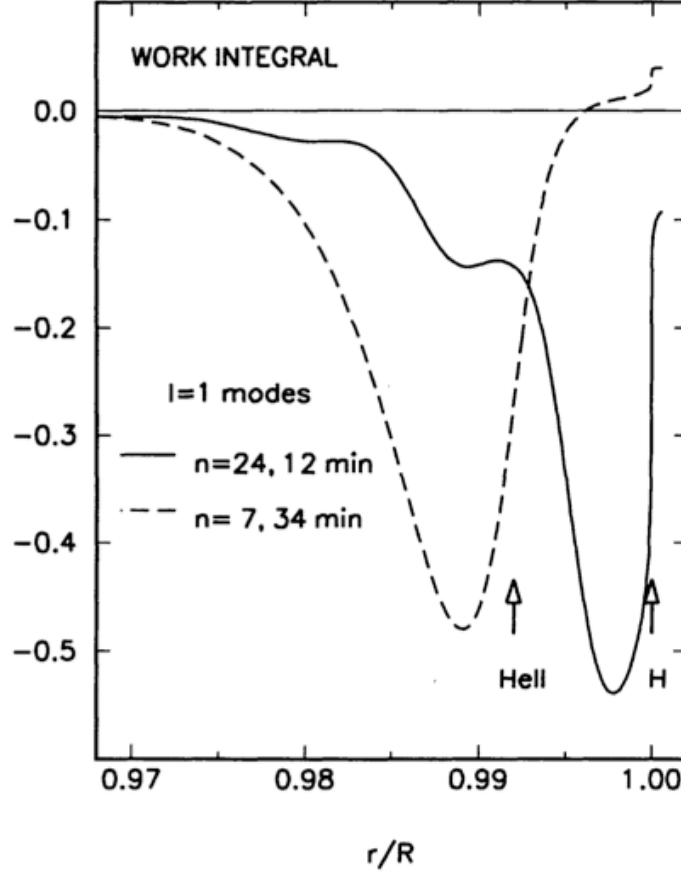


Figure 1.3: The cumulative work integral for two $\ell = 1$ modes in a $2M_{\odot}$ star as a function of stellar radius. Regions of driving due to He II and H ionisation are shown. (Taken from Dziembowski & Goode (1996))

1.2.3 Excitation mechanism and driving of roAp pulsation

Initially, the most puzzling question was how to excite roAp pulsation. Although their frequencies are in the regime of the stochastically excited solar-type oscillations, their amplitudes and mode stability point at a different excitation mechanism. The first fundamental accomplishment in roAp theory and modelling, and especially concerning the question of mode driving, was published by Dziembowski & Goode (1996). The authors investigated opacity-driven pulsation under the influence of magnetic fields, based on standard stellar models with homogenous chemical composition in the stellar envelope, i.e., not accounting for He settling due to diffusion, and a grey atmosphere. Dziembowski & Goode explicitly mention that their work was based on assumptions and models which should be first adapted to include diffusion. An additional complication, already found by Campbell & Papaloizou (1986), is that the magnetic field leads to loss in pulsation energy via a generation of Alfvénic-type waves. Nonetheless, they already identified H ionisation as the most plausible cause of driving the oscillations in roAp stars.

Figure 1.3 is part of a plot from their publication, in which the impact of the H ionisation zone

on the driving is apparent. It shows the cumulative work integral for two different $\ell = 1$ p-modes of a $2M_{\odot}$ model of radial order $n = 7$ and $n = 24$. Where the integral increases driving occurs, while a decrease signals dissipation, and positive values indicate that the mode is unstable to pulsation. Evidently, the $(n = 7)$ -mode is excited due to He II ionisation, but the frequency is in the regime of δ Sct-pulsation. On the other hand, driving of the $(n = 24)$ -mode, which is comparable to what has been observed for roAp stars in terms of its frequency, is not strong enough to make it unstable. However, it is obvious from Figure 1.3 that only H I ionisation is contributing significantly to driving such high-order modes. Dziembowski & Goode also found that efficient driving through this process requires radial orders $\gtrsim 20$, and that the driving is highest for frequencies above the acoustic cut-off frequency, the maximum frequency at which the pulsation wave is reflected and does not dissipate in the atmosphere. This poses the problem that such oscillations would essentially lose their energy and, as such, would require a very efficient driving mechanism to remain stable over time. Subsequent work by Audard et al. (1998) showed that improving atmospheric calculations, by taking into account frequency-dependent treatment of radiative transfer and general atmospheric properties of roAp stars, leads to higher acoustic cut-off frequencies. In addition, Gautschi et al. (1998) find that a temperature inversion above $\log \tau = 0$ of a few 1000 K also has a similar effect. However, their models predict for roAp pulsation an upper limit in T_{eff} which is clearly too low in comparison to observations.

A different approach developed by Balmforth et al. (2001), suggests that roAp stars can basically be divided into two components, namely the magnetic poles and the equatorial regions. At the magnetic poles convection is suppressed by the magnetic field, which produces all the previously discussed effects like He settling through diffusion. On the other hand, the authors argue that the equatorial regions would more closely resemble those of a normal A star, since there the magnetic field lines of a dipole are essentially parallel to the stellar surface, therefore allowing convection to occur. Balmforth et al. found that the suppression of convection at the polar regions is essentially the reason why pulsations could be driven through H ionisation. This model was subsequently employed in a study by Cunha (2002), in order to explore the theoretical instability strip of roAp stars. Again, however, some observations contradict the borders of this instability strip (e.g., Kochukhov 2003).

1.2.4 Effects of the magnetic field on the oscillations

Apart from driving the oscillations and exciting the modes, the effects of a magnetic field on the pulsation frequencies and the pulsation geometry itself has received much attention. One of the first studies, applicable to roAp stars although only considering radial modes, is Biront et al. (1982). The authors concluded that the problem of oscillations in a magnetic star would necessitate in a concept called the magnetic boundary layer. The total gravitational energy of a star is much larger than the total magnetic energy. Thus, for the most part within the stellar radius the gas pressure dominates over the magnetic pressure, and magnetic effects are negligible. In the outer layers close to the photosphere, however, the magnetic pressure can become of the same order as the gas pressure, and magnetic effects will influence the pulsation. A visualisation of this is given in Figure 1.4. Even for radial modes, non-radial components in the motion arise near the magnetic boundary layer. This concept was further developed by Roberts & Soward (1983), expanded to non-radial oscillations in Campbell & Papaloizou (1986), and also considered and improved in more recent studies (Dziembowski & Goode 1996; Cunha & Gough 2000). As a consequence, Dziembowski & Goode realized that the individual pulsation modes in magnetic stars can not be described by a single spherical harmonic. Therefore, from an observational point of view, mode identification using traditional tools is not feasible. In addition, due to this change in the oscillatory motion, the frequencies themselves are also directly affected. Cunha & Gough (2000) concluded

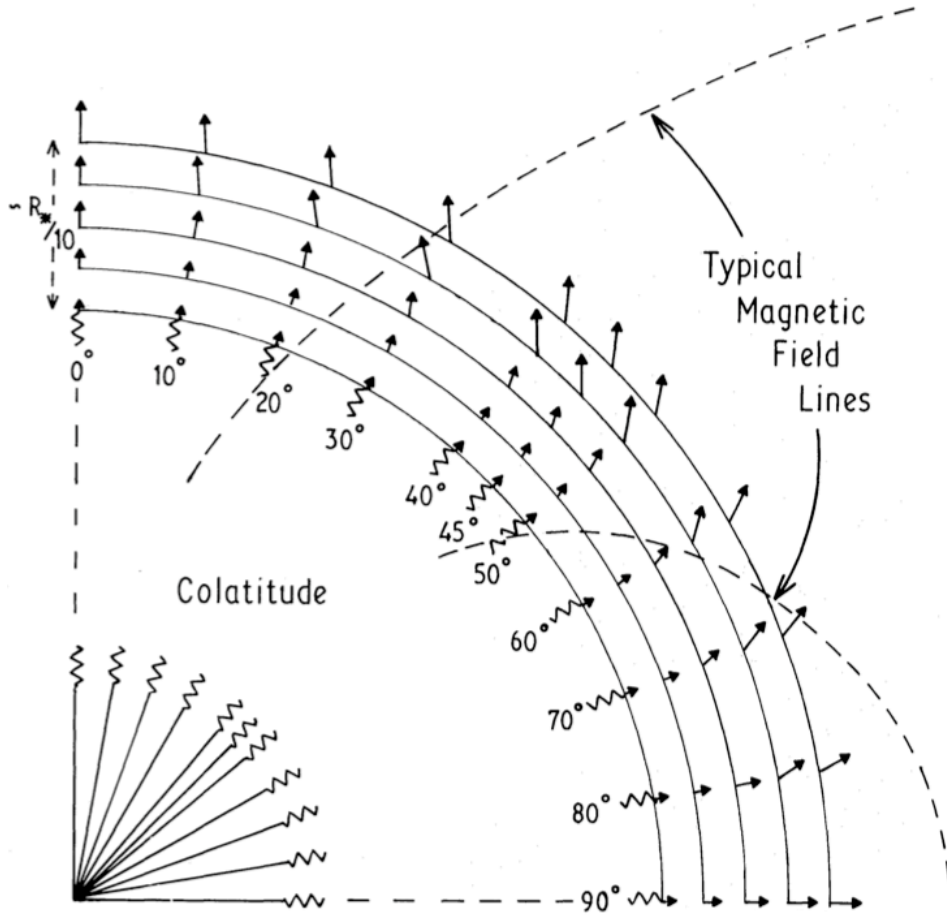


Figure 1.4: A schematic portrait of the displacement vectors as a function of colatitude and stellar radius for radial pulsation under the influence of a magnetic field. The scale of the magnetically influenced outer layers is exaggerated (Modified from Biron et al. (1982))

that frequencies shift significantly in comparison to non-magnetic models, which can be directly observed, and that the magnitude of these shifts is dependent on the individual modes. A very prominent case of frequency shifts that have been detected and analyzed is HR 1217 (e.g., Kurtz et al. 2005).

Since individual modes are affected differently by the magnetic field, i.e., their frequency values and energy budget changes as a function of magnetic field strength and geometry, Cunha & Gough (2000) suggested that this might be a very important agent of mode selection in roAp stars. More recently, the concept of the magnetic boundary layer has been revisited, and two regions within this layer have been studied in more detail: the magneto-acoustic layer, where magnetic pressure and gas pressure are of the same order, and the magnetically dominated layer, where the magnetic pressure is significantly higher than the gas pressure. These different regions also are very likely to influence the pulsation. A comprehensive review on this topic, and theory of roAp pulsation in general, can be found in Cunha (2007).

Another great contribution to roAp pulsation theory was published in Saio & Gautschy (2004) and Saio (2005). Since the modelling of γ Equ in my work is based on the theoretical models of these authors, in particular the contribution of pulsation models by H. Saio, the discussion of these articles will be postponed to section 4.1.1.

1.2.5 A summary

As a concise summary of the previous sections, the introductory paragraph of the article on which this thesis is based (Gruberbauer et al. 2008) is given below.

roAp stars form a class of variables consisting of cool magnetic Ap stars with spectral types ranging from A-F, luminosity class V, and were discovered by Kurtz (1982). Photometric and spectroscopic observations during the last 2 decades characterize roAp stars with low amplitude pulsations (< 13 mmag) and periods between 5 to 21 minutes. It is now widely accepted that the oscillations are due to high-overtone ($n > 15$) non-radial p-mode pulsations. The observed frequencies can be described in a first-order approximation by the oblique pulsator model as described by Kurtz (1982). In this model the pulsation axis is aligned with the magnetic axis, which itself is oblique to the rotation axis of the star. It has since been refined and improved to include additional effects like the coriolis force .

The oscillations in roAp stars are most probably excited by the κ mechanism acting in the hydrogen ionization zone (Dziembowski & Goode 1996), while the prime candidate for the selection mechanism of the observed pulsation modes is the magnetic field (e.g. Bigot et al. 2000; Cunha & Gough 2000; Balmforth et al. 2001; Bigot & Dziembowski 2002, 2003; Saio 2005; Cunha 2006). Similar to noAp stars, the group of roAp stars also shows a distinctive chemical pattern in their atmospheres, in particular an overabundance of rare earth elements, which points to stratification and vertical abundance gradients. Tackling the question of what drives the roAp pulsation, it is important to note that apart from the similar chemical composition, noAp stars show comparable rotation periods and magnetic fields but higher effective temperatures (Ryabchikova et al. 2004). Thus, their hydrogen ionization zone lies further out in the stellar envelope, which prevents efficient driving of pulsation. All together, roAp stars have given new impulse to asteroseismology and 2D mapping of pulsation (Kochukhov 2004), as well as detailed 3D mapping of (magnetic) stellar atmospheres, has become possible.

1.3 The observational history of γ Equ

γ Equ (HD 201601, HR 8097, A9p, $m_V = 4.7$, shown in Fig. 1.5) has been a favourite subject of research and a significant contributor to the studies of magnetic stars. Its observational history, spanning several decades, was eloquently summarised in our paper (Gruberbauer et al. 2008), which will serve as a blueprint for this section.



Figure 1.5: An image from the second Palomar Observatory Sky Survey (POSS, Reid et al. 1991) centred on γ Equ obtained via the ALADIN interactive sky atlas (Bonnarel et al. 2000).

γ Equ was long known to have a significant magnetic field (Babcock 1958) which is variable with a period of ~ 72 years (Bonsack & Pilachowski 1974; Scholz 1979; Leroy et al. 1994). Rotation, a solar-like magnetic cycle or precession of the star’s rotation axis due to a hypothesised binary companion are candidate mechanisms for this cyclic variation. The binary hypothesis was supported by Scholz et al. (1997), who observed a temporary drop in radial velocity for γ Equ during 4 consecutive nights. Their results are however contradicted by Mkrtichian et al. (1998, 1999). Magnetic field data spanning more than 58 years indicate that the variation is most likely due to rotation and therefore $P_{\text{mag}} = P_{\text{rot}}$ (Bychkov et al. 2006). This explanation is also supported by many spectroscopic observations showing very sharp absorption lines (e.g. Kanaan & Hatzes 1998) which are typical for a slow rotator (or a star seen pole-on).

Kurtz (1983) was the first to detect a pulsation period of 12.5 min (1.339 mHz) with an amplitude varying between 0.32 and 1.43 mmag and speculated about a rotation period of 38 days, inconsistent with the magnetic field measurements mentioned above. It was the 6th discovery as a roAp star. Aside from rotation, beating with a closely spaced frequency has been proposed as a cause, for which Gruberbauer et al. (2008) gives further evidence, which will also be discussed in this thesis. The pulsation was confirmed shortly after Kurtz’s study by Weiss (1983). Bychkov (1987) reported first evidence for radial velocity (RV) variations, but it took two more years for a

clear detection (Libbrecht 1988). Although unable to detect the 1.339 mHz oscillations reported by Kurtz (1983), Libbrecht discovered three frequencies at 1.365 mHz, 1.369 mHz and 1.427 mHz. He suggested that the amplitude modulation observed in the spectra of roAp stars may not be due to closely spaced frequencies, but rather caused by short mode lifetimes in the order of ~ 1 d. He concluded that both peaks therefore belong to a single p-mode oscillation. The follow-up study by Weiss & Schneider (1989) aimed at performing simultaneous spectroscopic and photometric studies but failed to confirm γ Equ's pulsation. The latter authors applied a correlation technique using more than 100 Å wide spectral ranges in order to improve the S/N ratio relative to previous techniques, based on individual lines. This approach turned out to be inapplicable, considering the peculiar abundance structure of roAp star atmospheres which is now well known. Matthews & Scott (1995) then claimed to have detected variability with rather large radial velocity amplitudes but their results were inconsistent with previous findings.

Detailed photometric observations were conducted by Martinez et al. (1996) using a multi-site campaign in 1992, spanning a total of 26 nights. Their results also suggested limited life times of pulsation modes, because additional frequencies appeared in their analysis of individual nights. However, all three frequencies detected so far were confirmed, and prewhitening of 1.366 mHz revealed a fourth eigenfrequency at 1.397 mHz. Using these four frequencies they concluded a spacing of consecutive radial overtones of $\Delta\nu \sim 30 \mu\text{Hz}$ based on the asymptotic theory for low-degree, high-overtone p-mode pulsations (Tassoul 1990). They did not detect any evidence for non-linear behavior of the eigenfrequencies (i.e. harmonics) which, as will be shown in this paper, is indeed present in the MOST data. Except for Gruberbauer et al. (2008), their observing campaign was the most recent photometric investigation of γ Equ. A period of spectroscopic studies focusing on pulsation, abundance and stratification analyses followed.

Kanaan & Hatzes (1998) reported on RV amplitudes for chromium and titanium and speculated that this is due to their concentration close to the magnetic – hence also pulsation – poles, while other elements (e.g. iron) showing no RV variations may be concentrated at the magnetic equator. Malanushenko et al. (1998) independently arrived at a similar conclusion and they are the first who identified the rare earth elements (REE) Pr III and Nd III to show the largest variations (up to 800 ms^{-1}). Most other atomic species had very low or non-measurable RV variations and the authors concluded that previous spectroscopic observations failed to detect significant radial velocity variations due to the chosen spectral regions and/or low spectral resolution. Savanov et al. (1999) further clarified the situation by drawing attention to a possible incorrect identification of spectral lines in Kanaan & Hatzes (1998) and concluded that Pr III and Nd III were responsible for the large RV amplitudes discussed in their analysis.

Further investigations by Kochukhov & Ryabchikova (2001) and Ryabchikova et al. (2002) impressively explained amplitude modulations of different elements and even ions of the same element by lines being formed at different atmospheric depths. The authors also tried a first mode identification based on rather short data sets of line profile variations (LPVs) and they argue for $\ell = 2$ or 3, and $m = -\ell$ or $-\ell + 1$ modes. Shibahashi et al. (2004) disagreed with this analysis and suggested a shock wave causing the observed LPVs which in turn was questioned by Kochukhov et al. (2007) who argued that the pulsational velocity should not exceed the local sound speed. The latter authors propose a modified oblique pulsator model where LPVs are caused by pulsation velocity fields superposed by sinusoidal line width changes due to convection, but which previously was thought to be suppressed. In any case, they agree with Shibahashi et al. that the identification of the primary frequency as an $\ell = 1, m = 0$ mode is still the most likely explanation, which is also supported by Gruberbauer et al. (2008). The issue is still being debated though (Shibahashi et al. 2008).

A still unsolved issue are magnetic field variations synchronized with pulsation. Leone & Kurtz (2003) showed evidence for this, but subsequent investigations (Kochukhov et al. 2004b; Bychkov et al. 2005; Savanov et al. 2006) could not confirm their findings. Hubrig et al. (2004) corroborate this null detection for γ Equ with ESO-FORS1 data. Eventually, as hinted at throughout this section, the results of the analysis of MOST observations of γ Equ, which are presented in this thesis, have been published in Gruberbauer et al. (2008).

1.4 Motivation for this work

As presented in section 1.2.3 and 1.2.4, theorists have struggled since the discovery of roAp stars to explain mechanisms of exciting pulsation in these objects, and to quantify the influence of the magnetic fields on their frequencies. The fact that these stars “suffer” multiple convoluted physical effects (diffusion, magnetic fields, chemical peculiar atmospheres, rotation) that need to be treated rigourously in order to arrive at a complete description of their pulsation, makes it very difficult to test the individual components of the theory. Moreover, roAp stars are heterogeneous group of objects. Their magnetic fields range from a few hundred G to a few kG, they pulsate in either a single frequency or half a dozen modes simultaneously, and their rotation periods range from a few days to tens of years. Therefore, in most of the studies conducted until today, the goal was not to match the observations of a specific roAp star by modelling, but to build a theoretical framework that is able to reproduce their general characteristics.

This sensible approach has delivered very exciting results. However, it is the opinion of the author of this thesis that with almost 30 years of progress in theory and a wealth of observations, the potential for testing very specific theoretic predictions, like the mode frequencies, is already feasible for some stars. γ Equ, in particular, is one of the best choices to make for this type of investigation. It is a well-studied object with relatively small uncertainties in effective temperature, luminosity, and magnetic field strength. Furthermore, it is a rather well-behaved specimen in that all observations indicate a relatively low rotation rate. Finally, γ Equ is multi-periodic, thus putting more constraints on the models with each additional observed mode. In summary, γ Equ should thus enable us to test today’s most sophisticated roAp theories by fitting observed frequencies to model predictions. Models following the theory by Saio (2005) are an ideal testing ground. They neglect rotation but incorporate a full treatment of the magnetic effects on pulsation, including frequency shifts, the need for decomposing a single mode into a series of spherical harmonics, and stability analysis.

First, though, there is a need to resolve the ambiguity that lies within the frequencies found in previous analyses. Despite a history of more than 25 years of observations, the pulsation frequency spectrum of γ Equ was poorly understood prior to the MOST observations: several frequencies have been published, but never were all of them found to be observable simultaneously or confirmed by subsequent studies. A reliable set of frequencies is necessary to give meaning to comparing asteroseismic observations with theoretic models. On the other hand, if this ambiguity were in fact an intrinsic property to γ Equ, meaning that the oscillations are not stable enough to be coherently detected over several months or even days, it would be an equally important finding. This is why an extended observational campaign, like the MOST run, on which this work is based, was necessary for any attempt to test roAp theory.

Chapter 2

The MOST satellite

In this chapter I introduce the MOST satellite and give a description of its properties. First, however, basics of time series analysis are discussed in context of the benefits of space photometry. As a conclusion, I describe a few problems that the MOST satellite encountered unexpectedly, and which have serious impact on the data quality. This knowledge will guide the reader to the next chapter, where the MOST data of γ Equ will be presented.

2.1 The benefits of observing from space

Percentage-wise, most studies of variable stars since pursuing research in this field have been supported by data from ground-based observations. The limiting factor in observational performance from ground that is mentioned most often is the Earth's atmosphere, which limits the optical resolution of the instrument. For research focussed on very dim, extended objects (e.g., galaxies), this is a serious restriction that can only be lifted through modern technologies like adaptive optics. In the case of stellar astronomy the objects of interest are point sources and cannot be resolved. While refractive properties of the atmosphere can be problematic for spectroscopic observations¹, photometric data is usually not seriously affected, as long as measurements of the sky background are taken regularly for calibration. Observing from ground has, however, some ramifications when it comes to time-resolved observations.

The quality of stellar variability observations, especially in the case of (at least partially) coherent and stable variations like pulsation, is basically determined by three factors.

- **The data point density of the time series:** The fewer gaps there are in a time series, the more signals can be recovered due to two reasons. When using tools such as the DFT for frequency analysis of a time series, in the case of equidistant sampling the well-known Nyquist frequency f_N (Nyquist 1928) amounts to

$$f_N = \frac{1}{2\delta t}, \quad (2.1)$$

where δt is the time difference between two adjacent observations (i.e., $\delta t = t_{i+1} - t_i$). It is the limit frequency of a periodic signal that can be fully recovered by such a data set due to the sampling theorem. Although with non-equidistant sampling the relation is not as well-defined as in equation 2.1, it is still proportional to the average sampling rate. Therefore,

¹E.g., the stellar image might wander from the slit of the spectrograph due to atmospheric turbulence, or telluric lines might appear in the observed spectrum.

in order to sample higher-frequency signals, like solar-type oscillations or roAp pulsation, many data points have to be collected in a relatively short amount of time. Also, larger gaps will introduce aliasing, i.e., frequencies that are not actually intrinsic signal but appear in the DFT because multiple frequencies can fit the observations equally well. This effect is usually dealt with by utilising the window function, which is the DFT of a constant time-series that only shows pseudo-periodicities caused by the sampling. In the DFT of the actual time series (the “amplitude spectrum”), this window function is then over-imposed on each individual signal. Fig. 2.1 shows two synthetic time series containing a periodic signal with a frequency of 3.15 d^{-1} , their window functions, and amplitude spectra. The left panels are based on equidistant, continuous sampling, while the right panels are continuously sampled over 8 hours but regularly interrupted by gaps of 16 hours. The window function of the uninterrupted data does not exhibit any other significant component than the one at zero frequency, while for the interrupted data there is significant power at 1, 2, 4, 5, 7, 8, and 10 d^{-1} . Finally, the amplitude spectra show that the gapless time series has only a single significant frequency, while the gaps introduce multiple pseudo-frequencies. In the case of 2 or more intrinsic frequencies, the amplitude spectrum will become even more convoluted, because each frequency produces its own aliases. In asteroseismology, this is a major issue that can only be resolved by observing as continuously as possible. In addition, as will be

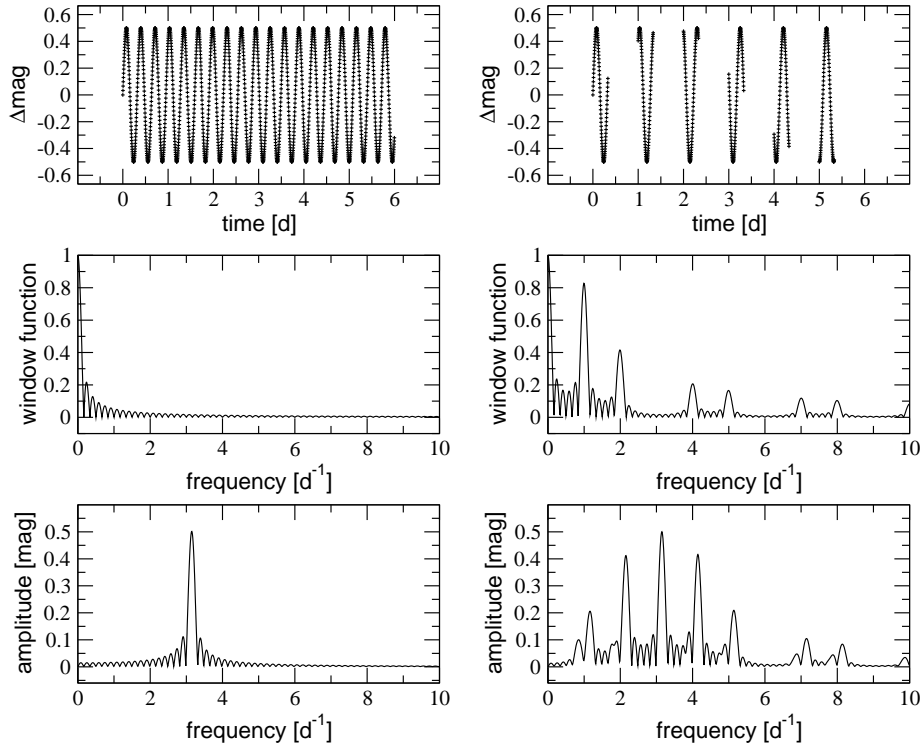


Figure 2.1: Synthetic, noiseless light curves (*left*) without gaps, and (*right*) with gaps mimicking single-site ground-based observations (8 hours of continuous observations between 16-hour gaps), as well as their corresponding window functions and amplitude spectra.

further elaborated in Section 3.2, the so-called spectral significance of a periodic signal in a time series is proportional to the number of data points. This essentially means that the noise level in the frequency domain decreases with increasing amount of observations. A

satellite is, in general, not able to produce data more often than a telescope from ground. However, with a wisely chosen orbit, it is unaffected by the day-night-cycle. This removes the aliasing problem and also increases the data point density, thereby reducing the noise level.

- **The length of the time series:** The DFT interprets a time series as superposition of a single periodic signal f_0 and an (in the optimal case) infinite number of integer multiples (“overtones” or “harmonics”) of this “fundamental frequency”. The latter is defined by

$$f_N = \frac{1}{\Delta T}, \quad (2.2)$$

where ΔT is the length of the data set in units of time (i.e., for a time series with N data points, $\Delta T = t_N - t_0$). f_N will be referred to as the “Rayleigh resolution”. This “Rayleigh resolution” can be used as an estimate for the very upper limit of the frequency uncertainty in an amplitude spectrum, and therefore also hints at a limit for the detection of close frequencies (e.g., Kallinger et al. 2007). Kallinger et al. show that this estimate is too restrictive, however, but that any kind of relation for this quantity is proportional to $1/\Delta T$.

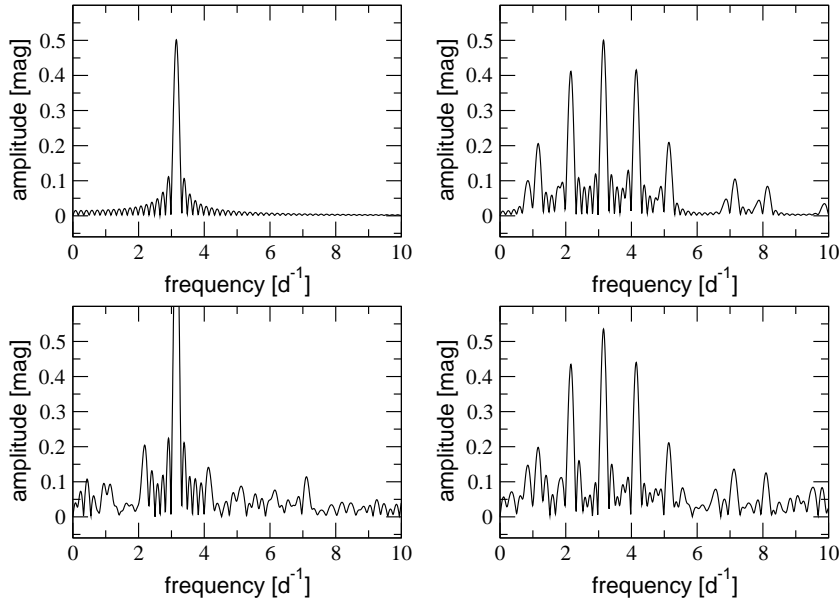


Figure 2.2: Amplitude spectra of the same synthetic light curves as in Fig., 2.1. (*Top*) without noise and (*bottom*) with an added high level of Gaussian noise ($\sigma_{noise} = 0.5$ mag).

- **The noise:** Assuming a strictly harmonic signal without any noise, the DFT will be able to recover this signal unambiguously, unless there are too many gaps in the data or if the frequency of the signal is higher than the Nyquist frequency (see Fig. 2.1). In reality, time series from observations will inherently contain noise (e.g., photon noise, readout noise).

The light curve will scatter around the actual values that would have been obtained by an ideal instrument under ideal/unphysical conditions (no photon noise, etc.). This leads to additional peaks in the amplitude spectrum, thus complicating the frequency analysis. It calls for methods to distinguish which peaks in the amplitude spectrum are caused by noise, and which are caused by intrinsic signal². Self-evidently, the more one reduces the noise in the observations, the more reliable are frequency analysis techniques. Fig. 2.2 shows the impact noise has on the amplitude spectra of the data sets in Fig. 2.1. Clearly, additional peaks arise and, in the case of the gapped time series, their convolution with the window function adds another level of complexity. One should also notice that the amplitude at the position of the intrinsic signal is slightly higher than in the noise-less data. Thus, also the signal parameters derived from noisy data are affected.

All in all, the effects that have been shown suggest that observing with a high-quality instrument as long as possible, with few gaps in between, is the desired situation for asteroseismology. This is especially important for studying objects with low-amplitude variations like the solar-like oscillators and the roAp stars. Obviously, satellites are very promising instruments for these types of investigations, since they give the opportunity to observe relatively independent of the Earth's day-night cycle. Depending on the satellite's orbit and the target's position in the sky, uninterrupted observations of the same object can be obtained for months and even up to years. Also, since the Earth's atmosphere has no influence on data quality in space, measurements taken with a satellite are likely to be more reliable. In addition, radiation at wavelengths that would be blocked by the atmosphere can be analysed. Asteroseismology, thus, would benefit tremendously from a dedicated satellite. The first satellite that made it into space with exactly this purpose was MOST.

²A short discussion of this problem is given in Section 3.2.1

2.2 MOST - design and relevant properties

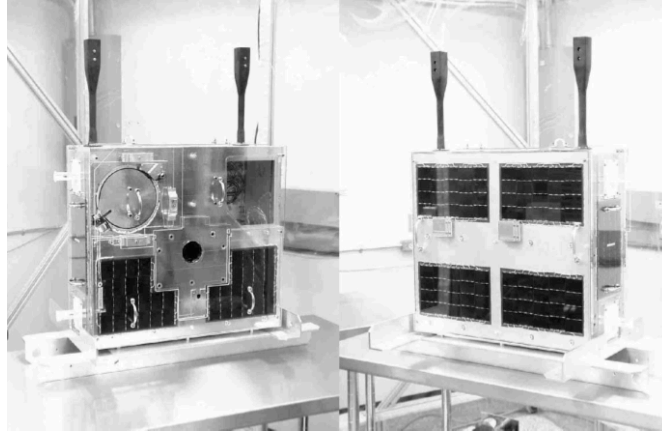


Figure 2.3: The MOST satellite almost ready for launch at UTIAS. Solar panels on the front side and back side of the instrument, magnetotorquers on top, and the entrance aperture with its protective cover closed are visible. (Taken from Walker et al. (2003))

MOST is a Canadian space satellite designed for the detection of stellar variability with amplitudes down to several ppm on time scales up to several days. A complete description of the instrument can be found in Walker et al. (2003), from which the majority of the following information has been taken. MOST was funded by the Canadian Space Agency (CSA), which assigned the development of the scientific instrument to the University of British Columbia (UBC), while the prime contractor for the satellite was Dynacon Inc. Several other institutions (Special Applied Research, CRES Tech) and the University of Toronto Institute for Aerospace Studies (UTIAS) also were involved in the design, testing and integration of the instrument. Additional funding was provided by the Canadian Natural Sciences and Engineering Research Council, as well as the Ontario Centre for Research in Earth and Space Technology.

The satellite's most remarkable property is its modest size. MOST has a mass of only 54 kg and has the dimensions of a larger suitcase (65 x 65 x 30 cm). Fig. 2.3 shows the satellite in the clean room environment prior to launch. With such a low mass MOST would be prone to jitter due to its low inertia, which results in poor pointing stability (about $\pm 2^\circ$). This would render such an instrument incapable of doing high-precision photometry of stars. Including a set of latest technology reaction wheels and magnetotorquers, however, the design of MOST allows pointing stability on the order of a few arcseconds (Reegen et al. 2006).

The satellite houses a 15 cm aperture Maksutov telescope, which is situated perpendicular to the entrance aperture surface normal and receives the light through a periscope mirror (see Fig. 2.4). The telescope has a focal ratio of f/6 and a focal length of 897 mm, and delivers light to two CCDs at the external Cassegrain focus. The CCD layout is displayed in Fig. 2.5. In the initial design, one of the CCDs (the "Guidance CCD") was employed to handle the observations of guide stars, which provide the necessary information for the Attitude Control System (ACS). The other CCD (the "Science CCD") carries a 6 x 6 Fabry microlens array, which covers about one quarter of the total CCD area, and was used to obtain the scientific observations. The microlenses serve the purpose of producing an image of the entrance aperture on the CCD rather than a Gaussian point spread function (PSF), which reduces the effects of jitter due to finite pointing precision. Fig. 2.6

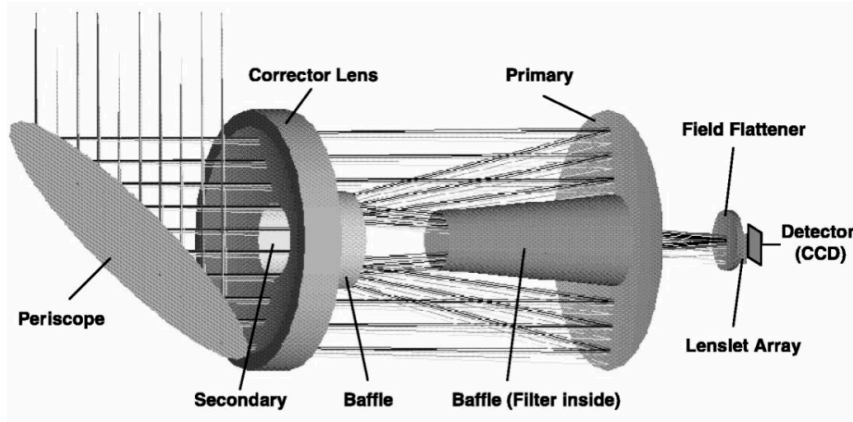


Figure 2.4: The design of MOST's optical system. Light arrives from the entrance aperture and is reflected by the periscope mirror towards the primary. (Taken from Walker et al. (2003))

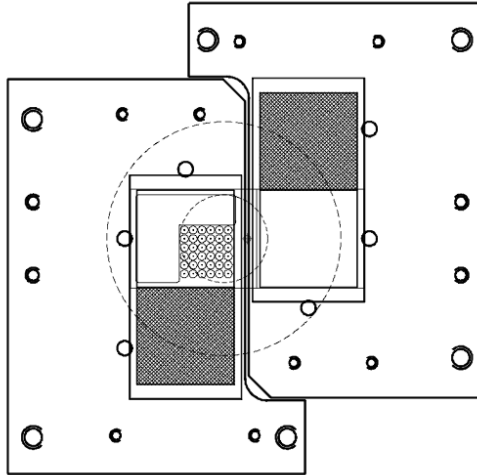


Figure 2.5: The layout of the CCD setup at the Cassegrain focus. Both, the Guidance (right) and the Science CCD (left, with microlens array), are bonded to Invar plates. The vignettted and unvignettted fields of view are shown as dashed circles, corresponding to radii of 0.4 and 1.28°. (Taken from Walker et al. (2003))

shows the resulting image of a point source produced by such a lens. Since these images do not wander across the CCD, fixed apertures for the bright, “doughnut-shaped” part of the image can be defined to separate the stellar contribution from the instrumental background. While the microlenses are employed for the brightest of targets, additional stars can be observed in the same field using the remaining area of the Science CCD. For the latter, traditional aperture photometry must be applied for each exposure (“direct imaging”). Alas, in 2006 the Guidance CCD stopped working, and the onboard software was adjusted to also perform guide star photometry with the Science CCD (Huber & Reegen 2008). As a consequence, multiple exposures have to be stacked, because both, the rate of guide star observations for the ACS and the SNR of the scientific measurements, had to remain as close to the initial design as possible.

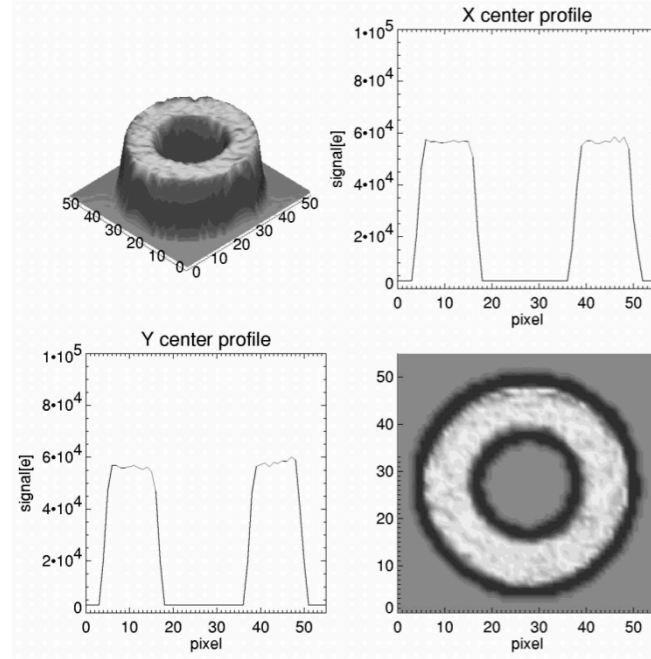


Figure 2.6: The properties of a point source imaged by a Fabry microlens. (Taken from Walker et al. (2003))

Since the MOST mission was envisioned with a focus on detecting low-amplitude variations, in particular solar-type oscillations, the filter system and overall spectral response were designed to maximize the number of photons. It allows sufficient transmission in the range from 380 nm to about 800 nm, closely resembling the visual spectral range. Fig. 2.7 shows a spectrum of a solar-like star together with the filter response, the properties of the high-transmission coating, and the overall the CCD response. In general, the instrument and the optics were planned to allow MOST to reach its maximum micro-magnitude precision when observing very bright primary targets with $V = 0.4 - 6.0$ mag using the microlens array. Simultaneously, secondary targets, which have to be at least 5.5 mag fainter than the respective primary target in order to avoid saturation, can be investigated via direct imaging with a very slight decrease in photometric performance.

MOST was launched into Sun-synchronous, near-polar, low-Earth orbit (LEO) with an inclination of 98.72° , which closely follows the terminator. Therefore, the instrument is able to have its telescope point in the direction opposite to the Earth-Sun vector. This exposes the solar panels on the satellite's back continuously to sunlight, while minimizing influence of the latter on the optical system. It also allows to observe the same field of view, which is only constrained in declination ($-19^\circ < \delta < +36^\circ$), for up to ~ 2 months or $\sim 60^\circ$ in right ascension. This is called the Continuous Viewing Zone (CVZ). MOST completes its trajectory around the Earth at an altitude of about 800 km roughly once every 101.5 minutes or at a frequency of 14.19 d^{-1} . A visualisation of the orbit taken from Walker et al. (2003) can be found in Fig. 2.8.

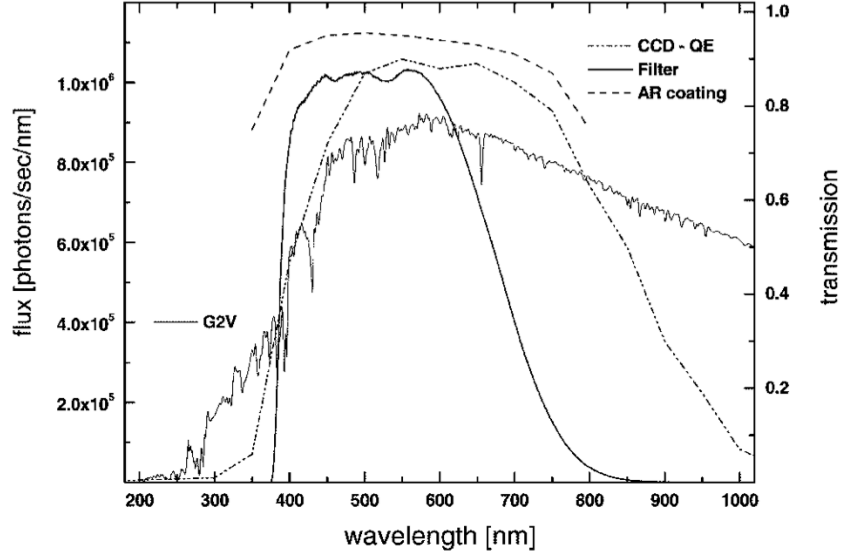


Figure 2.7: The transmission of the different optical elements as a function of wavelength in comparison to the spectrum of a G2V star. *dash-dotted line* : the CCD response; *dash line* : transmission of the coating; *solid line* : spectrum of a G2V star; *thick solid line* : filter transmission. (Taken from Walker et al. (2003))

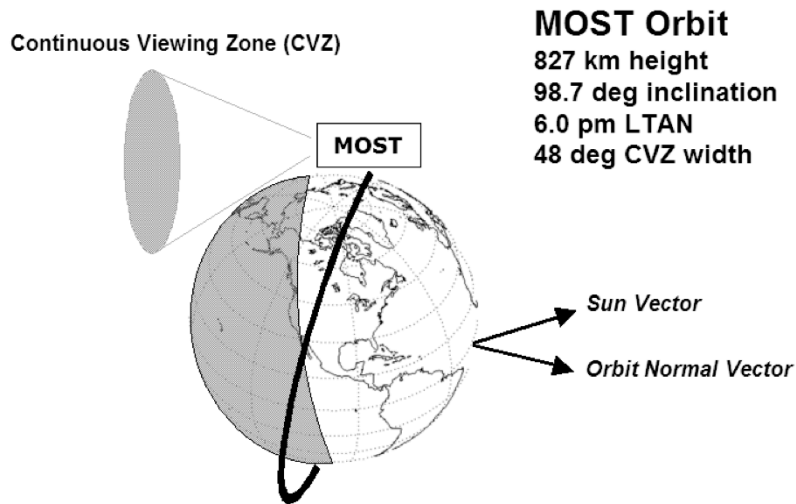


Figure 2.8: An illustration of the MOST orbit, annotated with its basic parameters. The orientation of the CVZ relative to the Earth-Sun vector is also shown. (Taken from Walker et al. (2003))

2.2.1 The stray light problem

Very soon after the initial data of the commissioning targets were received in 2003, a serious problem with the quality of the measurements was identified. Even though the instrument design included a baffling system, the data showed tremendous amounts of parasitic signal varying periodically with MOST's orbital period. It soon was realised that light reflected off the Earth is leaking into the instrument and finding its way to the detector. Since the Fourier transform is most often used to analyse stellar pulsation, the stray light additionally poses a problem because of its non-harmonic shape as depicted in Fig. 2.9. In order to decompose the stray light variations into a linear combination of harmonic components, the orbital frequency of 14.19 d^{-1} and many integer multiples are needed. Furthermore, the shape of the stray light variation varies throughout the observations, and even from one pass to another. This necessitates in additional frequencies clustered around the integer multiples of the orbital frequencies but differing by an integer number of cycles per day (e.g., $13.19, 12.19, 15.19 \text{ d}^{-1}$ or $27.38, 26.38, 29.38 \text{ d}^{-1}$).

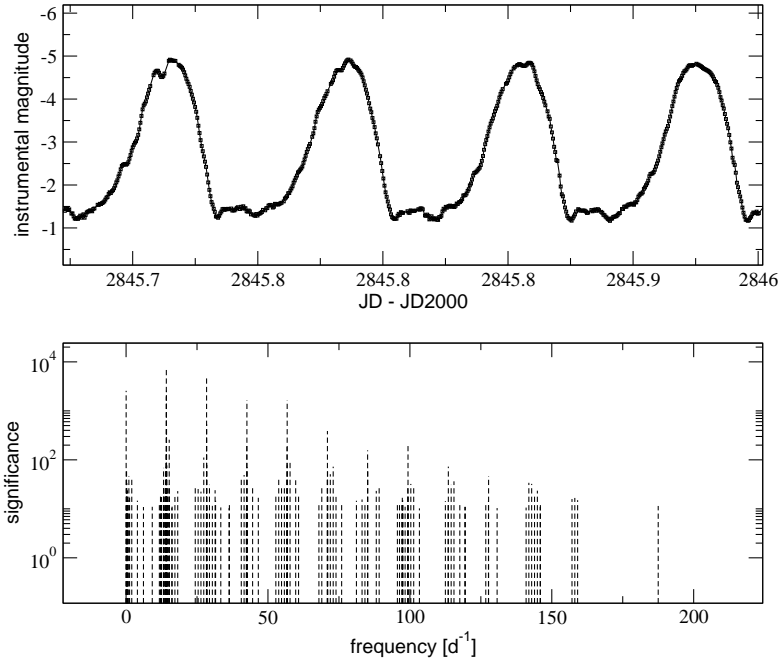


Figure 2.9: *Top panel:* a small subset of the background light curve of the MOST observations of HD 9289, another roAp star. The apparent large variation is due to stray light from the illuminated Earth entering the instrument. The target light curve is comparably affected. *Bottom panel:* the corresponding SIGSPEC-result, which clearly shows the large number of harmonic components needed to decompose this signal with the Fourier transform.

As MOST was designed to detect stellar variability down to a few ppm, this parasitic signal poses a huge problem, since it dominates the Fourier transform with its large amplitudes. Much time was thus spent on developing data reduction algorithms which remove the stray light but leave the stellar signal relatively unaltered. Simple aperture photometry, especially in the case of targets observed using the Fabry microlenses, was found to be insufficient, because of changes in the spatial and temporal correlation between the target and background pixels. Eventually, a method which decorrelates the stellar and the background signal was devised and delivered the desired results (Reegen et al. 2006). Although some artefacts still remain in the Fourier transform, the decorrelation lowers the magnitude of this signal to a level, where it does not interfere with the

detection of micro-magnitude variations in many cases. The quality of the MOST data and the success of the decorrelation, however, are still very much dependent on the properties of the stray light signal, which varies significantly in shape and magnitude from run to run, as well as on the relative brightness of the observed targets.

2.2.2 The CCD crosstalk problem

In the initial phases of the MOST-mission, another problem was identified to originate from a slight asynchronicity between the clocks used to define the time stamp of each exposure. Although this issue was soon removed by adjusting these clocks, it resulted in artifactual periodicities in the data of the first few target runs. These artefacts can be found around multiples of $\sim 3.2 \text{ d}^{-1}$, but are usually not present beyond 14 d^{-1} . It is only in the data of $\gamma \text{ Equ}$ that there is evidence for these artifactual signals at higher frequencies (see Sec. 3.2.2). As an example, Fig. 2.10 presents the case of $\tau \text{ Boo}$, where the crosstalk signal is very strong. The problem has also been addressed in Reegen et al. (2006).

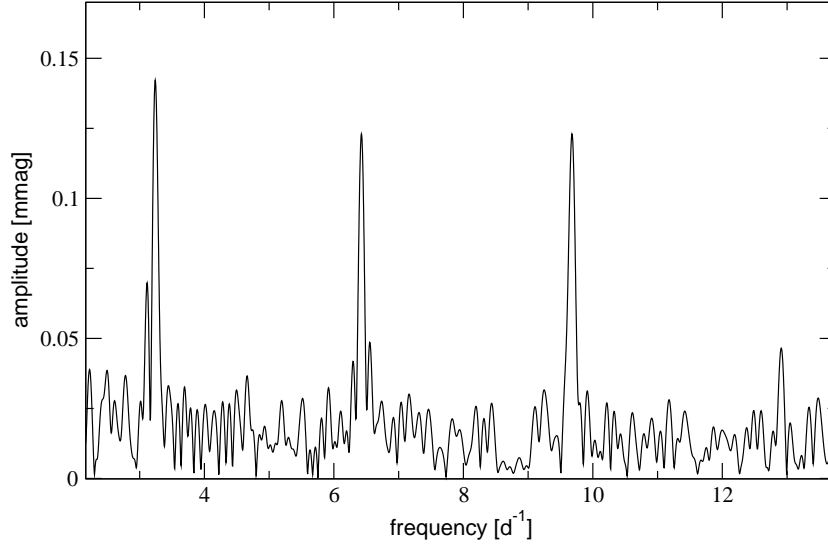


Figure 2.10: Amplitude spectrum of the MOST data on $\tau \text{ Boo}$ from one of the first runs in 2004. The obvious signal at 3.2, 6.4, 9.6, and 12.9 d^{-1} is an artefact produced by the CCD-cross talk problem.

Part II: Data reduction and analysis

Chapter 3

The MOST data of γ Equ

In this chapter the properties of the MOST observations of γ Equ will be discussed. I give a step-by-step guide on how the data were reduced, as well as on how the pulsation frequencies were obtained. I then proceed to investigate the time-dependent properties of these frequencies. A discussion of the new knowledge about γ Equ, gained from the MOST observations alone thus far, concludes the chapter.

3.1 The γ Equ data set in the time domain

MOST observed γ Equ from 07/28/2004 to 08/16/2004 with exposures (integration time = 11 sec) taken continuously once every 30 sec. In total, 49213 frames were gathered over a time base of 19 days. As already mentioned, every MOST data set suffers from a slightly different stray light contamination, and different regions of the CCD might be exposed to this signal with varying intensity (see Reegen et al. 2006). Moreover, other effects like long-term trends due to changes in the satellite components' temperature are also individual artifacts for every observing run. Consequently, the raw data must be carefully examined for every target, and the reduction parameters must be individually set in order to obtain the best reduced light curve. Since invasive reduction techniques are required to remove the instrumental signal and the stray light, it is important to compare results of multiple reduced versions of the same raw data. This might not be necessary in the case of obvious signal with amplitudes of several thousands to tenths of a magnitude, but for newly detected signals closer to the noise level the benefits of such a procedure are obvious.

The primary frequencies of γ Equ that had already been observed from ground were expected to show significant amplitudes well above the noise level. Even though the broad MOST passband is not advantageous for this kind of pulsation, the intention was to also check for additional frequencies which had not been detected before with less sensitive instruments. Hence, two different reduction techniques were employed.

3.1.1 Data reduction using decorrelation

As mentioned before, the decorrelation technique developed by the Vienna team (Reegen et al. 2006) is the obvious first choice, since it strongly diminishes the stray light amplitudes. What follows is a brief explanation of the procedure. The stray light effects are corrected by computing a correlation between target and background pixels. The doughnut shape of the Fabry image provides a natural aperture, with *target pixels* inside the aperture (the bright torus) and *background*

pixels outside the aperture (the dark regions of the inner circle and the regions outside the doughnut). The latter are assumed to contain no stellar signal. In addition, “neutral” pixels around the edges of the aperture are flagged and not used for further analysis, as they might contain stellar and background signal. Once the correlation between target and background has been calculated, the background time series, multiplied by the correlation coefficient, is subtracted from the target light curve. The average of the target light curve is then added to the residual time series. This procedure is usually performed in subsets with a time base of a few orbital periods, since the shape and magnitude of the stray light changes with time.

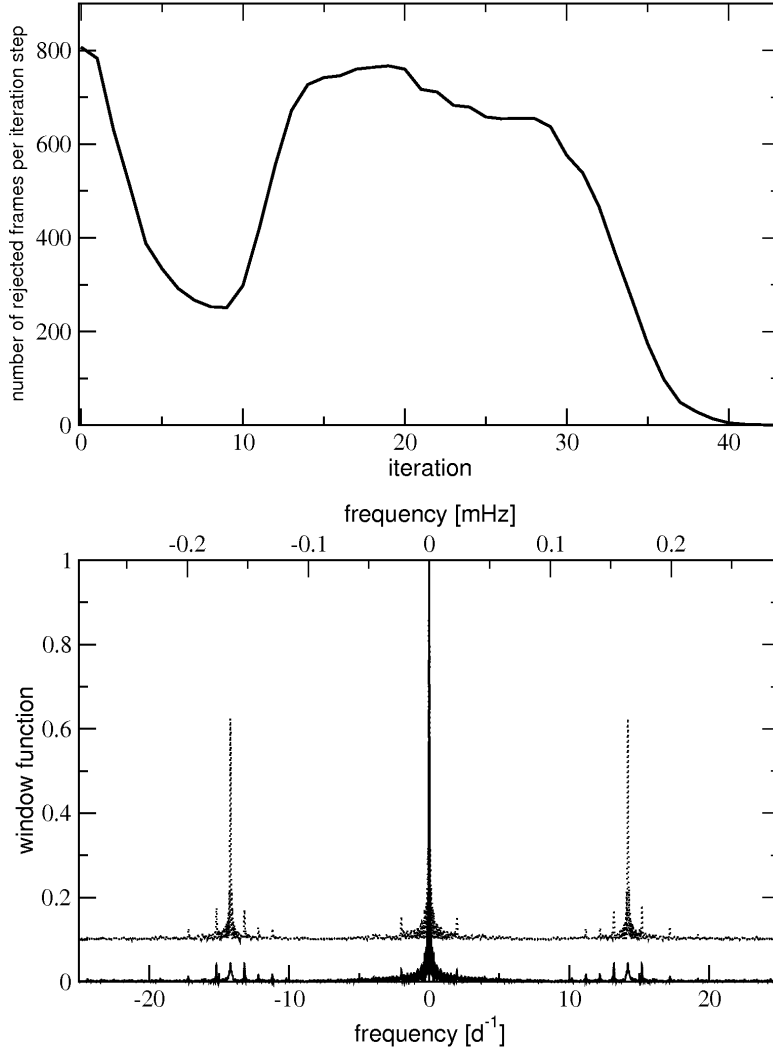


Figure 3.1: *Upper panel:* Iterative elimination of frames with deviating image geometry. The increasing number of rejections with higher iterations followed by a second decline indicates two separate mechanisms responsible for distorting the Fabry image geometry.

Lower panel : Window function of the data sets including (solid line) and excluding (dotted line) frames with deviating image geometry. The dotted graph has been shifted by 0.1 for better visibility. This figure can also be found in Gruberbauer et al. (2008).

Preparatory steps prior to the actual decorrelation involves the determination of the quality for each individual frame and the correction of outliers in an otherwise acceptable exposure. Frames of low quality are not considered in the analysis. This reduces the sampling density of the light curve, but also results in a decreased scatter in the time domain. The reduced scatter, of course, is beneficial for any least squares fits to the data. Also, while aliasing arises as a consequence in the Fourier transform of the time series, the noise level is simultaneously lowered in the frequency domain. The number of rejected frames is usually not high enough to cause serious aliasing as it is common in ground-based observations, because the MOST sampling rate is much higher and the time base of the observations is much longer. Whether or not to reject a frame is determined by comparison to a mean normalised Fabry image - the reference image. If the pixel values in an individual (normalised) frame are deviating from the reference image by more than $g\sigma$, where g is an integer that has to be set by the user and σ is the standard deviation of the mean normalised frame, the frame is rejected. After testing all frames, a new reference image is constructed from the remaining frames, and the test is repeated. This process is stopped when no more frames are being rejected. The cosmic ray correction is a similar procedure, where pixel values of subsequent frames are compared. If one of the frames contains a value that cannot be reconciled with the former and latter frames, it is replaced the running average of the comparison frames' pixel values. An in-depth and complete description of the reduction algorithm can be found in our paper (Reegen et al. 2006).

Due to bad data quality at the beginning of the γ Equ-run about 1060 frames had to be rejected. Additional frames needed to be eliminated due to pointing problems in the early days of MOST operations which resulted in distorted Fabry image geometries. Performing this elimination, it turned out that the number of images in which pixels are deviating by more than 5σ first decreased as expected, but increased after about ten iterations and later decreased again. This indicates that two different effects are responsible for the deviating Fabry image geometry and presented in the upper panel of Fig. 3.1. Fig. 3.2 presents the raw data light curve after correcting for cosmic rays, phased with the orbital period. It shows which orbital phases are responsible for the image geometry deviations. The majority of the frame rejections, unsurprisingly, concern exposures taken during high stray light phases and therefore cause regular gaps in the final data set (see Fig. 3.3).

To ensure that this reduced duty cycle does not impair the identification of intrinsic frequencies, the analysis was repeated with the data set obtained after the first iteration step in the image geometry evaluation, which eliminated only 807 frames. In the lower panel of Fig. 3.1 the spectral windows of both reductions are compared. It shows that the rejections mainly affected orbit-induced artifacts ($f_{\text{orbit}} = 14.19 \text{ d}^{-1}$). The final analysis did not yield a different set of intrinsic, but considerably fewer instrumental frequencies. The summary statistics of the reduction process are shown in Table 3.1.

Table 3.1: Reduction statistics for the decorrelation technique performed on the data set of γ Equ. A total of 49213 frames were obtained by the satellite. ACS: MOST Attitude Control System. This table can also be found in Gruberbauer et al. (2008).

Reduction step	# rejected	% rejected
saturated pixels	1	0.002
saturated ACS errors	1637	3.33
deviating image geometry	21679	44.35
excessive number of cosemics	1002	3.87

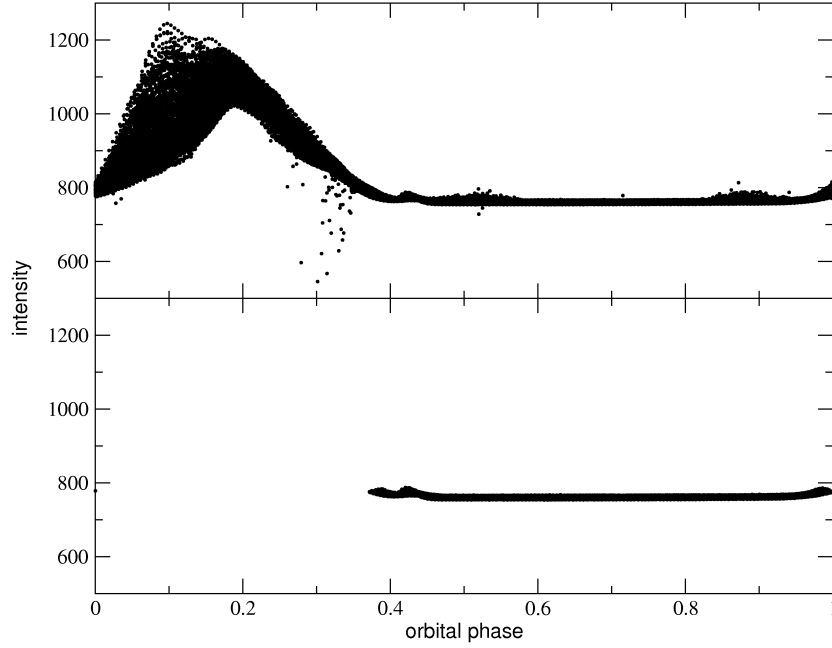


Figure 3.2: *Upper panel:* The raw light curve after cosmic ray correction, phased with the Most orbital period. The stray light contamination is mostly confined to orbital phases 0 - 0.4. *Lower panel:* Same as in the upper panel, but after correcting for deviating image geometry. This figure can also be found in Gruberbauer et al. (2008).

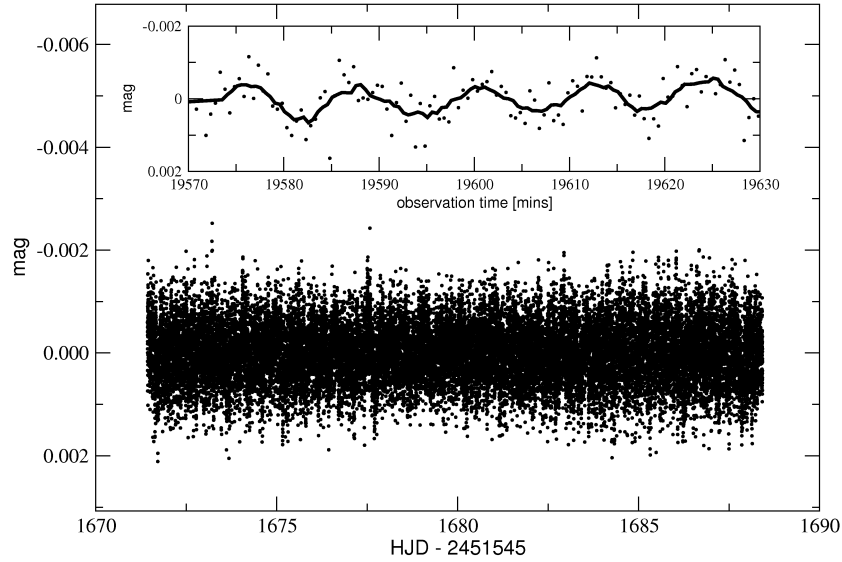


Figure 3.3: Final light curve using decorrelation resulting in a duty cycle of $\sim 53\%$. All long-term variations with periods > 1 d have been prewhitened. The inset shows a subset spanning about 50 min together with a 10 point (~ 4 min) running average. The ~ 12 min oscillation is clearly visible. This figure can also be found in Gruberbauer et al. (2008).

3.1.2 Data reduction using “doughnut” fitting

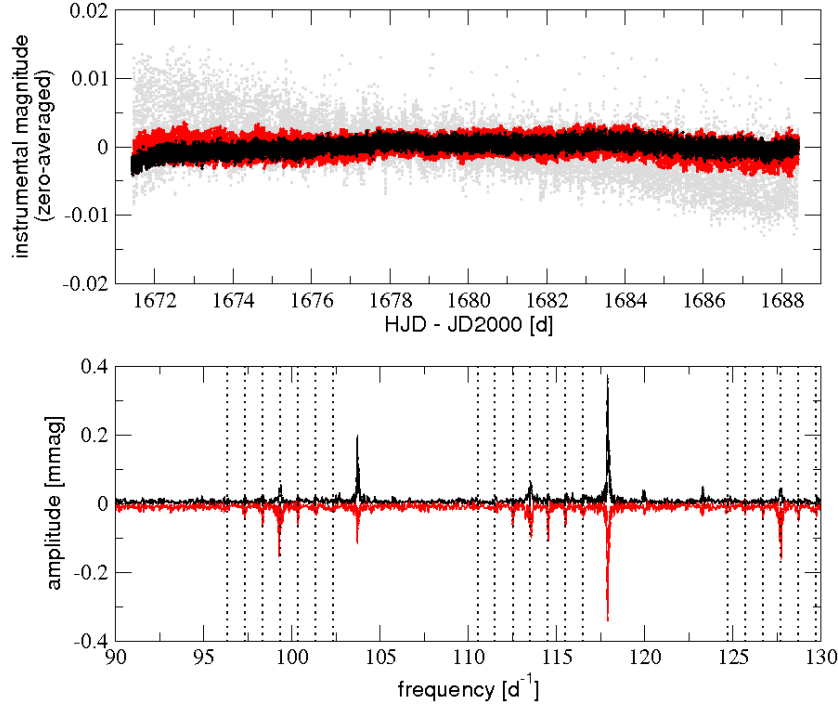


Figure 3.4: *Top panel:* comparison of the reduced light curves resulting from the decorrelation (black - 26409 data points) and the doughnut fitting (red - 40792 data points; after outlier removal) procedures. The grey dots show the doughnut fitting results before performing 3 σ -outlier removal. *Bottom panel:* the DFT of the decorrelated (black) and doughnut fitted (red) time series. The dotted lines indicate frequencies where one could expect peaks produced by the stray light variability.

In order to verify the consistency of the frequency analysis following the data reduction in the time domain, a less invasive reduction method is given by the “doughnut” fitting procedure. First, an average Fabry image is determined from the frames of highest quality, e.g., those at phases with very low stray light and the fewest number of cosmics. The mean intensity, derived from the background pixels which are defined just as described in Sec. 3.1.1, is subtracted from all pixels. The resulting image is then scaled to the mean intensity of the N pixels with the highest intensity values, where N is of the order of 100. The result serves as sort of normalized point spread function (PSF) for a Fabry image. Subsequently, a linear regression between pixel intensities of each image and the corresponding pixel intensities of the mean PSF frame is performed. For each of these images the slope k of the linear fit gives a scaling factor, while the offset d corresponds to the image mean background intensity. Each frame is replaced by the PSF frame multiplied with the corresponding scaling factor k , and the mean background intensity d is added. The average intensities of all target and background pixels result in the target and background light curve, respectively. Finally, a linear fit between the background and target light curve is determined and subtracted from the target light curve resulting in the final light curve. In the case of γ Equ, the latter consists of 48955 datapoints.

The advantage of this method is the insensitivity of the linear regression to extreme pixel values, for instance due to cosmic ray hits or local stray light effects. In addition, there is no danger

of significantly decreasing the signal, which is a possibility in the decorrelation technique when a large number of decorrelation iterations are performed. Also, contrary to the method described in Sec. 3.1.1, the data set is not split into subsets and processed individually, which could distort the low frequency signal. The entire data set is reduced en-block, no subsets are created which qualifies this procedure as a perfect cross-check for detecting artifacts due to data reduction. The disadvantage of this method, however, is the stray light correction which is less efficient as for the decorrelation method. Nonetheless, the stray light effects are sufficiently removed in order to use the results of the “doughnut” fitting procedure in parallel to the decorrelation method for confirmation of signals with very low amplitudes.

The results of both techniques are compared in Fig. 3.4. The scatter of the light curve resulting from doughnut fitting is clearly larger than the decorrelated light curve. Hence, also the noise level in the frequency domain is higher. Nonetheless, both methods clearly enable to find γ Equ’s most prominent pulsation at $\sim 118 \text{ d}^{-1}$. A few small peaks between 110 and 130 can also be identified in both methods. The extraction and evaluation of these frequencies will be dealt with in the following section.

3.2 Frequency analysis

3.2.1 SIGSPEC

The time series resulting from both reductions outlined in the previous sections were analyzed individually using SIGSPEC. A description of the concepts behind SIGSPEC can be found in Reegen (2007). Roughly summarized, SIGSPEC is a program which extracts significant frequencies from a given time series by evaluating the false-alarm probability for an amplitude at a given frequency and phase. It calculates the so-called spectral significance for each frequency bin, where the i -th frequency bin f_i for a given time series is

$$f_i = f_{\min} + i \times \frac{f_{\max} - f_{\min}}{\Delta T} \frac{1}{k}, \quad (3.1)$$

where f_{\min} and f_{\max} are the lower and upper frequency limits for the resulting significance spectrum, ΔT is the length of the time series ($T_{\max} - T_{\min}$), and k is the oversampling ratio set by the user. The corresponding spectral significance is defined as

$$\text{sig}(A|\omega_i, \tau) = -\log \Phi_{\text{FA}}(A|\omega_i, \tau), \quad (3.2)$$

where $\Phi_{\text{FA}}(A|\omega_i, \tau)$ is the false-alarm probability, i.e., the probability that a signal with an amplitude A at frequency $\omega_i = 2\pi f_i$ and phase τ is caused by white noise. The significance is proportional to the number of data points, as well as inversely proportional to the variance of the noise in the data set. The latter can, for instance, be estimated from the variance of the time series. For further details concerning the derivation and the properties of $\Phi_{\text{FA}}(A|\omega, \tau)$ the reader is referred to Reegen (2007). Once SIGSPEC has calculated the spectral significances for all frequency bins, a sinusoidal signal with the frequency corresponding to the bin with the highest significance is fitted to the data. This is accomplished using a least-squares algorithm to further improve the accuracy of the frequency, amplitude, and phase parameter of the sine. Subsequently, the fitted signal is subtracted from the time series and the process is repeated for the residuals to the fit. Iteration after iteration, the most significant frequencies in the data are extracted, until a lower significance threshold is reached. As an established convention, the lower limit of $\text{sig} = 5.46$, which roughly corresponds to an amplitude SNR of 4, is commonly used when working with SIGSPEC. This limit therefore was applied in the analysis of the MOST data of γ Equ.

3.2.2 Finding intrinsic frequencies

SIGSPEC was set to analyze the final light curves resulting from the decorrelation and doughnut fitting technique for significant frequencies between 0 and 360 d^{-1} . The upper limit was chosen to also include 2 harmonics, i.e., integer multiples, of γ Equ’s most prominent signal at $\sim 118 \text{ d}^{-1}$, in order to study the possibility of a non-harmonic shape of the pulsation. The oversampling was set to the standard value of 20. The results delivered by SIGSPEC then were automatically searched for orbital artefacts and other possibly instrumental frequencies (see Sec. 2.2.1) by using CINDERELLA (Reegen et al. 2008). CINDERELLA compares frequencies derived from the target time series to signal found in a comparison time series in terms of their significance. In the case of MOST data this translates to the target light curve and the background light curve. However, one assumption is that these signals common in both data sets are additive in intensity. This applies to the stray light signal but not to long-term trends or features produced by the CCD crosstalk effect. Nonetheless, any frequencies identified by CINDERELLA as artefacts were removed from the list of candidate frequencies.

As a next step, all remaining frequencies in the results of the decorrelated and the doughnut-fitted light curves were compared, and only frequencies found in both data sets were used for further analysis. As a criterion for a match the Kallinger resolution (Kallinger et al. 2007), which explicitly contains the spectral significance, hence implicitly the SNR of each frequency, was employed. In total, 32 matching significant frequencies not due to stray light variation could be identified in the decorrelated and the doughnut-fitted time series. These are presented in Fig. 3.5.

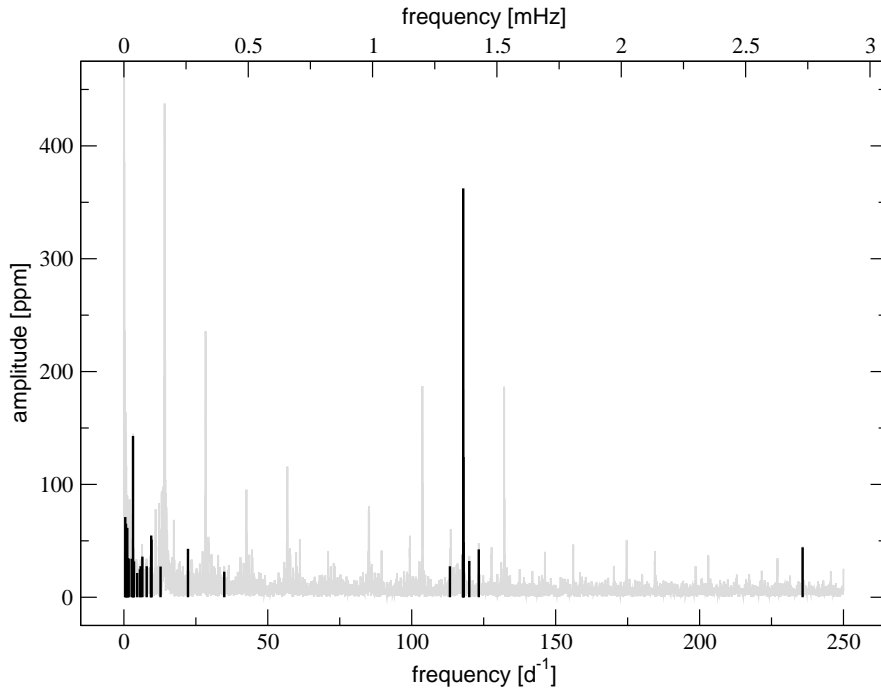


Figure 3.5: The amplitude spectrum of the final light curve (gray) presented in Fig. 3.3 and all frequencies found by SIGSPEC in both reduction methods. Only frequencies with $f > 50 \text{ d}^{-1}$ should be considered unaffected by the instrument. γ Equ’s pulsation is obvious in the range of 100 to 125 d^{-1} and the first of two harmonics of f_1 is evident at $\sim 235 \text{ d}^{-1}$. This figure can also be found in Gruberbauer et al. (2008).

Of those 32 frequencies, 22 are below 13 d^{-1} . The CCD crosstalk problem discussed in Sec. 2.2.2, by which the γ Equ data set was also affected, justifies the rejection of many of these frequencies. The identification of the remaining low-frequency signal mostly remains unclear. Some of the remaining power excess in the low frequency region might be of stellar origin, but the current data is inconclusive. Variability due to stellar rotation cannot be expected, since all studies concerning the rotation period for γ Equ point at a value of several years, as mentioned in Sec. 1.3. Other variability caused by pulsation, which would indicate the presence of gravity modes, is equally unlikely, since these oscillations have never been observed to be excited in roAp stars (or γ Equ in particular). Considering the instrumental instability in the early MOST runs, especially in the low-frequency domain, it would require to confirm this power excess by an additional MOST run on γ Equ in order to draw any conclusion about their origin. An additional problem are a few frequencies between 10 and 35 d^{-1} which seem to be multiples of 3.16 d^{-1} . While these signals appear to be related to the CCD crosstalk problem, no other MOST data set shows these instrumental artefacts at such high frequencies. Due to the conservative approach employed, however, these were not included in the final list of intrinsic frequencies.

The remaining significant frequencies all have frequencies $f > 100 \text{ d}^{-1}$. A cluster of peaks around $\sim 118 \text{ d}^{-1}$ marks the region of pulsational variability of γ Equ. In addition, the first harmonic to γ Equ's most apparent mode could be identified in both data sets. Also, even the corresponding second harmonic can be found to be significant in the decorrelated light curve. The noise level in the doughnut-fitted light curve, however, seems to be too high to allow for its detection. Still, this frequency is included in the final list of intrinsic signals, because of its obvious relation to γ Equ's pulsation.

The results in terms of numbers of identified frequencies for both reduction techniques are summarised in Tab. 3.2. Furthermore, Tab. 3.3 contains the final set of intrinsic frequencies due to pulsation. Two additional significant frequencies not included in Tab. 3.3 can be found very close to f_1 . They have amplitudes of $\sim 40 \text{ ppm}$, but including them in a Period04 multi-sine fit (Lenz & Breger 2005) fails, because the solution does not converge. The nature of these is not yet understood.

Table 3.2: Statistics on the number of significant frequencies ($\text{sig} > 5.46$) identified by SIGSPEC for the decorrelated/doughnut-fitted light curves. The lower number of significant frequencies in the decorrelated light curve is due to the more efficient stray light removal. The decorrelated time series shows an additional, clearly stellar, frequency which can be identified as the 2nd harmonic to γ Equ's most prominent mode.

	decorrelation	doughnut fitting
significant frequencies	95	231
matching frequencies (no stray light)	33	33
stellar frequencies due to pulsation	9	8

Evidently, no obvious spacing, as predicted by the asymptotic theory of non-radial pulsation, can be found in the final set of frequencies. This suggests that either the regular spacing of modes with the same degree ℓ is disturbed, e.g. by the magnetic field, or that modes of different degree are excited in γ Equ and were observed by MOST. It also means that there is no evidence for any of the frequencies to be part of a multiplet according to the oblique pulsator model. Therefore, from the presented observations it is not possible to derive any rotation period. Most importantly, though,

Table 3.3: The list of frequencies considered to be intrinsic to γ Equ. σ_f : 1σ -uncertainty in frequency, derived according to Kallinger et al. (2007); σ_a : uncertainty in amplitude; sig: spectral significance according to Reegen (2007); θ : phase in radians corresponding to $\cos(2\pi f_i t - \theta)$. This table can also be found in Gruberbauer et al. (2008).

	f mHz	$\sigma_f \cdot 10^6$ mHz	a ppm	σ_a ppm	sig	θ
f_1	1.364594	6	362	2.9	963	2.7704
f_2	1.365411	13	124	2.4	175	2.6594
f_3	1.427102	34	43	2.1	25	1.8325
f_4	1.388872	44	32	2.1	15	1.3636
f_5	1.310914	51	27	2.1	11	2.7173
$f_6 = 2f_1$	2.729148	32	44	2.1	27	2.0870
$f_7 = 3f_1$	4.094687	70	18	3.7	6	3.1012

it is not possible to derive the spherical degree of the individual modes without resorting to model frequencies derived from theoretical considerations. An attempt at comparing the observations to theoretical models will be described in the next chapter. First, though, a detailed discussion of the properties of the identified frequencies is necessary.

3.3 The frequencies and amplitudes of γ Equ

3.3.1 Comparison to previous studies

After having arrived at a conservative list of intrinsic frequencies that are due to pulsation, it is possible to evaluate previous time-resolved observations of γ Equ. These are characterized by the fact that no study had been able to clearly reproduce the frequency values that other campaigns had yielded. The biggest accomplishment in terms of giving a general picture and reconciling multiple asteroseismic investigations of γ Equ, was made by Martinez et al. (1996). Their study, which has already been mentioned in Sec. 1.3, was able to group all hitherto identified frequencies, as well as their findings from a profound photometric campaign, into 4 compartments. Nonetheless, their grouping was still ambiguous and a clear picture did not arise, except for hinting at multiple simultaneously excited modes.

The data obtained by MOST allow to unambiguously identify 7 frequencies (Tab. 3.3) above 1.3 mHz, including the first two harmonics of the primary frequency, which significantly exceed the mean noise level of ~ 10 ppm between 1.15 and 1.75 mHz. The comparison with Martinez et al. gives a match for f_1 , f_3 , and f_4 . f_2 , however, has never been detected before, probably because f_1 and f_2 could not be resolved as individual frequencies. This is also important for the discussion on amplitude modulation of the primary frequency, for which I refer to the next section. The value for f_5 is comparable to Martinez et al.'s $\nu_1 = 1.321$ mHz (taken from Weiss 1983), but differs by ~ 0.01 mHz. It can be assumed that they have misidentified a 1-day alias of the real frequency but this is difficult to assess, since no frequency uncertainties are known for this data set. Given that the data set from Weiss (1983) spans only three nights, the poor frequency resolution $1/T_{\text{obs}} \simeq 0.33 \text{ d}^{-1} = 0.004 \text{ mHz}$ supports the assumption of a misidentification.

The presence of additional frequencies even above the noise level of the MOST data set should not be ruled out. Due to the influence of the stray light, frequencies which are related to the satellite's orbital period have to be excluded from the analysis. Since the MOST data of γ Equ where

obtained relatively early on in the mission, revisiting the star with this instrument, which has since shown a tremendous increase of data quality, might help to provide further evidence for such signals. It would also help to re-evaluate the significant low-frequency power that was found but cannot be explained. Moreover, the pair of significant frequencies that was not included in Tab. 3.3, remain a puzzling fact. These could originate from a Fourier representation of intrinsic amplitude modulation, the likes of which have already been proposed in earlier works on γ Equ. When discussing previously published amplitudes, however, one has to keep in mind that the properties of MOST prevent a direct comparison. It has been well known since the eighties that amplitudes (Weiss & Schneider 1984) and phases (Weiss 1986) depend on wavelength, and the former are rapidly decreasing towards the red. The passband of MOST is broad compared to the Strömgren system, frequently used for roAp star photometry, hence the observed MOST amplitudes are intrinsically smaller.

Nonetheless, the frequencies listed in Tab. 3.3, derived from the MOST data set, can for the first time confirm and expand the previous set of frequencies unambiguously.

3.3.2 Amplitude modulation

Amplitude modulation of γ Equ's most prominent frequency has often been mentioned in the literature, and rotation or closely spaced frequencies have been proposed as possible explanations. Because of the relatively small effect and the limited accuracy of the data across all studies, a specific modulation period could never be accurately determined. This situation, however, changed with MOST. To distinguish between amplitude modulation of a single frequency and beating of two closely spaced frequencies one needs to discuss simultaneous phase *and* amplitude changes (Breger & Pamyatnykh 2006). If amplitude variation of a mode is due to some physical property of the mode, rather than caused by the beating with additional modes, the phase is expected to remain stable even when the amplitude changes. The cause for such changes, however, is not clearly established. One explanation for the amplitude modulation is damping and re-excitation of the oscillations, like in the solar-type pulsators. In this case, while the phase during damping is basically constant, the difference in phase prior to and after re-excitation is in principle random. Such stochastically excited pulsation, however, is not expected in roAp stars, because of the lack of profound convection in the envelopes of these objects. Periodic amplitude variation under constant phase of the amplitudes that is not due to some geometric effect or damping and re-excitation, on the other hand, is difficult to explain from a physical standpoint. The apparent change of amplitude due to beating with an unresolved frequency, however, goes hand in hand with a continuous, cyclical change in phase. Therefore, the time-resolved behaviour of the amplitude of γ Equ's most prominent frequency gives great insight into the actual properties of this stars' pulsation.

Figure 3.6 illustrates the results of a time-resolved analysis of the amplitude and phase for f_1 . All stellar frequencies except f_1 and f_2 have been prewhitened from the decorrelated light curve. Subsequently, a sinusoidal signal at fixed frequency f_1 , but with variable phase and amplitude, was fitted to subsets of the residual light curve with lengths of 0.5 days, using a least-squares approach. Obviously, the phase changes which already indicates beating with an additional frequency. The correlation of amplitude and phase variations is apparent, and a relative phase shift of $\frac{\pi}{2}$ between phase and amplitude variations is found. This is also indicative for beating of a close pair of frequencies. Judging from the estimated period of the apparently harmonic variation, these close frequencies should be spaced by $f_{\text{beat}} \sim 0.07 \text{ d}^{-1}$ ($\sim 0.0008 \text{ mHz}$).

Immediately, one finds $f_1 + f_{\text{beat}} \simeq f_2$. No convincing evidence is found for the modulation of the other frequencies in the frequency domain. This is inferred from the significance spectrum

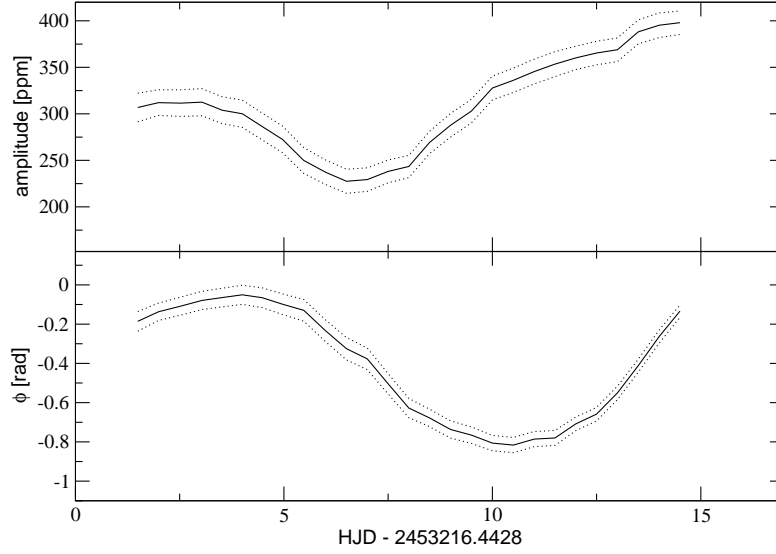


Figure 3.6: *Upper panel:* Amplitude modulation of the primary frequency, f_1 , as found by a least-squares fit with a fixed frequency to subsets of the light curve. *Lower panel:* Phase changes of f_1 determined in the same way as the amplitude modulation. The dotted lines represent the 1σ -confidence limits. This figure can also be found in Gruberbauer et al. (2008).

of the time series, since variable amplitudes would introduce additional significant peaks. Moreover, the scatter in the time domain is simply too high to make a meaningful assessment of the time-resolved properties of the low-amplitude modes. As already mentioned, two other significant frequencies with amplitudes ~ 40 ppm close to f_1 are found, which are not instrumental. These frequencies appear to be Fourier artifacts produced by irregularities in the beating of f_1 and f_2 . Section 3.2 it has already been reported that a multi-sine fit fails to converge if they are included in the solution. Their origin might very well be the presence of additional frequencies, but could also hint at intrinsic amplitude modulation of the f_1 or f_2 . In any case, Fig. 3.6 shows that the amplitude modulation of f_1 is not as smooth as if the were caused only by beating with f_2 .

Nonetheless, these effects are so miniscule that they would have been very difficult to detect from ground. Previous reports of amplitude changes in γ Equ, consequently, are most probably consistent with the beating effect. It comes as no surprise that previous studies, especially using time-resolved spectroscopy, could not explain the observations, since it is impossible to resolve f_2 with short time bases. The possibility of unresolved modes in such data should be taken into account when studying pulsation via residual spectra, produced by subtraction of a mean spectrum phased by only a single pulsation frequency. For ground-based photometry, the aliasing problem and the higher noise level might also have contributed to the difficulty of detecting f_2 .

Part III: Modelling

Chapter 4

Modelling γ Equ's pulsation

In this chapter I describe the process of modelling γ Equ. I start with a short description of the basic properties of Hideyuki Saio's roAp models, and then proceed to give a detailed summary of all models, and their parameters, that were used to test the MOST observations. I will also focus on what I did to improve these models for the subsequent fitting process. Furthermore, the technique that I employed to compare models and observations is explained. Finally, I present the fitting results and discuss the many implications that follow from them.

4.1 Pulsation models

It was mentioned in Sec. 3.2.2 that only theoretic models of γ Equ's pulsation frequencies can help to provide more detailed information about the modes excited in this star. Therefore, in collaboration with Hideyuki Saio from the University of Tokyo, such models were produced to not only probe the observations for their possible physical meaning, but also to create one of the first profound challenges for Mr. Saio's theory.

4.1.1 Non-adiabatic, axisymmetric pulsations in the presence of a magnetic field

The theoretic model for calculating roAp mode frequencies used in this work follow the method of calculating non-adiabatic frequencies of axisymmetric ($m = 0$) high order p-modes under the presence of a dipole magnetic field as described in Saio (2005). In this work, Saio expanded his earlier work (Saio & Gautschi 2004) into the non-adiabatic regime. His models neglect stellar rotation, which seems to be sufficiently valid in the case of γ Equ, and include the magnetic effects on stellar structure and evolution, and on the p-mode oscillations produced by a polar magnetic field in the form of

$$\mathbf{B}_0 = \frac{B_p}{(r/R)^3} \left(\mathbf{e}_r \cos \theta + \mathbf{e}_\theta \frac{1}{2} \sin \theta \right), \quad (4.1)$$

where r/R is the fractional distance with respect to the stellar radius from the star's centre, θ is the co-latitude with respect to the magnetic axis, and \mathbf{e}_r and \mathbf{e}_θ are unit vectors in the radial and θ directions. B_p denotes the strength of the magnetic field at the magnetic poles on the stellar surface. Since stellar rotation is neglected the magnetic axis defines the frame of reference for the pulsation. Before pulsation frequencies can be calculated, an (unperturbed) stellar model is constructed. As usual, this is done by choosing a starting mass and metallicity, and then evolving

the model to a desired state via stellar evolutionary models. Here, Saio states that the only influence of the magnetic field on stellar evolution is due to suppression of convection. To simulate this throughout the calculations in the stellar evolution code, the mixing length parameter is set to zero. Once the star is in the desired state of evolution, Saio then proceeds by perturbing the stellar model and solving the linearized perturbation equations. The magnetic field enters the calculations using the ideal magnetohydrodynamics approximation.

Since the displacement due to pulsation, and, therefore, the latitudinal dependence of amplitude, under the presence of a magnetic field cannot be expressed by a single Legendre function, it is expanded into a truncated series of components proportional to Legendre functions P_{l_j} with $l_j = 2j - 1$ for odd modes and $l_j = 2j$ for even modes. In total, twelve terms are included, i.e., $j = 1, 2, \dots, 12$. The latitudinal degree ℓ is not a definite quantity for a pulsation mode any more, because pulsation energy is distributed among twelve components associated with P_{l_j} . For convenience, Saio still uses ℓ representing the l_j value of the component associated with the largest kinetic energy. Sometimes the distribution of the kinetic energy among the components is broad so that the identification of ℓ is ambiguous, and the value of ℓ may change as the strength of the magnetic field changes. As a condition for convergence, Saio requires that the kinetic energy related the last term in the expanded series must be less than half than that of the strongest contribution. For more details about the pulsation models, the reader is referred to Saio's work (Saio & Gautschi 2004; Saio 2005).

One of the most interesting properties of roAp pulsation derived from Saio & Gautschi's work, is the fact that for a mode associated with ℓ , the latitudinal dependence of amplitude on the stellar surface may be considerably different from that of $P_\ell(\cos \theta)$. Usually, it is assumed that whole-disk observations can only reliably detect modes from $\ell = 0$ to 3. Fewer nodes in the pulsation geometry lead to a more uniform temporal behaviour of displacement over large parts of the stellar discs. On the other hand, oscillations of high spherical degree cancel out when integrated over the whole disk. Increasingly smaller areas on the stellar disk vary in phase and lie adjacent to areas comparable in size but varying in anti-phase to the former. In roAp stars, however, the magnetic field leads to a different pulsation geometry and latitudinal dependence of amplitude, so that modes of higher ℓ can still be detected.

4.1.2 Modelling γ Equ

To compare theoretic frequencies with observed ones of γ Equ, Hideyuki Saio has computed main-sequence evolutionary models, which were then subjected to pulsation, just as described in the previous section. These models were intended to match the currently estimated parameter space of γ Equ, which is $\log T_{\text{eff}} = 3.882 \pm 0.011$ K, $\log L/L_\odot = 1.10 \pm 0.03$, and $M \sim 1.74 \pm 0.03 M_\odot$ (Kochukhov & Bagnulo 2006). Some models outside these observational constraints were devised to serve the purpose of evaluating the validity of the pulsation models, i.e., to see whether good fits are constrained to the actual position of γ Equ in the HRD. In particular, most models have been calculated with higher masses, since the initial tests showed that a mass lower than $1.75 M_\odot$ were not able to fit to the observations. Therefore, H. Saio used in his calculations a mass range of $1.75 M_\odot - 1.85 M_\odot$ with heavy element abundance of $0.015 \leq Z \leq 0.025$ and OPAL opacities (Iglesias & Rogers 1996). For the pulsation calculations, outer boundary conditions were imposed at an optical depth of 10^{-3} , and a reflective mechanical condition ($\delta p/p \rightarrow \text{constant}$) was adopted. Only modes, where the most kinetic energy is provided by components $l_j < 5$, were included in the final list of model frequencies. As a first success, the observed frequencies of γ Equ are below the critical acoustic cut-off frequencies for all calculated models.

A list of the individual models, and how they were organised into grids, is presented in Tab. 4.1. A primary intention for the modelling was to test how the calculated frequencies would react and

Table 4.1: List of all stellar evolution models computed for γ Equ with polar magnetic field strengths ranging from 0 to 10 kG in steps of 0.2 kG, except of *Grid 7* which was calculated up to a magnetic field strength of 12 kG. Model 1c in Grid 1, indicated by parentheses, was only used for the convective version of the grid, and all models in Grid 4 have been calculated with a homogeneous He abundance in the stellar envelope (see text). This is an extended version of a table published in Gruberbauer et al. (2008).

Grid ID	M/M_{\odot}	Z	$\log L/L_{\odot}$	$\log T_{\text{eff}}$
1a	1.75	0.02	1.0252	3.8810
1b	1.75	0.02	1.0229	3.8825
(1c)	1.75	0.02	1.0206	3.8840)
2a	1.80	0.015	1.1574	3.8990
2b	1.80	0.015	1.1558	3.9004
2c	1.80	0.015	1.1542	3.9017
3a	1.80	0.02	1.0880	3.8809
3b	1.80	0.02	1.0871	3.8818
3c	1.80	0.02	1.0861	3.8826
4a	1.80	0.02*	1.0899	3.8794
4b	1.80	0.02*	1.0880	3.8810
4c	1.80	0.02*	1.0871	3.8819
4d	1.80	0.02*	1.0861	3.8827
5a	1.80	0.025	1.0284	3.8701
5b	1.80	0.025	1.0267	3.8714
5c	1.80	0.025	1.0243	3.8726
6a	1.85	0.02	1.1388	3.8885
6b	1.85	0.02	1.1368	3.8903
6c	1.85	0.02	1.1345	3.8917
6d	1.85	0.02	1.1325	3.8934
7a	1.85	0.025	1.0753	3.8806
7b	1.85	0.025	1.0734	3.8819
7c	1.85	0.025	1.0715	3.8832

fit to the observations when different physical properties, some of which are still being debated, were imposed on these roAp models. For standard models, envelope convection was suppressed ($\alpha = 0.0$). Furthermore, to mimic depletion of helium abundance in the outermost layers of the star, the helium abundance Y was parameterized as $Y = 0.01 + 0.27(x_2 + x_3)$, where x_2 and x_3 are fractions of singly and doubly ionized helium, respectively (cf Balmforth et al. 2001). This conforms to the currently accepted picture of a star which envelope and atmosphere is dominated by the strong magnetic field effects of a large-scale dipole field.

Nonetheless, even though convection is not expected to play an important role in the envelopes of roAp stars, its effects on the pulsation were also tested by computing all grids except *Grid 4* with $\alpha = 1.5$ and homogeneous He abundance in the outer layers. For these convective models all other parameters remained the same. Finally, *Grid 4* included a homogeneous distribution (mixing) of He in the envelope but no convection, which represents another interesting hybrid model between a normal and a magnetic star.

All models were calculated taking into account a magnetic dipole with polar field strength, B_p , up to 12 kG. Fig. 4.1 shows the position and parameters of all models involved. From this figure, it is obvious that the grid resolution could be improved. The reason for the model scarcity is mostly related to computer resource limitations. However, calculating a large number of models might not even be a good approach for such an initial test of theory and observations. Only when it has been established that H. Saio's models represent reality to a sufficient degree, it makes sense to use many months of CPU time to create dense grids of models. A more convenient approach for increasing the grid density for this initial test was therefore to evaluate whether it might be valid to use interpolation in order to increase the number of models within each grid of Tab. 4.1.

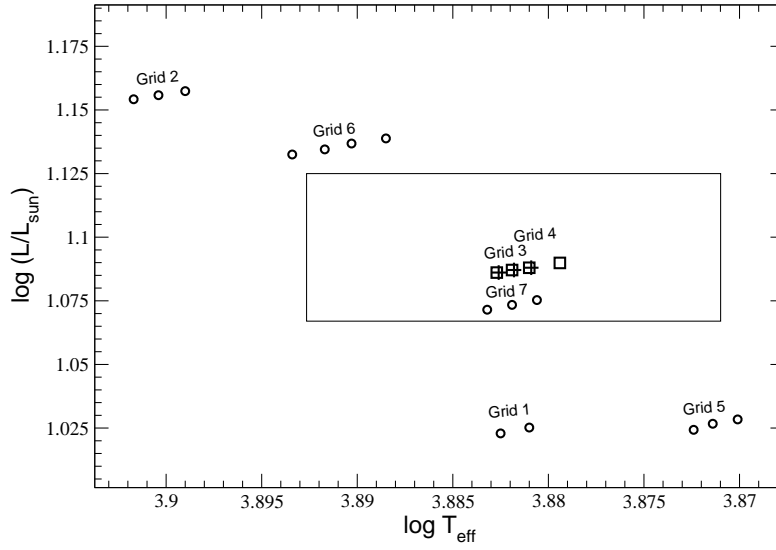


Figure 4.1: A schematic diagram of the calculated grids and their model parameters following the notation of Tab. 4.1. Since *Grid 3* and *Grid 4* partially overlap, all grid points for *Grid 3* are shown as + symbols, while *Grid 4* is indicated by rectangles. Observational uncertainties for γ Equ's estimated position in the HR diagram (Kochukhov & Bagnulo 2006) are represented by the large rectangle. This figure can also be found in Gruberbauer et al. (2008).

4.1.3 Increasing the grid resolution by interpolation

To increase the resolution of the model grids, the mode frequencies were interpolated linearly in B_p and $\log T_{\text{eff}}$ for a fixed mass and chemical composition. First, models with the same polar magnetic field strength yield new models through interpolation in effective temperature. Subsequently, these are expanded by interpolation in the B_p -coordinate. The step width for the interpolation was chosen to be 0.00002 in $\log T_{\text{eff}}$ and 0.02 kG in B_p . Since not all modes with the same degree ℓ and radial order n converge in the model calculations, due to the influence of the magnetic field, the sequence of frequencies for a specific mode may not cover the entire chosen stellar fundamental parameter space ($\log T_{\text{eff}}$, $\log L/L_\odot$, and M).

A linear interpolation in both, B_p and $\log T_{\text{eff}}$, is most likely an oversimplification for the change of frequencies in between the genuine models. Thus, it may be questioned if it is a sensible approach. As a test, interpolated values were compared to the genuine models originally provided by H. Saio. The interpolation in effective temperature was tested in the following way: For all genuine models m_g in all grids, enclosed by 2 additional genuine models $m_{g,1}$ and $m_{g,2}$, equivalent frequencies at

the position of m_g were produced by linear interpolation between $m_{g,1}$ and $m_{g,2}$. The deviation of the interpolated frequencies from their genuine values, normalized to the gap in $\log T_{\text{eff}}$ between the enclosing and the enclosed models, was calculated and over 16000 frequencies were compared. Fig. 4.2 shows a histogram of the results. It illustrates that the interpolation delivers a reasonable approximation to genuine models, as long as the gaps in between the reference models remain reasonably small. The interpolation in B_p performs equally well, as shown in the bottom panel of Fig. 4.2. Due to the fixed step size in polar magnetic field strength, no normalization is required.

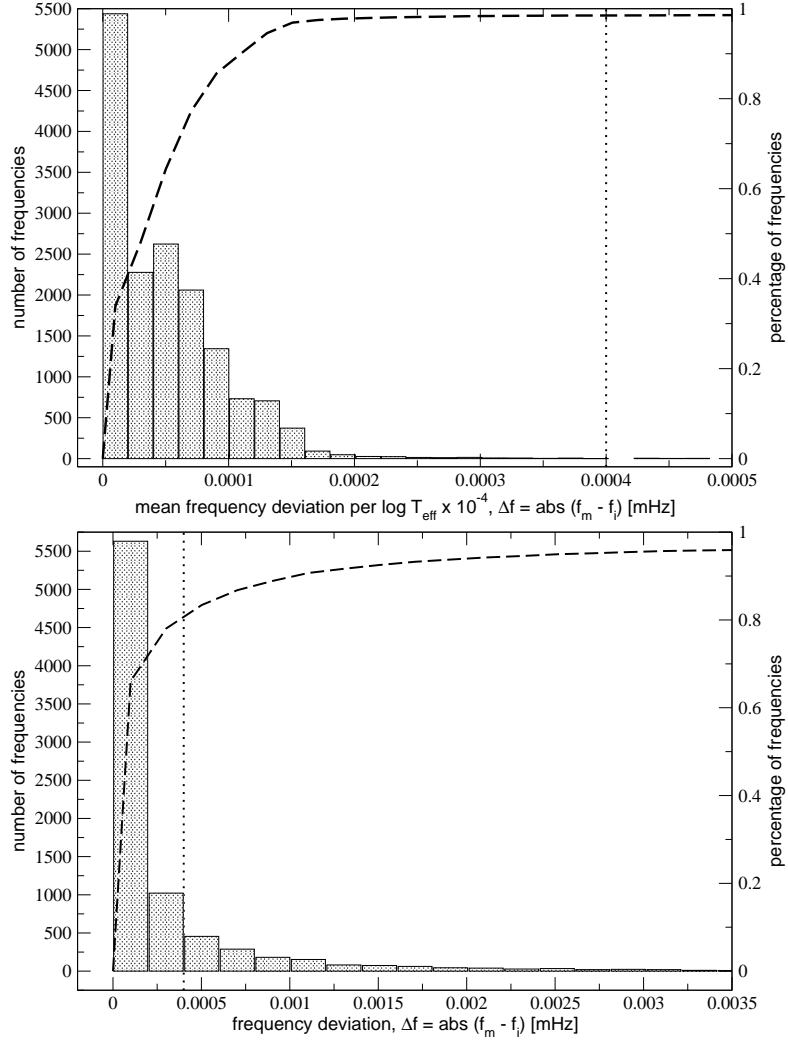


Figure 4.2: *Upper panel:* A histogram of the normalized deviation of 16050 frequencies, interpolated as a function of $\log T_{\text{eff}}$, from their values in genuine models. The bars show the number of frequencies deviating within a certain range. The dotted line gives the estimated upper limit of the model uncertainties. The dashed line shows the total percentage of frequencies, as indicated by the right-hand side ordinate, as a function of frequency deviation. *Lower panel:* A histogram of the absolute frequency deviation of 8523 frequencies, interpolated as a function of B_p , from their genuine counterparts. The dashed and dotted lines have the same meaning as in the upper panel. This figure can also be found in Gruberbauer et al. (2008).

In conclusion, the interpolated models seem to be an appropriate approximation to the results of genuine numerical solutions. Nonetheless, it is not intended to treat their frequencies as correct representations of roAp pulsation at the respective positions in the fundamental parameter space. Rather, the interpolated models are a convenient way to track changes in the model frequencies, following the evolutionary track in each grid of Tab. 4.1. These changes are then reflected in the fitting result. For instance, if modes that fit best to the observations were only present in one of the genuine models of a specific grid, these could as well be artefacts from numerical computation. The interpolation procedure would ignore such modes and the fitting result would deteriorate sharply along a single step in parameter space - from the genuine to the closest interpolated models. This ensures that the fitting structure of a specific grid is dependent on the presence of modes in all genuine models within the specific grid. Therefore it is important that any good fit is part of an extended patch of reasonably well fitting models, rather than a singularity. In addition, the size of the patch will reflect the magnitude of change in the frequency values between adjacent genuine models. This cannot be verified, and visualized, without employing the interpolation procedure.

4.2 Model fitting

4.2.1 The χ^2 -statistic

For the model fitting a procedure similar to what is described in Guenther & Brown (2004) was followed. Guenther & Brown developed this method for the analysis of solar-type oscillations, but it is applicable to any type of pulsating star where individual modes are sufficiently well separated in frequency in comparison to the observational uncertainties. They propose a χ^2 -test for fitting some model to the observations, using the statistic

$$\chi^2 = \frac{1}{N_{\text{obs}}} \sum_{i=1}^{N_{\text{obs}}} \frac{(f_m - f_i)^2}{\sigma_m^2 + \sigma_i^2}, \quad (4.2)$$

where N_{obs} is the number of observed pulsation frequencies f_i , f_m is the frequency given by the model that deviates the least from the observed value, σ_m is the uncertainty of f_m , and σ_i is the corresponding uncertainty for f_i . The χ^2 -statistic has the property of smoothly dropping to a minimum when the differences between observed and model frequencies approach their lowest value, and provides an unambiguous measure for the goodness-of-fit with respect to the observational and theoretical uncertainties. If the uncertainties for both, the observed frequencies and the model frequencies, are assumed to be normally distributed, σ_m and σ_i should be equivalent to the 1σ -uncertainties of these quantities. In Guenther & Brown this statistic is used after a successful mode identification, i.e., after the spherical degree ℓ of the observed frequencies could be established. The χ^2 -statistic then only compares model frequencies and observations that correspond to the same ℓ .

However, it has already been established in the previous sections that no mode identification of γ Equ's frequencies can be inferred from the MOST data without ever fitting the observations to the model frequencies. Moreover, it must again be stressed that mode identification is very difficult for roAp stars *ab initio*. The strong magnetic field influences the pulsation and leads to the necessity of describing each pulsation mode using a linear combination of multiple spherical harmonics. Hence, in the case of axisymmetric oscillations, the pulsation amplitude as a function of stellar latitude does not conform to the usual behaviour of a single spherical harmonic. As a consequence the frequency with the largest amplitude does not necessarily correspond to a purely radial or ($\ell = 1$)-mode. The same is true for all other frequencies found in the data. Also, if there

is no additional information about the mode configuration for frequencies derived from whole-disk observations, it usually is safe to assume that no modes with $\ell > 3$ could be detected. This simplification is not applicable here. Therefore, the fitting procedure needs to ignore the mode configuration and all model frequencies are subjected to the χ^2 -test.

Accordingly, all models in all grids presented in Tab. 4.1 were compared to the observed frequencies using Equ. 4.2. In order to visualize the goodness-of-fit, the fitting procedure was carried out in the $(B_p, \Delta\nu)$ -space. Here, $\Delta\nu$ is the heuristically determined large frequency separation, which can be calculated according to

$$\Delta\nu = 0.1349 \cdot \left(\frac{\langle\rho\rangle}{\langle\rho_\odot\rangle} \right)^{0.5}, \quad (4.3)$$

where $\langle\rho\rangle$ is the mean density of the stellar model, $\langle\rho_\odot\rangle$ is the solar mean density, and the factor of 0.1349 originates from the large frequency separation observed in the Sun. The mean density of the stellar model was calculated from the mass, luminosity, and effective temperature given by the models. Assuming spherical symmetry, $\langle\rho\rangle$ is then given by the well known equation

$$\langle\rho\rangle = \frac{3M}{4\pi R^3}, \quad (4.4)$$

where M is the mass and R is the radius of the star. R can be calculated from the effective temperature and luminosity according to

$$R = \sqrt{\frac{L}{4\pi\sigma_{\text{SB}}T^4}}, \quad (4.5)$$

where σ_{SB} is the Stefan–Boltzmann constant. Since the stellar mass is known for each model, $\Delta\nu$ can be immediately determined.

The 1σ -uncertainties of the observed frequencies were estimated to be roughly 0.25 of the upper frequency error derived according to Kallinger et al. (2007). This assumption holds if the frequency uncertainties conform to a normal distribution, and the upper frequency error is comparable to a 4σ -uncertainty. The 1σ -uncertainties assigned to the individual model frequencies were provided by H. Saio, who assumed them to be on the order of $0.2\mu\text{Hz}$.

4.2.2 Results

The best fitted models, represented by a minimum in the χ^2 -statistic, are listed in Table 4.2, and the visualization of the χ^2 -results for all grids can be found in the Appendix. The minimum χ^2 varies by more than a magnitude, indicating that the general characteristics of the frequency spectra are vastly different among all tested grids. *Grid 3*, as defined in Table 4.1, outperforms the other models by far. It is the only model grid that manages to produce frequencies that fit all five observed frequencies, on average, to within the uncertainties ($\chi^2 \leq 1$). The result is illustrated in the upper panel of Fig. 4.3. As a comparison, the lower panel of Fig. 4.3 shows the fitting results to *Grid 6*, which produces considerably larger χ^2 values. Meeting the expectations, including convection for *Grid 3* leads to a radically different result, because the underlying stellar model is subject to different physics.

Surprisingly, for grids with large χ^2 it has the opposite effect. This is not necessarily an argument for convection and different fundamental parameters. Rather, it shows that all grids without convection have very particular characteristics, and gives even more weight to the fact that the good fits among these grids are very strongly constrained to *Grid 3*. The best fit is located at the center of an extended patch, rather symmetric in $\Delta\nu$. Therefore, as argued in the Sec. 4.1.3, the

Table 4.2: χ^2 values of the best fits in the corresponding model grids. Models taking convection into account are denoted by an index α . The visualization of the χ^2 -results for all grids can be found in the Appendix. This table is a revised version of a table in Gruberbauer et al. (2008).

Grid ID	$\min(\chi^2)$	$B_p[\text{kG}]$
1	41.0	6.0
1 α	4.4	8.8
2	6.0	6.5
2 α	22.4	6.5
3	0.7	8.1
3 α	7.7	2.8
4	8.0	0.0
5	22.6	0.4
5 α	2.2	4.6
6	4.6	7.3
6 α	4.6	6.0
7	17.8	0.0
7 α	2.0	3.7

modes fitting to the observations are present in all of the 3 stellar models of which *Grid 3* is composed. Moreover, its proximity to a genuine calculated model ensures that this good fit is not an artifact produced by the interpolation. The mean parameter values for the $\chi^2 \leq 1$ region with the mentioned interpolation step size are $\log T_{\text{eff}} = 3.8818$, $\log L/L_{\odot} = 1.0871$ and $B_p = 8.1$ kG.

In Fig. 4.3 obvious discontinuities can be seen in the fitting results. A number of effects cause these sudden increase in χ^2 . First, they are produced when the interpolation routine cannot find two modes of equal spherical degree ℓ and radial order n in both models that are acting as sampling points. This can happen, as already mentioned in Section 4.1, when the ℓ -value of a mode formally changes, because the former associated spherical harmonic does no longer supply most of the kinetic energy. Where this is the case, the drop in the quality of the fit is located close to a genuine model. As an example, in the upper panel of Fig. 4.3, at $B_p = 3.8$ kG, the χ^2 -values suffer an instantaneous increase when proceeding from the genuine models at $\Delta\nu \approx 63.375$ towards lower values of $\Delta\nu$. Towards higher values of $\Delta\nu$ this increase does not occur. This indicates that, around $B_p = 3.8$, the genuine models with the lowest $\Delta\nu$ in this grid do not contain one or more specific modes which fit reasonably well to the observations.

As a second reason for the discontinuities, the cyclic variation of the damping rate as a function of B_p , as shown in Saio & Gautschi (2004), has an effect on the “availability” of certain modes. Around the maximum of the damping rate, the kinetic energy is so broadly distributed among the different ℓ -components that convergence of the model calculations starts to fail. This effect is clearly visible as the two large discontinuities in each panel of Fig. 4.3, which bears resemblance to what is presented in Saio & Gautschi (2004). Overall, both causes can easily be distinguished when visualizing the goodness-of-fit as in Fig. 4.3. The cyclic variation of the damping rate causes discontinuities in the B_p direction, while those along the $\Delta\nu$ -coordinate are mostly artefacts due to interpolation.

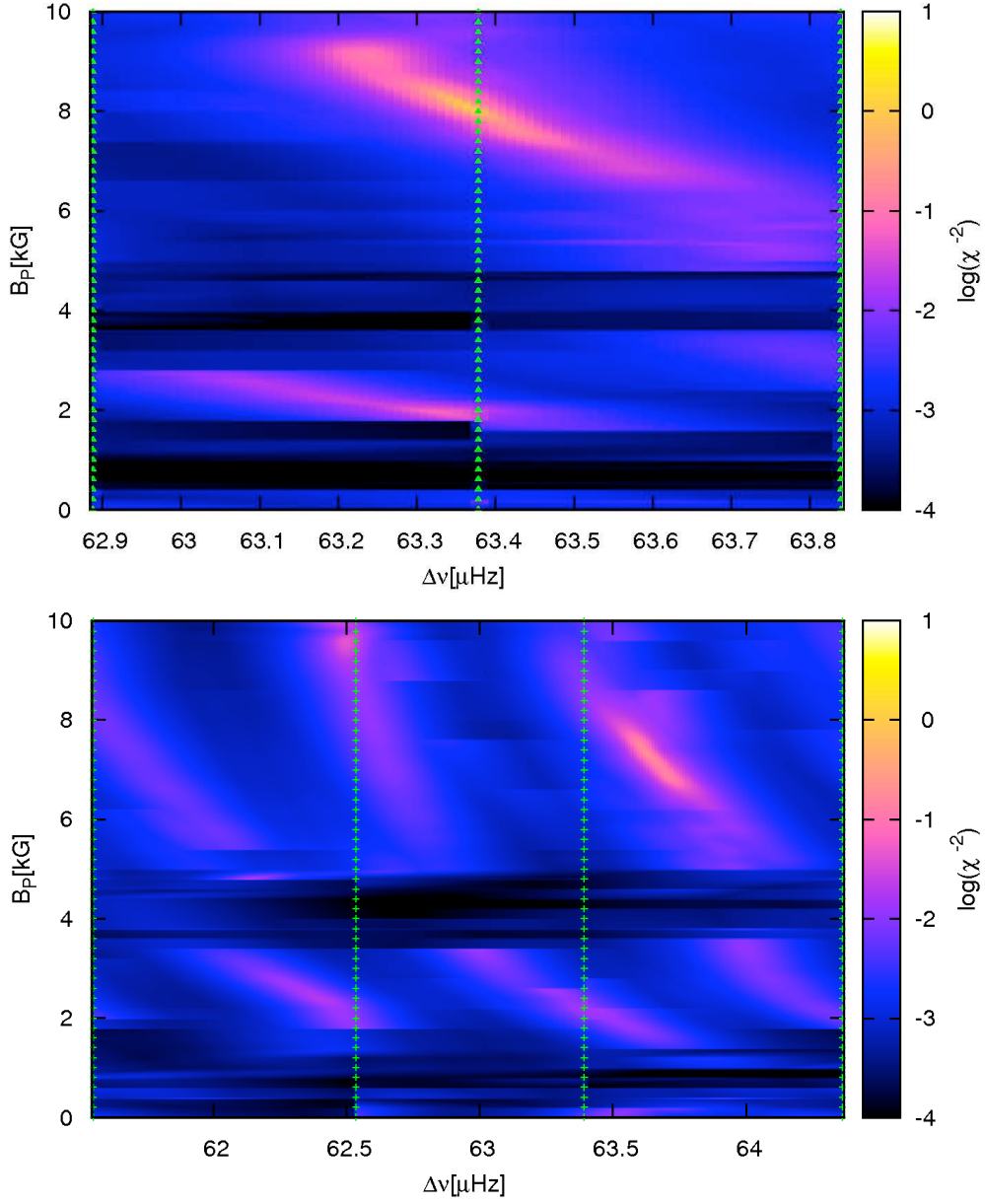


Figure 4.3: *Upper panel:* Color coded inverse χ^2 values obtained when fitting the 5 intrinsic frequencies of γ Equ to model frequencies of *Grid 3*. The vertically aligned symbols represent the calculated model positions – all other model frequencies are derived via linear interpolation. Discontinuities are due to a lack of converging model frequencies. Some modes of a certain degree and radial order are missing in the individual genuine models. Also, sudden changes of the frequency spacing due to the magnetic field, can change the quality of the fit quite rapidly. *Lower panel:* *Grid 6* shows a pattern similar to *Grid 3* but delivers larger χ^2 values. It gives, however, the same mode identification. Note the different scale of the abscissa! This figure can also be found in Gruberbauer et al. (2008).

Fig. 4.4 shows an échelle diagram of the best fitted model together with the observations. f_1 , the most prominent frequency, is identified as an ($\ell = 1$)–mode. f_2 and f_3 are matched by consecutive ($\ell = 4$)–modes. The remaining two frequencies, f_4 and f_5 , are fitted by modes of degree $\ell = 2$ and $\ell = 0$. Interestingly, while all grids except *Grid 3* fail at delivering ($\chi^2 < 1$)–results, the mode identification remains stable for grids with $\chi^2 < 4$. In particular, the two closely spaced model frequencies in the vicinity of f_1 and f_2 are found to fit the same degrees $\ell = 1$ and 4 for *Grids 3*, 7α , 5α , and 6. This is not the case for 6α and 1α . Again, comparable to the properties of *Grid 3* and 3α , for *Grid 6* convection is shown to radically influence the model frequencies. To conclude, the calculated model grids seem to favour the mode identification provided by the best fit in *Grid 3*, which is again presented in Tab. 4.3 for the purpose of reviewing, as a condition for good fitting.

Table 4.3: The mode identification as given by the best fit of *Grid 3* (see Tab. 4.1). The frequencies are labelled following the convention introduced by Tab. 3.3.

id	$f[\text{mHz}]$	ℓ
f_1	1.364594	1
f_2	1.365411	4
f_3	1.427102	4
f_4	1.388872	2
f_5	1.310914	0

It must be noted here that although the model frequencies fit the observations very well and provide a consistent picture, none of the fitted modes are actually excited according to the stability analysis of H. Saio. This of course remains an issue worth investigating and might even point at some fundamental flaw in the theoretic modelling. However, it is beyond the scope of this thesis to investigate this topic, and it must suffice to trust in H. Saio’s opinion, which is that the stability analysis needs improvement. Any change in this part of the theory behind his models, however, should not influence the resulting frequency values.

It is also interesting to note that comparable fitting results are returned if f_2 is excluded from the list of observed frequencies. This has at least two implications:

1. The remaining observed frequencies still strongly constrain which models are a good match. This suggests that for roAp stars not many frequencies are necessary to obtain a reliable fit to theoretic models, as long as the magnetic effects in the star are large enough to sufficiently distort the usual asymptotic behaviour of high-order p-modes. Nonetheless, from a purely statistical point of view, less observed frequencies and an increasing number of models in the grid, respectively a grid that spans a larger region in the fundamental parameter space, will of course still produce ambiguous results.
2. Beating is generally predicted by the models. Due to frequently intersecting ridges of modes with different ℓ -values among the model grids, beating should be expected in many roAp stars, as long as the corresponding modes are excited. It could be that numerous reports of amplitude modulation in the literature are actually misinterpretations of beating phenomena.

Now that the fitting properties of all models have been discussed, and the best fit has been shown to yield impressive results, it is important to test the reliability of this result. Although the overall validity of the interpolation routine has already been established in Sec. 4.1.3, the specific case of

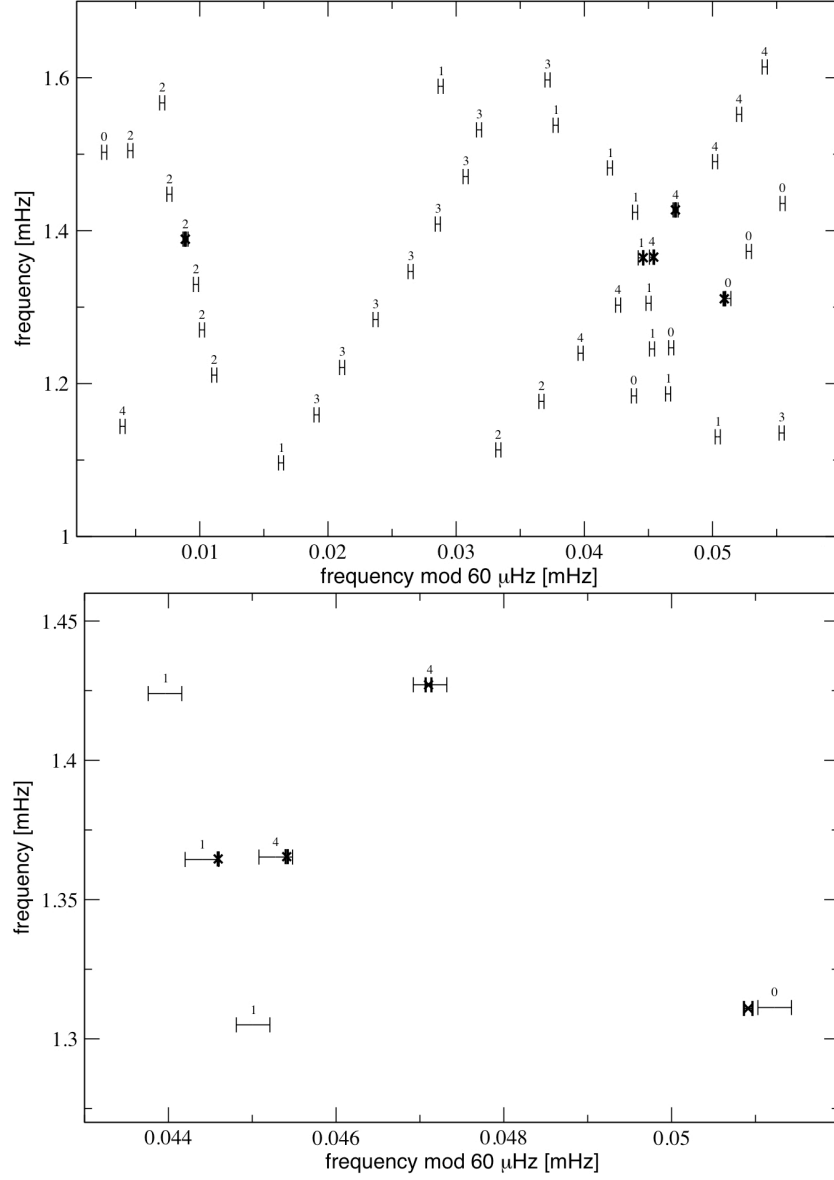


Figure 4.4: *Upper panel:* Échelle diagram of the best fitted stellar model ($\chi^2 = 0.744$, Grid 3). The corresponding parameters are $\log T_{\text{eff}} = 3.8818$, $\log L/L_{\odot} = 1.0871$, and $B_p = 8.06$ kG. The model frequencies are represented by their estimated error bars, the numbers above denote the mode degree ℓ . Black cross symbols indicate the position of the observed frequencies with error bars.

Lower panel: A close-up of the region in the échelle diagram including f_1 , f_2 , f_3 , and f_5 illustrating the quality of the fit more clearly. f_5 is not matched to within the 1σ -error, but f_1 to f_3 dominate the χ^2 statistics because of their high significance. This figure can also be found in Gruberbauer et al. (2008).

Grid 3, and the influence of interpolation on those frequencies in *Grid 3* that match the observations in the best fitted model, has to be evaluated. In order to do this, *Grid 3* was recalculated.

This time, however, the *3b*-models (see Tab. 4.1) were omitted, and all models between *3a* and *3c* were created through interpolation. Subsequently, the fitting process was repeated. Figure 4.5 shows the χ^2 -statistics for the new *Grid 3* based on interpolation between *3a* and *3c* (best fit with $\chi^2 = 2.642$). Obviously, the best fit is worse than when the *3b*-models are considered in the calculations. However, a comparison of Figure 4.5 with the upper panel of Fig. 4.3 shows that the general shape of the extended patch with good χ^2 values is comparable in both cases. This again suggests that interpolation is applicable for small gaps in between genuine models.

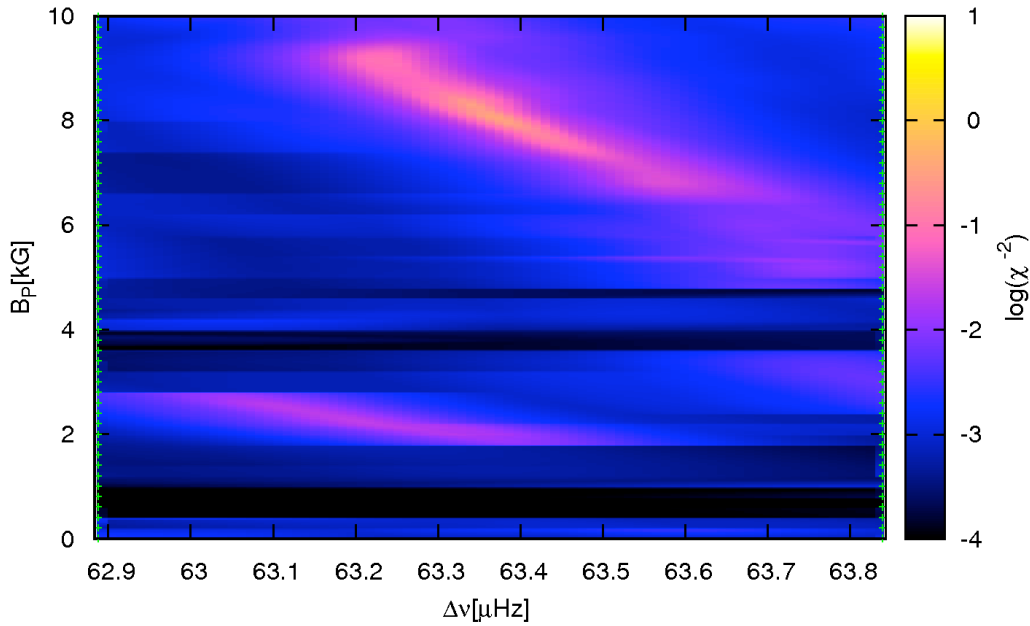


Figure 4.5: The result of fitting the observed frequencies to a model grid calculated by interpolation between *3a* and *3c*. Although the *3b*-models are omitted and no fit with $\chi^2 \leq 1$ is found, the figure compares well to the upper panel of Fig. 4.3. Linear interpolation in B_p is therefore a reasonable approximation to genuine models for our fitting procedure. This figure can also be found in Gruberbauer et al. (2008).

Not all modes can be approximated sufficiently through linear interpolation, as indicated by the bars in Figure 4.2 which lie outside the estimated uncertainties of the model frequencies. It is highly unlikely, but still possible, that the model frequencies that fit the observations best are among those distorted by the interpolation. Therefore, it is necessary to check whether these frequencies satisfy the assumption of a linear variation between the different genuine models. Figure 4.6 presents the absolute (rather than the normalized) deviation of the interpolated frequencies from the genuine frequencies for the *3b*-models. It shows that the interpolated values of all 5 modes that fit the observations are hardly deviating from their genuine values - the deviations lie well within the model uncertainties.

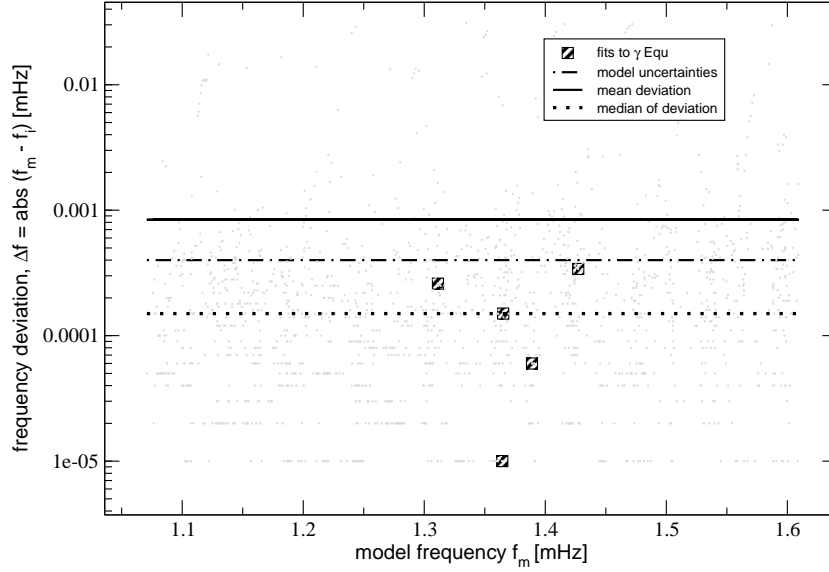


Figure 4.6: The absolute deviations of all interpolated frequencies at the position of 3b, using Grid models 3a and 3c, from the genuine frequency values. All 5 modes, which match the observed frequencies of γ Equ best and are indicated by boxes, are deviating less than the model uncertainties. This figure can also be found in Gruberbauer et al. (2008).

4.2.3 Latitudinal amplitude dependence

As discussed in Sec. 4.2.2 the observed frequencies of γ Equ are identified as modes of $\ell = 0, 1, 2$, and 4. Those modes, however, have amplitude distribution on the stellar surface considerably deviating from that of a single spherical harmonic due to the strong magnetic effect (Fig. 4.7). The amplitude for f_1 ($\ell = 1$) and f_4 ($\ell = 2$) is more concentrated toward the polar regions than $P_1(\cos \theta)$ and $P_2(\cos \theta)$. It is interesting that the amplitude distribution of f_4 ($\ell = 2$) on a hemisphere is not very different from that of f_1 ($\ell = 1$) having very small amplitude near the equator, although f_1 is antisymmetric and f_4 symmetric to the equator.

For f_2, f_3 ($\ell = 4$) and f_5 ($\ell = 0$) the amplitude distributions are strongly concentrated around $\cos \theta \approx 0.65$, drastically different from those for non-magnetic stars. Therefore, although the light variation from an $\ell = 4$ mode of a non-magnetic star is expected to suffer from a strong cancellation on the stellar disk, Fig. 4.7 indicates that, in the case of γ Equ, f_2 and f_3 seem hardly affected by this. This is another indication that pulsation in roAp stars can only be analyzed in terms of mode identification, if the observed frequencies are compared to theoretical values. A spectroscopic analysis of the line profile variations, as well as photometric studies investigating phase shifts and amplitude ratios aiming at mode identification, is highly ambiguous since completely different modes might appear similarly to the observer.

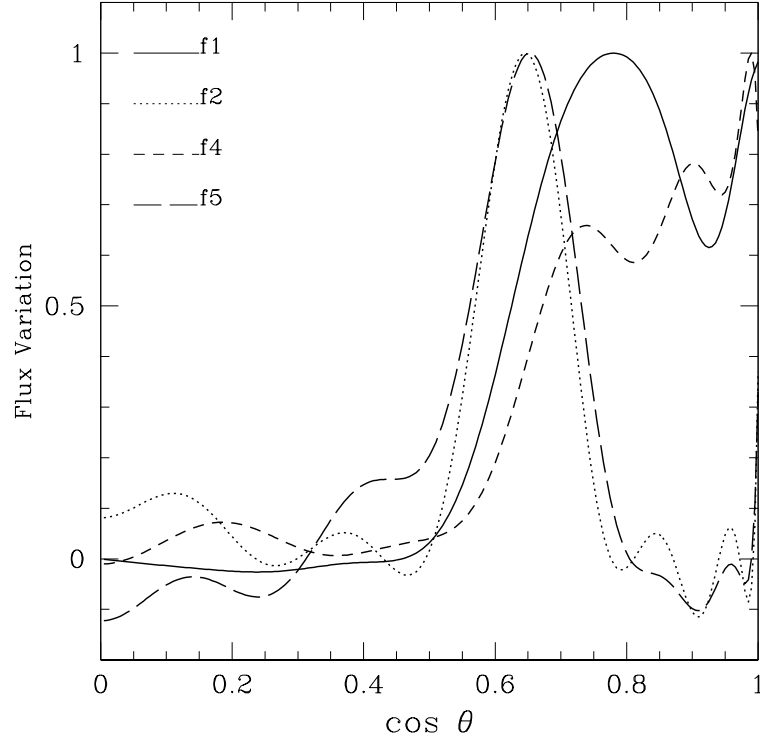


Figure 4.7: Latitudinal variation of the perturbation of radiative flux on the surface is shown for each mode matched to γ Equ. (The case of f_3 is not shown because it is very close to that of f_2 .) The ordinate shows $\cos \theta$ with θ being co-latitude ($\cos \theta = 1$ at poles). The plots are the real parts of the eigenfunctions for the flux perturbation at $B_p = 8$ kG for model *3b* (Table 4.1). Each curve is normalized so that the maximum is unity. The calculations have been performed by H. Saio. This figure can also be found in Gruberbauer et al. (2008).

Conclusion and outlook

Chapter 5

Conclusion and outlook

In this final chapter of my thesis I will summarize the results of my analysis. A list of discoveries is given which divides my findings into several emphasized points, which I will then discuss in terms of what the consequences should be for future observations of roAp stars with MOST and in general. This section is based on conference proceedings that I wrote, with editorial support by my advisor, and which have been published (Gruberbauer & Weiss 2008). I here give an extended discussion, however, and draw the conclusion to this thesis.

5.1 A list of discoveries

The 19 days of MOST observations of γ Equ, culminating in almost 49000 exposures, delivered highly precise measurements with unprecedented time sampling for this star. Many new discoveries have been made using this data and discussed in this thesis, which greatly help to clarify the previously confusing picture of the pulsation of γ Equ. Among these are the following:

1. 7 frequencies intrinsic to γ Equ were identified, with semi-amplitudes as low as 18 ppm.
2. Due to the relatively long time base, in comparison to single-site spectroscopic observations, the 1σ -frequency uncertainties are estimated to lie below $0.1 \mu\text{Hz}$
3. 2 of the 7 frequencies correspond to the first and second harmonic of the most prominent frequency.
4. All 4 frequencies from Martinez et al. (1996) have for the first time been found consistently in this single data set.
5. Most important though is the detection of an additional 5th frequency, closely spaced to the primary frequency.
6. After excluding the 2 harmonics, all 5 remaining frequencies were fitted to magnetic pulsation models. The model corresponding to the best fit reproduces the observed frequencies to within the observational uncertainties. Its parameters match γ Equ's assumed position in the HR diagram quite well. Even when excluding the newly discovered 5th frequency, the same results are achieved. The 5th frequency is thus predicted by the models because of the particular values of the remaining 4 frequencies. The parameters of the best fit are $\log T_{\text{eff}} = 3.8818$, $\log L/L_{\odot} = 1.0871$, and $B_p = 8.06 \text{ kG}$. This places γ Equ in an area of the HRD where it is expected to lie from previous observations. However, the magnetic field strength is about twice as large as it had been observed using spectro-polarimetric measurements. Also, the mass of the model is slightly higher than expected.

5.2 Implications for future studies - space photometry as a keyplayer

In reference to the previous section, the benefits of space photometry for the future development of roAp theory are obvious. Each finding points at a different observational shortcoming that can be overcome using new instruments like MOST.

As stated in point 1 of Section 5.1, MOST observed very small amplitudes in γ Equ. One can expect that these small light variations will be accompanied by small changes in radial velocity. Today, radial velocity measurements are becoming more precise than ever, and high quality time series can be constructed. A large number of data points is needed, though, in order to reduce the noise in Fourier space to a level that enables the detection of such weak signal. Alas, it is still almost impossible to obtain enough observing time at the best spectroscopic instruments in order to compete with space instruments. Also, daily aliasing would make it difficult to identify all 7 frequencies of γ Equ unambiguously. This eventually results in an incomplete picture of the star's pulsation, reducing the observations' potential to be a test for roAp theory, and could lead to false conclusions.

Point 2 mentions very small observational uncertainties on the frequency values. Small frequency uncertainties are necessary for resolving closely spaced frequencies, but also for testing theoretical models. A goodness-of-fit test, like the χ^2 -statistic explained in Sec. 4.2.1 only makes sense, if the observations put enough constraints on the model frequencies. Therefore, in order to test roAp theory, long time bases are inevitable, since the frequency uncertainty is inversely proportional to the time base of the data set.

Point 3 has a special relevance for recent studies of γ Equ and other roAp stars. Kochukhov & Ryabchikova (2001) found strange blue-to-red-moving features in the line profile variations (LPV) of γ Equ. According to them, these features might be explained through modes with $m \neq 0$. This led to a discussion about other possible explanations, e.g. whether these features might be caused by shock waves or turbulence (Shibahashi et al., 2004; Kochukhov et al. 2007; Shibahashi et al. 2007). Since similar characteristics have been found in many other roAp stars, they need to be understood in context of the roAp phenomenon. The detection of the first and second harmonic to the dominant frequency by MOST shows that photometry is also sensitive to these effects. This might help to rule out explanations, which are only applicable to spectroscopic observations. However, the first harmonic, as found in the MOST data, only has a semi-amplitude of about 40 ppm, and the second harmonic is an even weaker signal. As such, very precise photometry is needed for its detection.

Point 4 confines the answers to a question that has often been posed: Are roAp pulsations consistent over a longer time base, or is the signal damped and re-excited, similar to solar-like oscillations? The MOST observations of γ Equ show no convincing evidence that indicates a mode lifetime shorter than the observation run (19 days). Spectroscopic observations are currently obtained for a few hours at a time, often with daily or even longer gaps in between. To gather more evidence for the determination of mode lifetimes, extended observations with sufficient precision and a low detection threshold are necessary. Only space missions like MOST or COROT, and, to some extent ground-based observation networks like the Whole Earth Telescope (WET), currently meet these requirements.

The most unexpected result from the presented analysis probably concerns point 5. Amplitude

modulation or amplitude change, unrelated to stellar rotation, in roAp stars has been reported or suggested multiple times. One of the possible explanations is that we simply see the beating of two closely spaced frequencies. Beating can be misinterpreted as amplitude modulation, if the time base of the observations is not long enough to resolve the involved frequencies, or if the data quality is not good enough to reliably derive time-resolved amplitudes and phases. It has been shown that MOST has detected a previously unresolved frequency close to the most prominent frequency. This frequency doublet would result in a beating period of about 14.3 days. Observations with short time bases would not be able to distinguish between amplitude modulation and beating. An investigation of the pulsation models fitted to the MOST data also reveals, why such a beating phenomenon might be more common in roAp stars. The influence of the magnetic field can lead to closely spaced modes of different spherical degree ℓ , because the sequences of different ℓ sometimes intersect.

Mode identification is perhaps the most important prerequisite for asteroseismology. Only when the assignment of mode parameters (ℓ, m, n) to a specific observed frequency is established, can it be used to obtain information about the interior of the star. Usually, spectroscopy is the preferred tool. The mode parameters can be deduced from the line profile variations, and (in contrast to mode identification through photometry) $m \neq 0$ modes can also be analysed.

In the case of roAp stars, line profile variations are a much more difficult problem. As shown in Saio (2005), theory predicts that a single mode cannot be assigned to a single spherical harmonic because of magnetic effects. To describe the latitudinal distribution of amplitude of a pulsation mode over the stellar disc of magnetic stars, a single Legendre function is not sufficient. One needs to “construct” a mode which distributes its kinetic energy amongst a series of spherical harmonics.

A latitudinal amplitude dependence, as predicted by the magnetic pulsation models, can be tested by means of studying the line profile variations. An excellent example for this proposal are the excellent results in Kochukhov (2004). However, mode identification for roAp stars, as an unbiased observational effort, cannot work the way it is currently established. The only approach to mode identification in an unbiased fashion, therefore, has to rely on the frequency values alone, and on fitting them to magnetic model frequencies. Currently, only space photometry and ground-based networks like the WET can currently achieve uncertainties and detection thresholds that are low enough to make this a feasible task.

All together, the results presented in this thesis show great potential for space photometry, in combination with theory, to obtain a better picture of roAp pulsation. However, it is not only the knowledge about the stars’ oscillations that is improving. Knowing the pulsation frequencies, and whether they are stable, is important for most research on these objects. The corresponding variations in light and radial velocity affect the data used in studies that are not even concerned about pulsation. Thus, even if it should not be possible to determine the fundamental parameters of each roAp star from the oscillations alone, it will pay off to perform these observations.

5.3 Conclusion

Many researchers have focussed their efforts in previous years on understanding roAp stars and γ Equ in particular. Tremendous insight in the inner workings of these stars’ atmospheres has been gained, and pioneering observations of their pulsation behaviour have been made. However, only recently instruments and theory are finally good enough to answer some of the more elaborate questions. It has been established in this work that the continuous and extended high-precision

photometry obtained by the MOST satellite was a requirement to obtain an accurate overall picture of γ Equ's mode spectrum. This provided the possibility of comparing the observed frequencies with theoretical models, which resulted in impressive results. This fruitful symbiosis of observation and theory led to a consistent interpretation of all that is currently known about γ Equ's pulsation.

The presented result of course cannot be final. There might still be additional modes lurking in the noise of current observations and the MOST data, which are simply too faint to be observed without even more powerful telescopes and satellites. These might provide a different picture of γ Equ when compared to theory. Another possibility is that theory itself might be flawed. For instance, it is interesting that none of the fitted model frequencies belong to a mode that is actually expected to be excited. Also, the polar magnetic field value of $\sim 8\text{kG}$ is too high by a factor of two in comparison to spectro-polarimetric observations of γ Equ. A similar result, also obtained using MOST data and H. Saio's models in the case of 10Aql (Huber et al. 2008), suggests that this might be a systematic difference either originating from theory, observations, or some conceptual mistake of how to relate those to each other.

In conclusion, there are still some questions that need to be answered. Nonetheless, the presented analysis shows that for moderately-to-slow rotating roAp stars, where H. Saio's theory can be applied, space photometry might be the ultimate tool to take further steps down the road of progress. Looking even further into the future of this field, the next big leap obviously must be to incorporate rotational effects into the stellar evolution and pulsation models. This would provide the potential of comparing theoretic results to the observations of many more roAp stars. Asteroseismology of roAp stars might or might not be the long-sought key to unravel all the mysteries of these enigmatic objects. In any case, the groundwork has been laid and only the future will tell.

Acknowledgements

First and foremost, I want to thank my parents, Wieland and Ilse Gruberbauer, for supporting me throughout my childhood, adolescence, and my life as a student at the University of Vienna. It is because of them that I was able to make all the right decision which finally led to studying astronomy. Without their support it would not have been possible for me to follow all my childhood dreams, culminating in the pursuit of scientific endeavours. I also want to extend the same gratefulness to my sister Elisabeth, as well as to my grandmother Margarethe. Thank you!

I further want to thank you, Marlene, for putting up with me when I needed to work after hours at the institute, or when I spent weekends at home in front of the computer, hammering away at some manuscript or work for this thesis. I am eternally thankful that most of the time everything is fun because of you – and that you always know exactly which kind words you need to say in those few more desperate moments.

I also want to thank my best friends Stephan, Bernd, Matthias, and Christoph for their support, understanding, and all those fun times, where, thank goodness, science and astronomy were not the most important topics to discuss.

Furthermore, of course, I want to thank my advisor, Werner W. Weiss, for welcoming me as a member in his team, for providing all the freedom in the world to chose any topic (that is at least peripherally connected to his research) I want to work on, even if the results take time or don't lead anywhere. I also need to thank him for the financial support, without which it would have been very difficult to spend so much time with research. I also want to thank the MOST Science Team, especially Jaymie M. Matthews, Rainer Kuschnig, and David Guenther for their support and their confidence, which made it possible for me to work on data that would be on the wish list of many, many astronomers. Of course, I also want to thank Hideyuki Saio for his collaborational efforts - without him providing his models, most of the work presented in this thesis would simply not exist.

A number of colleagues which helped me in this work by either contributing their experience in data analysis and stellar astrophysics, or simply raising important points in interesting discussions also need to be credited. More importantly, though, they make the working hours even more fun - who would have though that science regularly descends into silly madness ... So, thank you Daniel, Thomas, Alex, David, and Markus! Last but not least, my thanks go out to Piet Reegen for introducing me to many, many important concepts, including the ethics of research, at the beginning of my "research internship". Also, thanks for giving me a hard time in the first couple of weeks :o).

Appendix A

χ^2 -plots

In the following appendix, all χ^2 -plots, indicating the quality of the fits and hinting at common structures in observations and models, are presented. For the sake of orientation, Tab. 4.1 and Tab. 4.2 are reprinted here.

Table A.1: Copy of Tab. 4.1 from Chapter 4.

Grid ID	M/M_{\odot}	Z	$\log L/L_{\odot}$	$\log T_{\text{eff}}$
1a	1.75	0.02	1.0252	3.8810
1b	1.75	0.02	1.0229	3.8825
(1c	1.75	0.02	1.0206	3.8840)
2a	1.80	0.015	1.1574	3.8990
2b	1.80	0.015	1.1558	3.9004
2c	1.80	0.015	1.1542	3.9017
3a	1.80	0.02	1.0880	3.8809
3b	1.80	0.02	1.0871	3.8818
3c	1.80	0.02	1.0861	3.8826
4a	1.80	0.02*	1.0899	3.8794
4b	1.80	0.02*	1.0880	3.8810
4c	1.80	0.02*	1.0871	3.8819
4d	1.80	0.02*	1.0861	3.8827
5a	1.80	0.025	1.0284	3.8701
5b	1.80	0.025	1.0267	3.8714
5c	1.80	0.025	1.0243	3.8726
6a	1.85	0.02	1.1388	3.8885
6b	1.85	0.02	1.1368	3.8903
6c	1.85	0.02	1.1345	3.8917
6d	1.85	0.02	1.1325	3.8934
7a	1.85	0.025	1.0753	3.8806
7b	1.85	0.025	1.0734	3.8819
7c	1.85	0.025	1.0715	3.8832

Table A.2: Copy of Tab. 4.2 from Chapter 4.

Grid ID	$\min(\chi^2)$	$B_p[\text{kG}]$
1	41.0	6.0
1 α	4.4	8.8
2	6.0	6.5
2 α	22.4	6.5
3	0.7	8.1
3 α	7.7	2.8
4	8.0	0.0
5	22.6	0.4
5 α	2.2	4.6
6	4.6	7.3
6 α	4.6	6.0
7	17.8	0.0
7 α	2.0	3.7

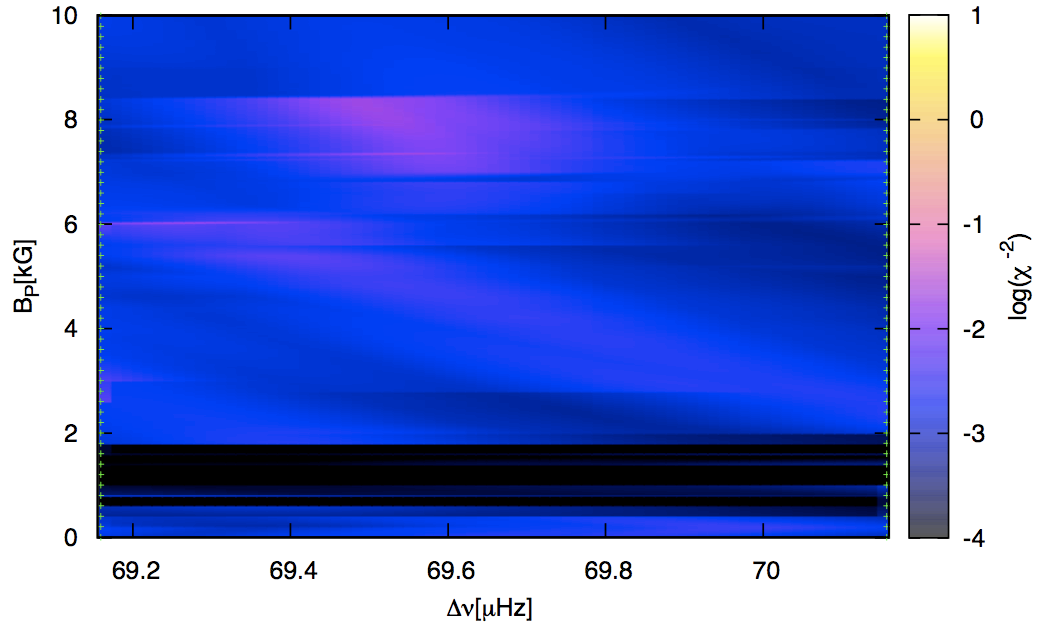


Figure A.1: χ^2 -results for Grid 1; no convection.

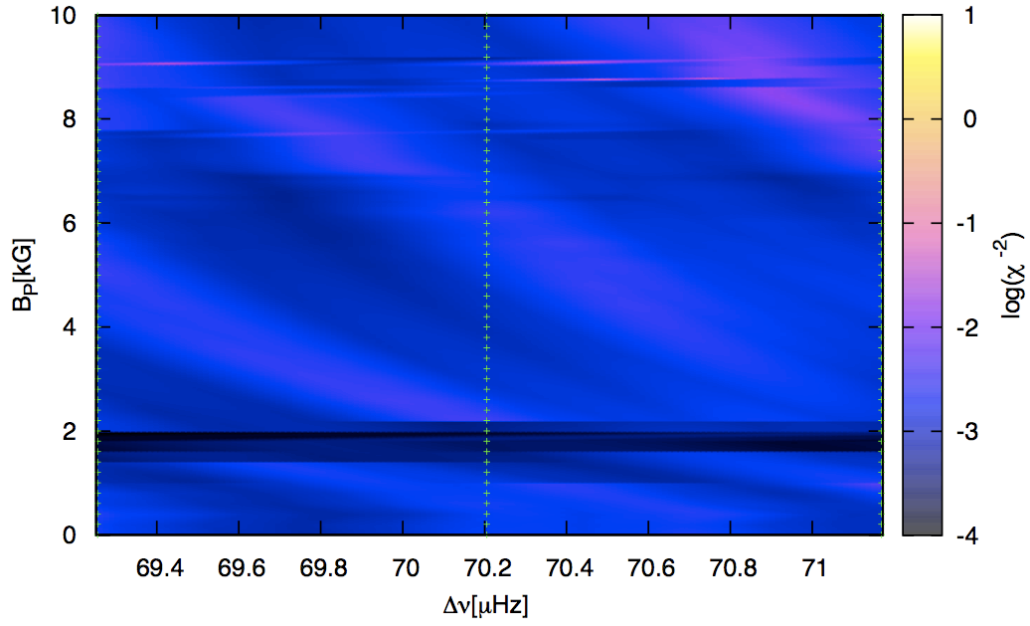


Figure A.2: χ^2 -results for the extended Grid 1α; includes convection.

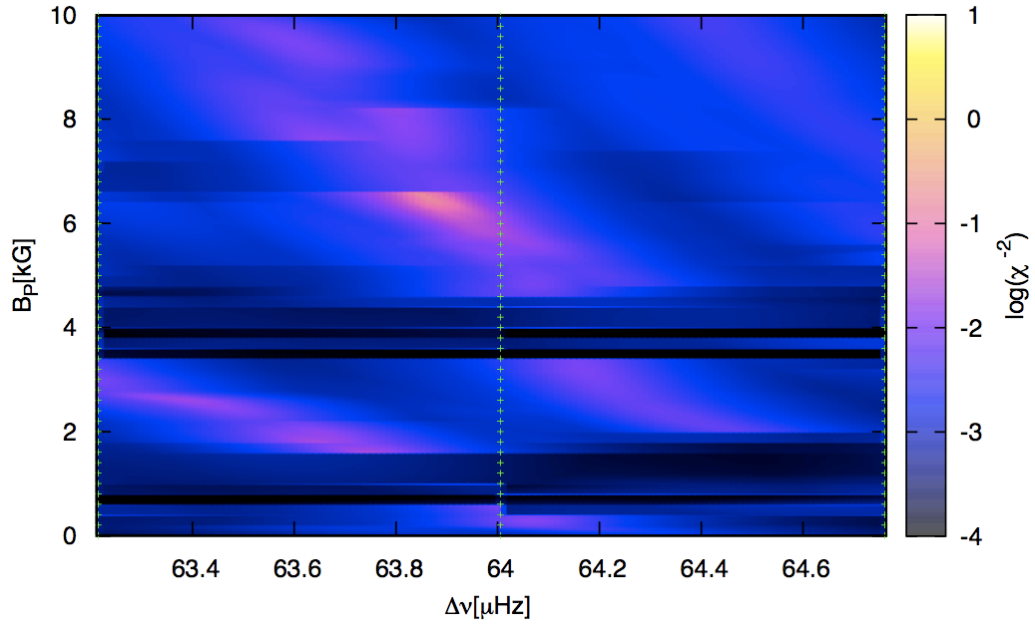


Figure A.3: χ^2 -results for Grid 2; no convection.

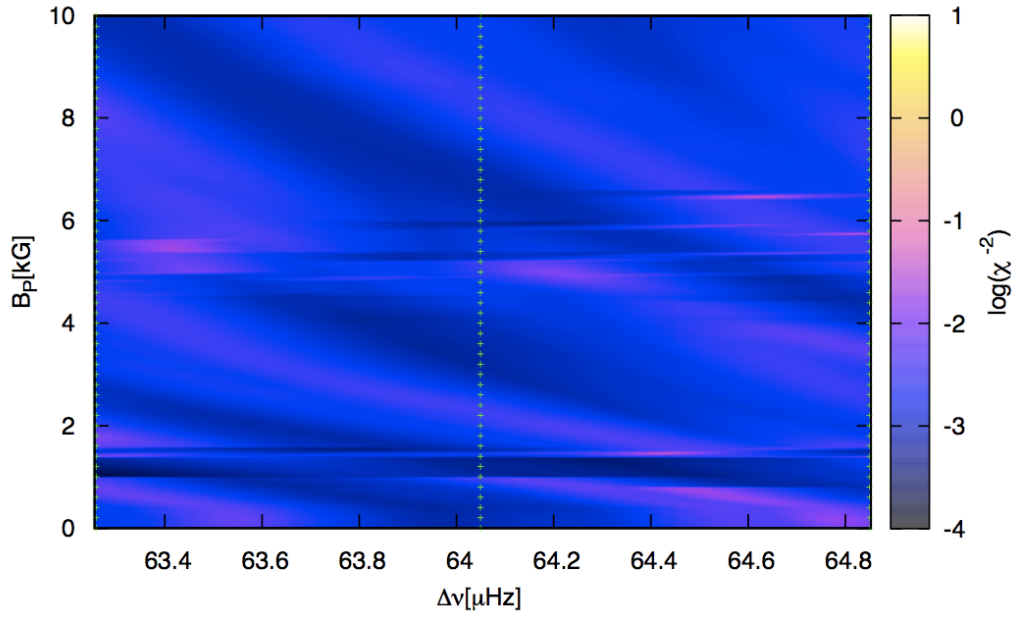


Figure A.4: χ^2 -results for Grid 2 α ; includes convection.

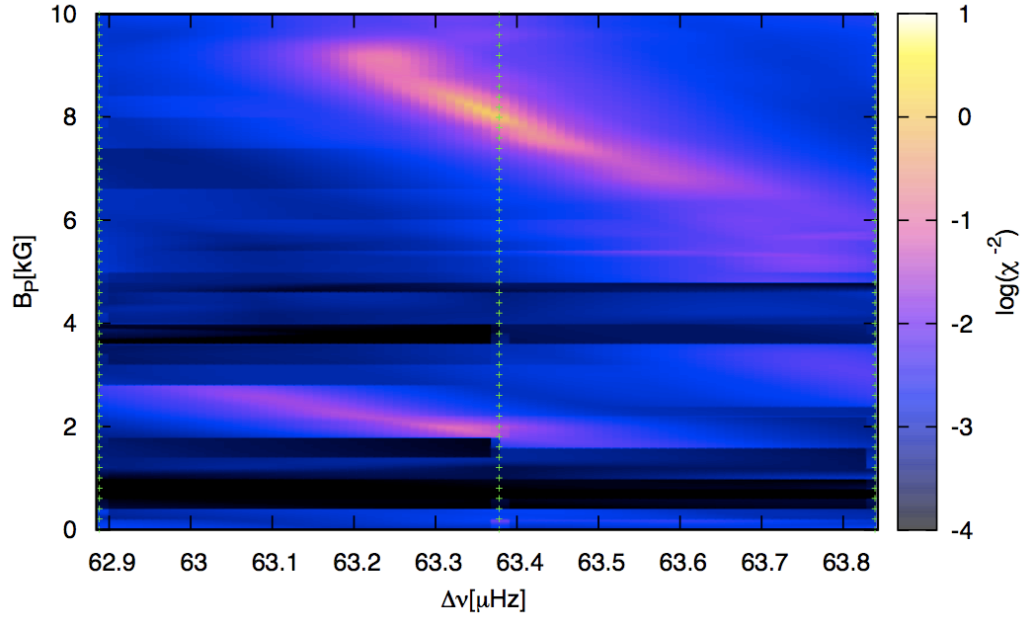


Figure A.5: χ^2 -results for Grid 3; no convection.

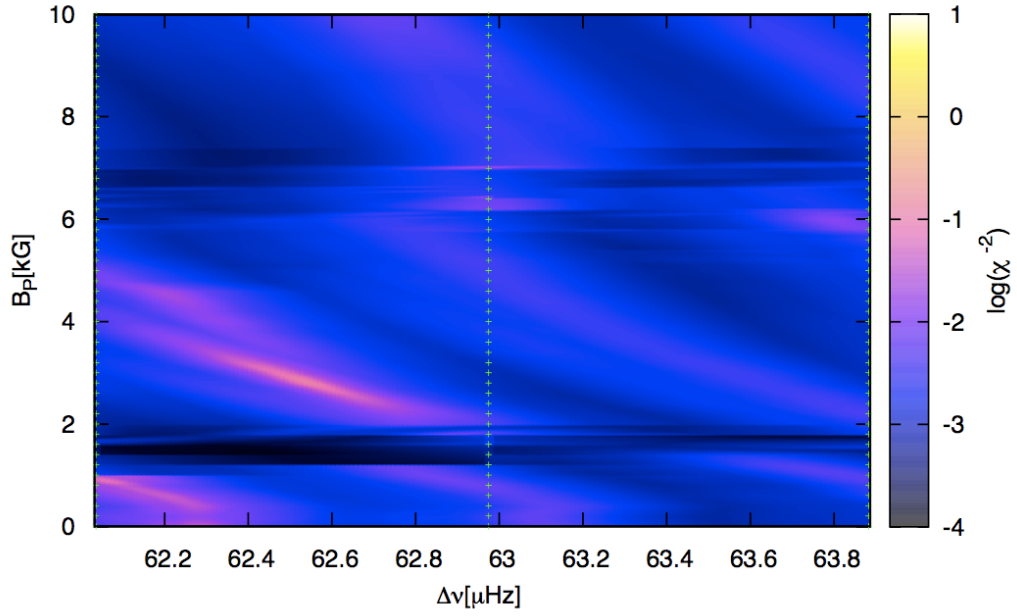


Figure A.6: χ^2 -results for Grid 3 α ; includes convection.

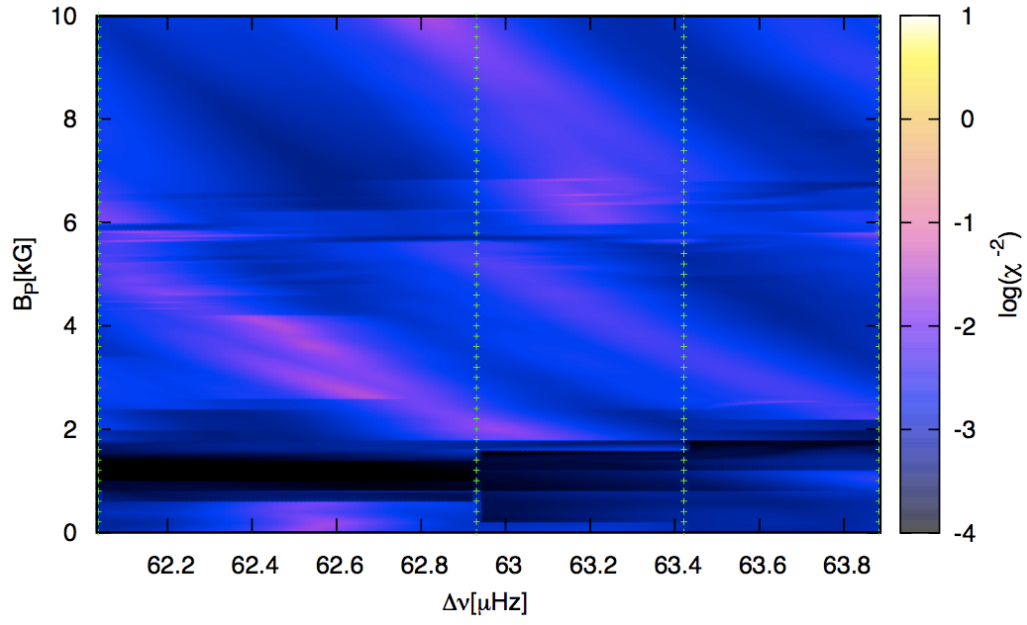


Figure A.7: χ^2 -results for Grid 4; no convection but homogenous He abundance in the envelope.

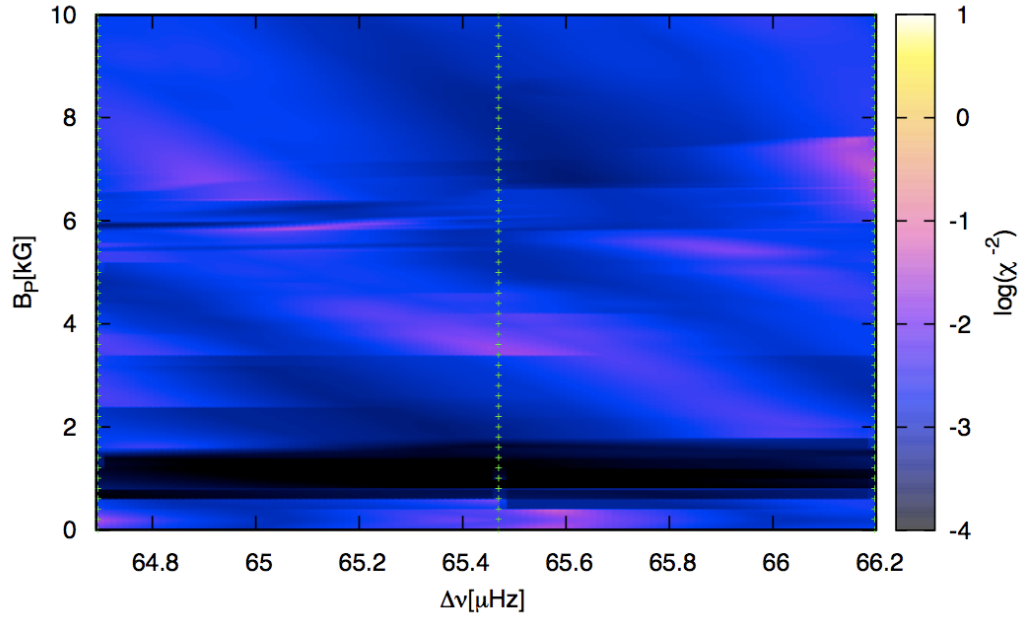


Figure A.8: χ^2 -results for Grid 5; no convection.

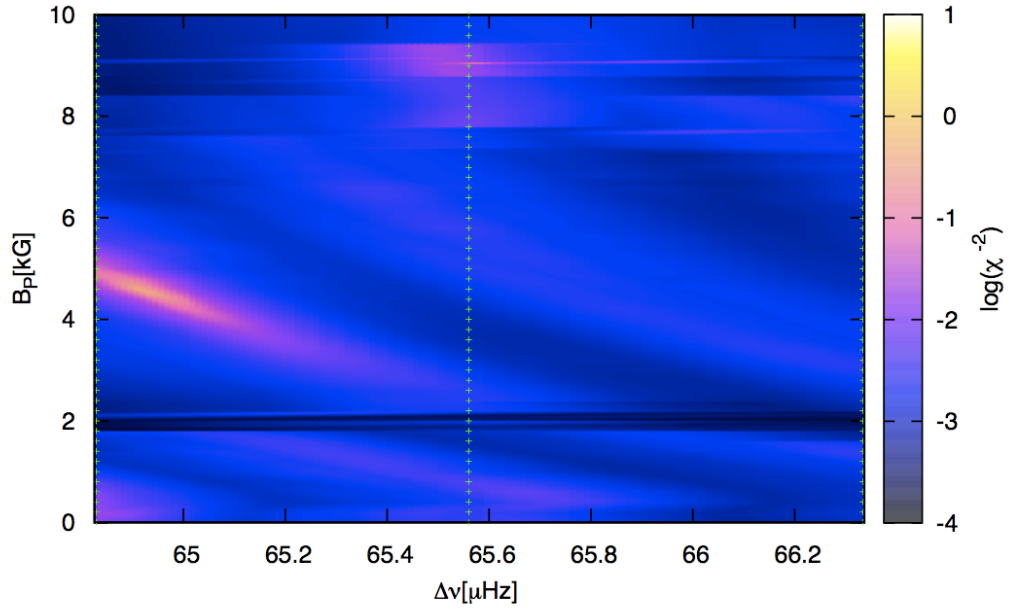


Figure A.9: χ^2 -results for Grid 5a; includes convection.

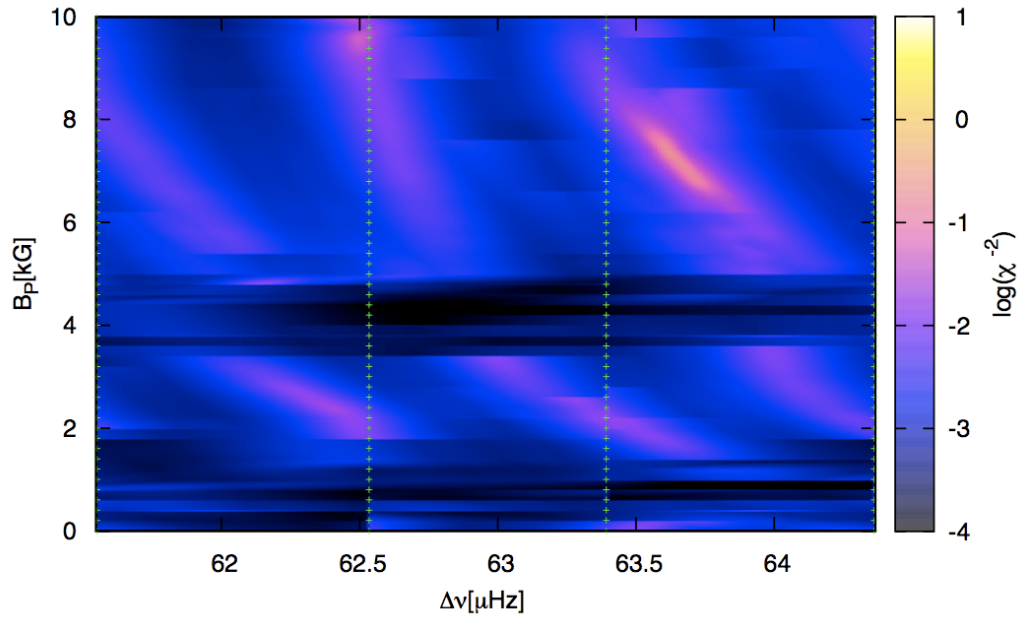


Figure A.10: χ^2 -results for Grid 6; no convection.

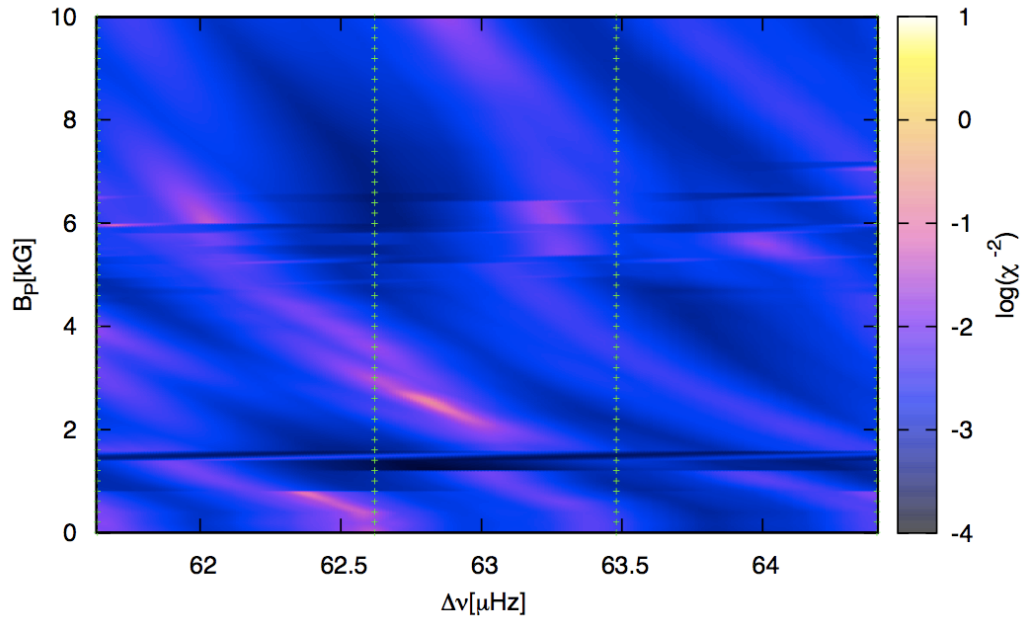


Figure A.11: χ^2 -results for Grid 6 α ; includes convection.

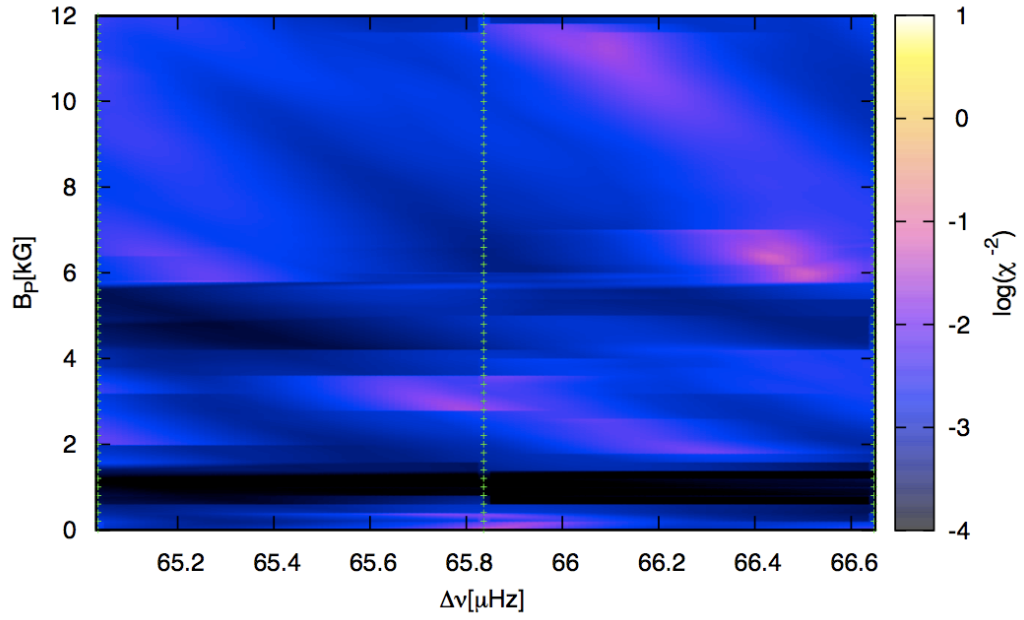


Figure A.12: χ^2 -results for Grid 7; no convection, calculated up to 12kG.

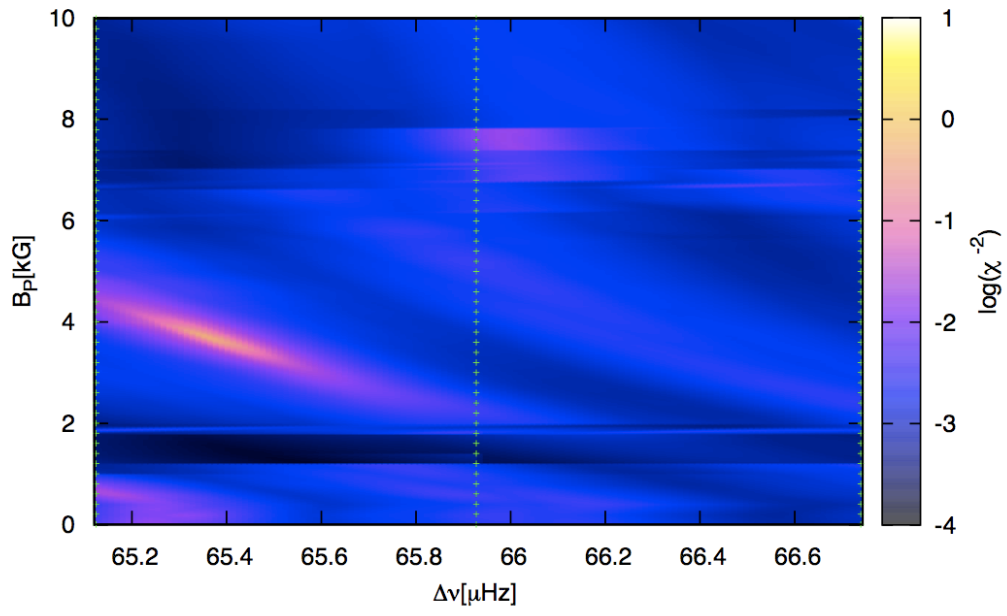


Figure A.13: χ^2 -results for Grid 7 α ; includes convection.

Bibliography

- Arlt, R. 2008, *Contrib. Astron. Obs. Skalnaté Pleso*, 38, 163
- Audard, N., Kupka, F., Morel, P., Provost, J., & Weiss, W. W. 1998, *A&A*, 335, 954
- Babcock, H. W. 1947, *ApJ*, 105, 105
- Babcock, H. W. 1958, *ApJS*, 3, 141
- Bahcall, J. N., Pinsonneault, M. H., & Wasserburg, G. J. 1995, *Reviews of Modern Physics*, 67, 781
- Balmforth, N. J., Cunha, M. S., Dolez, N., Gough, D. O., & Vauclair, S. 2001, *MNRAS*, 323, 362
- Berdyugina, S. V., Fluri, D. M., Afram, N., & Suwald, F. 2008, in *Astronomical Society of the Pacific Conference Series*, Vol. 384, 14th Cambridge Workshop on Cool Stars, Stellar Systems, and the Sun, ed. S. P. P. S. D. E. M. B. J. Messina, 175–+
- Bigot, L. & Dziembowski, W. A. 2002, *A&A*, 391, 235
- Bigot, L. & Dziembowski, W. A. 2003, *Ap&SS*, 284, 217
- Bigot, L., Provost, J., Berthomieu, G., Dziembowski, W. A., & Goode, P. R. 2000, *A&A*, 356, 218
- Biront, D., Goossens, M., Cousens, A., & Mestel, L. 1982, *MNRAS*, 201, 619
- Bonnarel, F., Fernique, P., Bienaymé, O., et al. 2000, *A&AS*, 143, 33
- Bonsack, W. K. & Pilachowski, C. A. 1974, *ApJ*, 190, 327
- Breger, M. & Pamyatnykh, A. A. 2006, *MNRAS*, 368, 571
- Bychkov, V. D. 1987, *Soviet Astronomy Letters*, 13, 325
- Bychkov, V. D., Bychkova, L. V., & Madej, J. 2005, *Acta Astronomica*, 55, 141
- Bychkov, V. D., Bychkova, L. V., & Madej, J. 2006, *MNRAS*, 365, 585
- Campbell, C. G. & Papaloizou, J. C. B. 1986, *MNRAS*, 220, 577
- Cunha, M. S. 2002, *MNRAS*, 333, 47
- Cunha, M. S. 2006, *MNRAS*, 365, 153
- Cunha, M. S. 2007, *Communications in Asteroseismology*, 150, 48
- Cunha, M. S. & Gough, D. 2000, *MNRAS*, 319, 1020

- Dziembowski, W. A. & Goode, P. R. 1996, *ApJ*, 458, 338
- Fleming, W. P. S. & Pickering, E. C. 1912, *Annals of Harvard College Observatory*, 56, 165
- Fowler, W. A., Burbidge, E. M., Burbidge, G. R., & Hoyle, F. 1965, *ApJ*, 142, 423
- Gautschi, A., Saio, H., & Harzenmoser, H. 1998, *MNRAS*, 301, 31
- Gruberbauer, M., Saio, H., Huber, D., et al. 2008, *A&A*, 480, 223
- Gruberbauer, M. & Weiss, W. W. 2008, *Contributions of the Astronomical Observatory Skalnaté Pleso*, 38, 311
- Guenther, D. B. & Brown, K. I. T. 2004, *ApJ*, 600, 419
- Handler, G., Weiss, W. W., Shobbrook, R. R., et al. 2006, *MNRAS*, 366, 257
- Huber, D. & Reegen, P. 2008, *Communications in Asteroseismology*, 152, 77
- Huber, D., Saio, H., Gruberbauer, M., et al. 2008, *A&A*, 483, 239
- Hubrig, S., Kurtz, D. W., Bagnulo, S., et al. 2004, *A&A*, 415, 661
- Iglesias, C. A. & Rogers, F. J. 1996, *ApJ*, 943
- Kallinger, T., Reegen, P., & Weiss, W. W. 2007, *A&A*, submitted
- Kanaan, A. & Hatzes, A. P. 1998, *ApJ*, 503, 848
- Kochukhov, O. 2003, *A&A*, 404, 669
- Kochukhov, O. 2004, *ApJ*, 615, L149
- Kochukhov, O. & Bagnulo, S. 2006, *A&A*, 450, 763
- Kochukhov, O., Bagnulo, S., Wade, G. A., et al. 2004a, *A&A*, 414, 613
- Kochukhov, O. & Ryabchikova, T. 2001, *A&A*, 374, 615
- Kochukhov, O., Ryabchikova, T., & Piskunov, N. 2004b, *A&A*, 415, L13
- Kochukhov, O., Ryabchikova, T., Weiss, W. W., Landstreet, J. D., & Lyashko, D. 2007, *MNRAS*, 376, 651
- Kurtz, D. W. 1982, *MNRAS*, 200, 807
- Kurtz, D. W. 1983, *MNRAS*, 202, 1
- Kurtz, D. W. 1990, *ARA&A*, 28, 607
- Kurtz, D. W. 1992, *MNRAS*, 259, 701
- Kurtz, D. W., Cameron, C., Cunha, M. S., et al. 2005, *MNRAS*, 358, 651
- Kurtz, D. W. & Martinez, P. 2000, *Baltic Astronomy*, 9, 253
- Landstreet, J. D. 1988, *ApJ*, 326, 967
- Ledoux, P. 1951, *ApJ*, 114, 373

- Lenz, P. & Breger, M. 2005, *Communications in Asteroseismology*, 146, 53
- Leone, F. & Kurtz, D. W. 2003, *A&A*, 407, L67
- Leroy, J. L., Bagnulo, S., Landolfi, M., & Degl'Innocenti, E. L. 1994, *A&A*, 284, 174
- Libbrecht, K. G. 1988, *ApJ*, 330, L51
- Malanushenko, V., Savanov, I., & Ryabchikova, T. 1998, *Informational Bulletin on Variable Stars*, 4650, 1
- Martinez, P., Weiss, W. W., Nelson, M. J., et al. 1996, *MNRAS*, 282, 243
- Mathys, G. 2004, in *IAU Symposium*, Vol. 224, *The A-Star Puzzle*, ed. J. Zverko, J. Ziznovsky, S. J. Adelman, & W. W. Weiss, 225–234
- Matthews, J. M. & Scott, S. 1995, in *Astronomical Society of the Pacific Conference Series*, Vol. 83, *IAU Colloq. 155: Astrophysical Applications of Stellar Pulsation*, ed. R. S. Stobie & P. A. Whitelock, 347
- Michaud, G. 1970, *ApJ*, 160, 641
- Mkrtychian, D. E., Samus, N. N., Gorynya, N. A., et al. 1998, *Informational Bulletin on Variable Stars*, 4564, 1
- Mkrtychian, D. E., Samus, N. N., Gorynya, N. A., North, P., & Hatzes, A. P. 1999, in *Astronomical Society of the Pacific Conference Series*, Vol. 185, *IAU Colloq. 170: Precise Stellar Radial Velocities*, ed. J. B. Hearnshaw & C. D. Scarfe, 331
- Morgan, W. W. 1933, *ApJ*, 77, 330
- Nyquist, H. 1928, *Trans. AIEE*, 41, 617
- Preston, G. W. 1974, *ARA&A*, 12, 257
- Reegen, P. 2007, *A&A*, 467, 1353
- Reegen, P., Gruberbauer, M., Schneider, L., & Weiss, W. W. 2008, *A&A*, 484, 601
- Reegen, P., Kallinger, T., Frast, D., et al. 2006, *MNRAS*, 367, 1417
- Reid, I. N., Brewer, C., Brucato, R. J., et al. 1991, *PASP*, 103, 661
- Roberts, P. H. & Soward, A. M. 1983, *MNRAS*, 205, 1171
- Ryabchikova, T., Nesvacil, N., Weiss, W. W., Kochukhov, O., & Stütz, C. 2004, *A&A*, 423, 705
- Ryabchikova, T., Piskunov, N., Kochukhov, O., et al. 2002, *A&A*, 384, 545
- Ryabchikova, T., Wade, G. A., & LeBlanc, F. 2003, in *IAU Symposium*, Vol. 210, *Modelling of Stellar Atmospheres*, ed. N. Piskunov, W. W. Weiss, & D. F. Gray, 301–+
- Saio, H. 2005, *MNRAS*, 360, 1022
- Saio, H. & Gautschy, A. 2004, *MNRAS*, 350, 485
- Savanov, I., Hubrig, S., Mathys, G., Ritter, A., & Kurtz, D. W. 2006, *A&A*, 448, 1165
- Savanov, I. S., Malanushenko, V. P., & Ryabchikova, T. A. 1999, *Astronomy Letters*, 25, 802

- Scholz, G. 1979, *Astronomische Nachrichten*, 300, 213
- Scholz, G., Hildebrandt, G., Lehmann, H., & Glagolevskij, Y. V. 1997, *A&A*, 325, 529
- Shibahashi, H., Gough, D., Kurtz, D. W., & Kamb, E. 2008, *PASJ*, 60, 63
- Shibahashi, H., Kurtz, D., Kambe, E., & Gough, D. 2004, in *Astronomical Society of the Pacific Conference Series*, Vol. 310, IAU Colloq. 193: Variable Stars in the Local Group, ed. D. W. Kurtz & K. R. Pollard, 287
- Stibbs, D. W. N. 1950, *MNRAS*, 110, 395
- Tassoul, M. 1990, *ApJ*, 358, 313
- Vauclair, S. 2003, *Ap&SS*, 284, 205
- Walker, G., Matthews, J., Kuschnig, R., et al. 2003, *PASP*, 115, 1023
- Wegner, G. 1981, *ApJ*, 247, 969
- Weiss, W. W. 1983, *Informational Bulletin on Variable Stars*, 2384, 1
- Weiss, W. W. 1986, in *Astrophysics and Space Science Library*, Vol. 125, *Astrophysics and Space Science Library*, ed. C. R. Cowley, M. M. Dworetzky, & C. Megessier, 219–231
- Weiss, W. W. & Schneider, H. 1984, *A&A*, 135, 148
- Weiss, W. W. & Schneider, H. 1989, *A&A*, 224, 101

Lebenslauf

Angaben zur Person

Name: Michael Gruberbauer
Geburtsdatum/-ort: 24. November 1983, St. Pölten, Niederösterreich
Staatsbürgerschaft: Österreich

Schulbildung

1994 - 1998 Unterstufe - BRG Krems, Ringstraße 33, 3500 Krems
1998 - 2002 Oberstufe - BORG Krems, Heinemannstraße 12, 3500 Krems,
mit Auszeichnung maturiert

Ehrenring der Stadt Krems: "*Summa Cum Laude*"
für außergewöhnliche Leistungen in der Schullaufbahn

Zivildienst

1.10.2002 - 30.9.2003 Rettungssanitäter beim Roten Kreuz Krems

Studium

2003 - 2006 Universität Wien
Bakkalaureat in Astronomie, mit Auszeichnung abgeschlossen

2006 - 2008 Universität Wien
Magisterstudium Astronomie

Ausgewählte wissenschaftliche Arbeiten

"*MOST photometry of the RRd Lyrae variable AQ Leo: two radial modes, 32 combination frequencies and beyond*",
Gruberbauer, M., Kolenberg, K., Rowe, J.F., Huber, D., Matthews, J.M., Reegen, P., Kuschnig, R., Cameron, C., Kallinger, T.,
Weiss, W.W., Guenther, D.B., Moffat, A.F.J., Rucinski, S., Sasselov, D., Walker, G.A.H.
Monthly Notices of the Royal Astronomical Society, Volume 379, Issue 4, pp. 1498-1506

"*MOST photometry and modeling of the rapidly oscillating (roAp) star γ Equulei*",
Gruberbauer, M., Saio, H., Huber, D., Kallinger, T., Weiss, W.W., Guenther, D.B., Kuschnig, R., Matthews, J.M., Moffat, A.F.J.,
Rucinski, S., Sasselov, D., Walker, G.A.H.
Astronomy and Astrophysics, Volume 480, Issue 1, March II 2008, pp.223-232

"*The Nature of p-modes and Granulation in Procyon: New MOST Photometry and New Yale Convection Models*",
Guenther, D.B., Kallinger, T., **Gruberbauer, M.**, Huber, D., Weiss, W.W., Kuschnig, R., Demarque, P., Robinson, F., Matthews, J.M.,
Moffat, A.F.J., Rucinski, S., Sasselov, D., Walker, G.A.H.
The Astrophysical Journal, Volume 687, Issue 2, pp. 1448-1459

"*CINDERELLA: Comparison of INDEpendent RELative least-squares amplitudes. Time series data reduction in Fourier space*",
Reegen, P., **Gruberbauer, M.**, Schneider, L., Weiss, W.W.
Astronomy and Astrophysics, Volume 484, Issue 2, 2008, pp.601-608

Unterschrift